# On the Stability and Imaging Applications of Metal-containing Coacervate Micelles

**Junyou Wang**

**Thesis committee**

**Thesis supervisor**

Prof. dr. M. A. Cohen Stuart
Professor of Physical Chemistry and Colloid Science
Wageningen University, The Netherlands

**Thesis co-supervisors:**

Dr. ir. J. van der Gucht
Associate professor, Laboratory of Physical Chemistry and Colloid Science
Wageningen University, The Netherlands

Dr. H. Van As
Associate professor, Laboratory of Biophysics and
Wageningen Nuclear Magnetic Resonance Centre
Wageningen University, The Netherlands

**Other members:**

| | |
|---|---|
| Prof. dr. A. H. Velders | Wageningen University, The Netherlands |
| Prof. dr. R. P. Sijbesma | Eindhoven University of Technology, The Netherlands |
| Dr. ir. T. Vermonden | Utrecht University, The Netherlands |
| Dr. ir. N. A. M. Besseling | Delft University of Technology, The Netherlands |

This research was conducted under the auspices of Graduate School VLAG

# On the Stability and Imaging Applications of Metal-containing Coacervate Micelles

Junyou Wang

**Thesis**

submitted in fulfilment of the requirements for the degree of doctor

at Wageningen University

by the authority of the Rector Magnificus

Prof. dr. M. J. Kropff,

in the presence of the

Thesis Committee appointed by the Academic Board

to be defended in public

on Monday 26 November 2012

at 4 p.m. in the Aula

Junyou Wang
On the Stability and Imaging Applications of Metal-containing Coacervate Micelles
120 pages
PhD thesis, Wageningen University, Wageningen, The Netherlands (2012)
with references, with summaries in English and Dutch

ISBN: 978-94-6173-399-3

# Contents


| | | |
|---|---|---|
| **Chapter 1** | Introduction | 1 |
| **Chapter 2** | Complex Coacervate Core Micelles from Iron-based Coordination Polymers | 15 |
| **Chapter 3** | Effect of pH on Complex Coacervate Core Micelles from Fe(III)-Based Coordination Polymers | 31 |
| **Chapter 4** | Stable Polymer Micelles Formed by Metal Coordination | 45 |
| **Chapter 5** | Controlled Mixing of Lanthanide(III) Ions in Coacervate Core Micelles | 63 |
| **Chapter 6** | Phase Diagram of Coacervate Complexes Containing Reversible Coordination Polymers | 77 |
| **Chapter 7** | Summary and General Discussion | 95 |

**Samenvatting**

**Acknowledgements**

**Curriculum Vitae**

**List of Publication**

**Overview of Completed Training Activities**

# Chapter 1

## Introduction

## 1.1 Polyelectrolytes and their self-assembly

Polyelectrolytes are polymers with a substantial portion of the constitutional units containing ionic or ionisable groups.[1] Quenched or strong polyelectrolytes are polymers with a constant charge density, while annealed, or weak polyelectrolytes are chains consisting of ionisable groups with a non-fixed degree of ionisation. Polyelectrolytes can be either synthetic polymers or natural macromolecules, such as DNA, proteins, teichoic acids, some polypeptides and polysaccharides. In aqueous solution, polyelectrolytes can acquire charges on the chain by either absorbing ions from solution or dissociating the groups on the backbone.[2] For example, poly(vinylpyridine) (PVP) can pick up protons at low pH and become positively charged; carboxylic groups on poly(methacrylic acid) (PMAA) can dissociate into $-COO^-$ and $H^+$ ions at higher pH ( > 6), giving a negative polymer chain. The charge formation process creates a polymeric ion and numerous counterions distributed near the polyion, leading to a double layer structure with condensed counterions near the polyion and free counterions staying a bit farther. Depending on the sign of the charges on the backbone, polyelectrolytes can be divided into polycations, polyanions, and polyampholytes, where the latter contain both cationic and anionic groups. Another typical feature of polyelectrolytes is the stretched chain conformation at low ionic strength in solution due to the strong electrostatic repulsion between the charged segments.[3]

Upon mixing oppositely charged polyelectrolytes in aqueous solution, a phase separation occurs. The dilute phase contains mainly water and released counterions while the dense phase at the bottom is rich in both polyions. The polyelectrolyte-rich phase was named a complex coacervate by Bungenberg de Jong and Kruyt who investigated such phase separation in colloidal systems.[4,5] The complexation is driven mainly by two contributions: the electrostatic attraction between the oppositely charged groups on the polyelectrolyte chains and the entropy gain of the counterions that are released upon complexation. Overbeek and Voorn developed the first theoretical model for complex coacervation, where they assumed that the total free energy of mixing is given by the sum of the mixing entropy and the electrostatic interaction free energy, based on Flory-Huggins expressions and the Debye-Huckel theory, respectively.[6] The model was modified subsequently by several other researchers.[7-10]

Self-assembly base on ionic interaction offers a straightforward and powerful strategy to organize the polyelectrolytes into highly ordered nano- or micro-structures. In recent years, assemblies based on a wide variety of polyelectrolytes have been investigated extensively, leading to various structures and functional materials.[11-13] One of the most popular structures is a core-shell micelle, prepared by mixing a polyion-neutral diblock copolymer with oppositely charged surfactants, polyions, proteins, peptides, or enzymes.[14] The linear ionic-neutral block copolymers can also self-assemble with nonlinear polyionic species, such as dendrimers, cylindrical brushes, star-shaped polyelectrolytes, organic dyes, DNA and polysaccharides, giving rod-like, star-shaped or other branched structures.[15-17] Hydrogels driven by ionic interaction have been studied systematically by Lemmers and co-workers, where the cross-link happened between an A-B-A triblock polymer with two ionic end blocks and an oppositely charged homopolymer.[18] Such hydrogels are totally reversible structures and respond to changes in temperature, concentration, ionic strength, cationic/anionic composition and pH. Besides complexes formed in bulk solution, homo-polyelectrolyte assembly on a substrate surface is another widely studied system.[19] The fabrication is mainly based on the layer-by-layer technique and provides multilayered films, functional coatings and capsules. All these structures have a great potential to be used as drug carriers, biosensors and microreactors.

## 1.2 Complex coacervate core micelles

One widely studied type of assemblies formed by polyelectrolyte complexation is that of micellar aggregates. The crucial point for forming a micelle is to introduce a hydrophilic polymer to the end of one or both homo-polyelectrolytes, so that macroscopic phase separation is prevented by the steric repulsion between the hydrophilic polymers. This leads to the formation of micelles with a core consisting of the complex coacervate and a corona of the neutral polymer (Figure 1.1). The first report on such micelles was published in 1995 by Kataoka.[20] Then the field has been investigated widely by many groups, leading to different names describing the micelles: polyion complex micelles (PIC micelles) named by Kataoka;[20] block ionomer complexes (BIC) by Kabanov;[21] complex coacervate core micelles (C3Ms) by Cohen Stuart[22] and polyelectrolyte complexes (PEC) by Gohy.[23] In this thesis, we use the name complex coacervate core micelles.

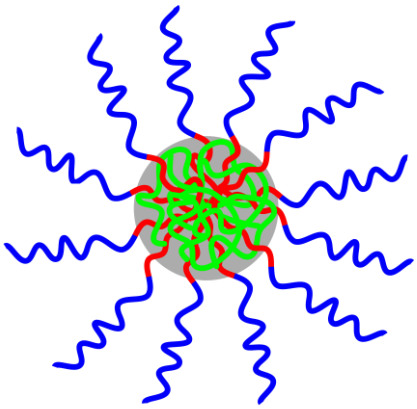

Figure 1.1 Schematic representation of complex coacervate core micelles.

Based on the results from literature, some typical properties of C3Ms are summarized below:

*a. constituents and mixing fraction*

C3Ms are formed by oppositely charged polyelectrolytes with at least one of the polyelectrolytes containing a neutral hydrophilic block. The micelle structure and stability depend strongly on the properties of the components, such as the length of the diblock copolymer, the block length ratio, the chemical structure of the corona block and the type of ionic groups. For example, the length ratio of the neutral block and the charged block $N_{corona}/N_{core}$ should be > 3 in order to avoid macroscopic phase separation completely.[22] The charge mixing ratio is another crucial factor for forming stable micelle structures. In general, well defined micelles can be formed only near the charge stoichiometric point, where the number of positively and negatively charged groups on the polymers is equal. Out of this mixing range, soluble complexes or loose structures are formed.[24]

*b. responsiveness to ionic strength and pH*

C3Ms are quite sensitive to ionic strength due to the fact that the electrostatic interaction between the polymers, which is the driving force for micellization, can be screened progressively with increasing ionic strength.[25-27] Upon increasing salt concentration, C3Ms typically swell into loose structures followed by a complete dissociation above the critical salt concentration, CSC. Accompanied with the internal structural changes, the morphology of the micelles also varies with changing salt concentration. The critical micelle concentration (CMC) increases with added salt and the micellar structures become

more dynamic and closer to thermodynamic equilibrium at high ionic strength. For C3Ms formed by strong polyelectrolytes, pH hardly affects the formation and structure, as the charge density of the polyelectrolytes is fixed. By contrast, C3Ms formed by weak or annealed polyelectrolytes are sensitive to pH. The dissociation degree of weak polyelectrolytes is governed by the solution pH, and the formed C3Ms can respond to pH reversibly to form micelles or fall apart.[28-30]

*c. structure and morphology*

C3Ms formed by linear and flexible polyelectrolytes normally have a core-shell structure with a spherical shape. As mentioned above, the internal structure and morphology of C3Ms depend on the conditions, such as charge mixing ratio, pH, and ionic strength. Since the corona of C3Ms contains only hydrophilic polymer chains, there is less interest in the corona structure. Most studies focus on the structure and properties of the core. One interesting question is the solvent content in the coacervate core. C3Ms are believed to have a considerable amount of water in their core, but no quantitative number has been obtained yet. By simply weighing a macroscopic coacervate complex before and after evaporating water, Spruijt et al. recently found that the water content in the coacervate complexes formed by linear polyelectrolytes was never lower than 65%, and the water fraction increased slightly with increasing salt concentration and decreasing polymer chain length.[31] Such results can be a good reference to estimate the water content in the coacervate cores of C3Ms.

*d. potential applications*

Amphiphilic block polymer micelles are believed to be good carrier and reactor materials due to their high stability, inert core and corona. For complex coacervate core micelles, the advantage is that both the micellar core and corona are hydrophilic, which is favorable especially for biomedical applications and for use as aqueous reactors and materials.[32-36] For example, enzymes, oligonucleotides, and hydrophilic drugs can aggregate with ionic-neutral diblock copolymers, forming C3Ms with functional components packed in the micellar core. The corona could be further modified with target groups or functional blocks responding to a biological signal. Surfaces coated with C3Ms were found to repel specific proteins efficiently, which could be used in biofouling applications. Hybrid quantum dots and metal nanoparticles could be prepared with C3Ms as templates in aqueous solution.

## 1.3 Metal-ligand coordination polymers and complexes

Metal-ligand coordination is a highly specific and directional interaction. The binding strength is intermediate between weak non-covalent interaction and covalent bonding, and can be tuned by selecting different metal-ligand pairs.[37] Kinetically inert metal-ligand coordination normally provides irreversible structures with high polydispersity because of the large binding constant and the extremely slow exchange of ligand at moderate conditions. Reversible structures are formed by kinetically labile coordination complexes with intermediate binding constants. These structures are of special interests due to the adjustability of the structure and their responsiveness to ambient factors.[38-40] To form reversible coordination polymers, the organic ligand needs at least two chelate groups at the ends of a spacer, allowing chain growth in one or multiple directions. Bisligands are the most studied system and the chelate groups are mainly based on pyridine derivates, such as terpyridine, pyridine with carboxylic groups and hydroxylic groups.(Figure 1.2) The metal ions used for reversible coordination structures are normally the first row transition metal ions, such as $Mn^{2+}$, $Fe^{2+/3+}$, $Co^{2+}$, $Ni^{2+}$, an $Zn^{2+}$. Lanthanides can also form reversible structures with pyridine-carboxylic ligands.

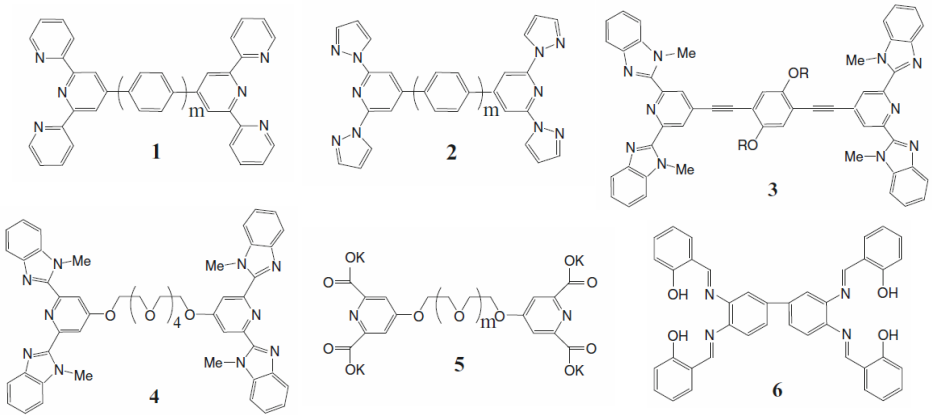


Figure 1.2 Structures of some bisligands.

Reversible coordination complexes have been studied by several groups. Kurth and co-workers have done a series of work based on 1,4-bis(2, 2`:6,2``-terpyridine-4`-yl)benzene ligands (Figure 1.2, 1). They found that a bisligand with a rigid spacer formed rod-like coordination compounds with $Fe^{2+}$ and $Ni^{2+}$, while a ligand with a flexible spacer gave

small coordination nanoparticles since the spacer could bend to form rings and stop the chain growth (Figure 1.3).[41]

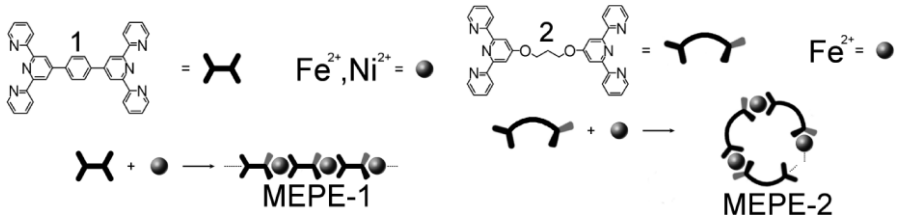


Figure 1.3 Rod-like and ring structures of coordination complexes based on terpyridine bisligand. (Ref. 42)

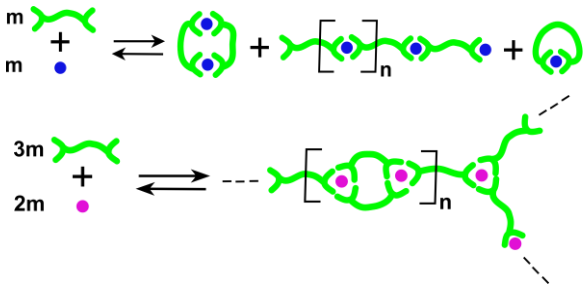


Figure 1.4 Coordination structures based on $L_2EO_4$ ligand with transition metal ions (top, first row) and lanthanides (bottom).

Another well investigated system is the 1,11-bis(2,6-dicarboxypyridin-4-yloxy)-3,6,9-trioxaundecane ($L_2EO_4$, Figure 1.2, 5) ligand developed by Vermonden and co-workers.[42-43] In Vermonden's work, ethylene oxide (EO) was used as a flexible spacer and the effect of the EO spacer length on the complexes was studied. Zn-$L_2EO_4$ (metal to ligand ratio M/L, 1/1) complexes formed small structures with both rings and linear chains (Figure 1.4, top). The ring fraction decreased with increasing concentration or increasing temperature. A longer spacer (6 EO units) gave more rings than a short spacer (4 EO units), because the EO-6 spacer is just long enough to form monomeric rings, while the EO-4 spacer needs at least two molecules to form a ring. $L_2EO_4$ ligands could also form reversible coordination complexes with lanthanides ($La^{3+}$, $Nd^{3+}$) at a M/L ratio of 2/3, but with a branched structure, because lanthanides have nine coordination sites and can bind with three chelate groups of $L_2EO_4$ (Figure 1.4, bottom). The metal-ligand complexes normally carry positive charges from the metal ions or negative charges from the ligand groups. These charges

make them an ideal component for the self-assembly with other polyelectrolytes to build up inorganic/organic hybrid complexes and materials.

## 1.4 Metal containing complex coacervate core micelles

Metal containing complex coacervate core micelles (M-C3Ms) are formed based on the electrostatic interaction between a polyion-neutral diblock copolymer and reversible coordination polymers or complexes. M-$L_2EO_4$ coordination polymer and complexes have been used as the construction components as they are reversible and very soluble in aqueous solution. Yan *et al.* reported the first paper about M-C3Ms, in which cationic Zn-$L_2EO_4$ coordination polymers aggregated with the oppositely charged block of $P2MVP_{41}$-$PEO_{205}$ diblock copolymers.[44] The coacervate complexes that were formed were stabilized by the long PEO chain, giving micellar structures successfully (Figure 1.5). Zn-C3Ms could be formed at a very low concentration of Zn-$L_2EO_4$ coordination complexes, where these should form mainly small rings and short oligomers based on previous observations.[42] However, in the absence of metal ions no micelles were formed , even though the free ligand molecules had more negative charges compared to the oligomers formed at M/L=1/1. This result suggests that the oppositely charged block induces a strong shift of the equilibrium from small rings or short oligomers to long coordination polymer chains, indicating that micellization is a cooperative process between ionic interaction and metal-ligand coordination.

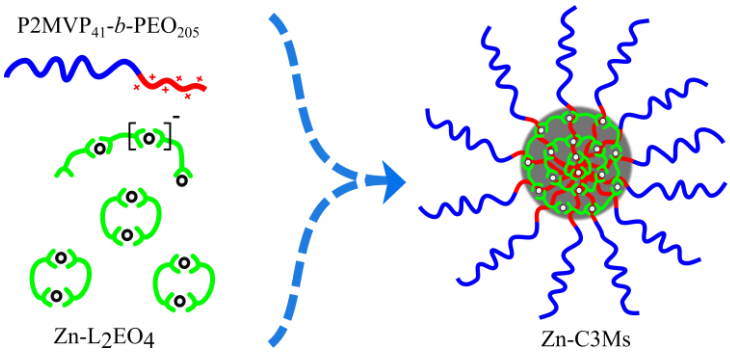


Figure 1.5 Illustration of the formation of Zn-C3Ms. (small dots present $Zn^{2+}$ ions)

M-C3Ms were only formed in the presence of all three components: metal ions, $L_2EO_4$ ligand and polycationic-neutral diblock copolymer; any two of the three components without the third one cannot make micelles. The metal to ligand ratio M/L should be at the

coordination stoichiometry to form polymer chains for transition metal ions (1/1) and branched structures for lanthanides (2/3).[45] The charge mixing ratio is another crucial factor to control the formation of M-C3Ms. At neutralized charge ratio, M-C3Ms are formed efficiently; while an excess of M-$L_2EO_4$ coordination complexes has almost no effect on the formed micelles, an excess of diblock copolymers are found to lead to a gradual dissociation of the micelles. This is different from C3Ms made of pure organic polyelectrolytes, for which the range where micelles can be formed is very narrow and excess of any component will dissociate the formed micelles. This difference confirms the reversibility of M-$L_2EO_4$ coordination complexes: they form small coordination rings or oligomers out of the micelle that can not destroy the formed micellar structures. Since the ionic interaction is the driving force for the micellization, M-C3Ms also show the typical response to ionic strength: the CMC increases and the aggregation number decreases with increasing salt concentration; their structure and morphology vary upon adding salt and the micelles fall apart completely above the critical salt concentration.[46] As a special category of C3Ms, M-C3Ms have much interest and advantages. First of all, the core structure and morphology of C3Ms is very difficult to probe for purely organic C3Ms. The core is invisible under microscopes (TEM, SEM) due to insufficient contrast of the organic components. With metal ions in the micellar core, this problem can be solved, opening new possibilities to investigate the core structure and properties of C3Ms.[47] What is more, different functionalities of C3Ms can be obtained and adjusted by applying and varying metal ions, giving great potential for fabricating functional materials.[48-49] For example, luminescent or magnetic lanthanides ($Eu^{3+}$, $Gd^{3+}$) can be packed in the core of C3Ms, providing good candidates for optical imaging or MRI probes;[50] Au or Pt containing C3Ms may be the good precursors for making polymer stabilized nanoparticles, which are good catalysts.[36] In this regard, M-C3Ms are worth to be investigated further.

## 1.5 Outline of this thesis

In this thesis we study metal containing complex coacervate core micelles (M-C3Ms). We prepare Fe-C3Ms and Gd-C3Ms with magnetic properties and Eu-C3Ms which have luminescent properties. The interest of these particles is their potential for application as MRI and optical imaging probes, for example in medical applications. The stability of these micelles against ionic strength and pH is studied, and an alternative micellization, based on a new type of diblock copolymers is presented. The study on the phase separation

of coacervate complexes from homopolyelectrolytes and coordination polymers gives additional information about formation and structure of coacervate complexes and M-C3Ms.

In **chapter 2**, we study the formation and stability of Fe-C3Ms by light scattering. Both Fe(II)-C3Ms and Fe(III)-C3Ms are found to form efficiently near charge stoichiometry and are very stable in time at room temperature. Fe(II)-C3Ms and Fe(III)-C3Ms show the typical salt response: increasing the salt concentration results in an almost linear decrease of the scattering intensity, an increase of the CMC, a linear decrease of the aggregation number, and swelling of micelles followed by full dissociation at the critical salt concentration. Fe(III)-C3Ms are more stable against salt than Fe(II)-C3Ms. In other words, Fe(III)-C3Ms are preferred above Fe(II)-C3Ms due to the high stability, especially, in developing novel properties and potential applications.

In **chapter 3**, the pH effect on Fe(III)-C3Ms is described. Light scattering and Cryo-TEM have been performed to study the variations of the hydrodynamic radius and the core structure with changing pH. The hydrodynamic radius of Fe(III)-C3Ms is determined mainly by the corona and does not change very much in a broad pH range. However, Cryo-TEM pictures and magnetic relaxation measurements indicate that the structure of the micellar cores changes upon changing the pH, with a more crystalline, elongated shape and lower relaxivity at high pH. We attribute this to the formation of mixed iron complexes in the core, involving both the bisligand and hydroxide ions. These complexes are stabilized towards precipitation by the diblock copolymer.

In **chapter 4**, we develop a salt-stable micelle system. We synthesize a diblock copolymer with a neutral hydrophilic block and a block with ligand groups grafted to the backbone. Added metal ions cross-link the ligand-carrying blocks together, while the hydrophilic blocks protect the formed coordination complex, leading to the formation of micelles. The micellization is driven directly by the metal-ligand coordination, providing a high stability against ionic strength.

In **chapter 5**, we investigate $Eu^{3+}$ and $Gd^{3+}$ combined micelles, Eu/Gd-C3Ms. The formed coacervate-core micelles contain a few hundred $Eu^{3+}$ and $Gd^{3+}$ ions in the core at a composition ratio between $Eu^{3+}$ and $Gd^{3+}$ that can be adjusted between 0 – 100%, resulting in a corresponding linear tunability of the luminescence and magnetic relaxation properties of the micelles. Light scattering, Cryo-TEM, luminescence spectroscopy and magnetic relaxation measurements indicate that the micelles are very stable under physiological

conditions and in the presence of scavenging ligands like EDTA, showing great potential for use as bimodal imaging probes.

In **chapter 6**, we study the phase separation and the binodal composition of coacervate complexes from cationic PDMAEMA [poly(N,N-dimethylaminoethyl methacrylate)] and anionic reversible Zn-$L_2EO_4$ coordination polymers. The charge mixing ratio and metal to ligand ratio, M/L are varied systematically. The composition of complexes in both the dilute phase and coacervate phase has been measured using $^1$H-NMR spectra (PDMAEMA and $L_2EO_4$) with an internal standard and ICP-AES tests ($Zn^{2+}$). An asymmetric phase diagram is obtained, which summarizes all the composition points together.

In **chapter 7**, finally, we summarize the thesis. A general discussion including potential directions for future research on C3Ms and M-C3Ms is given in the end.

## References


1. Hess, M.; Jones, R. G.; Kahovec, J.; Kitayama, T.; Kratochvil, P.; Kubisa, P.; Mormann, W.; Stepto, R. F. T.; Tabak, D.; Vohlidal, J.; Wilks, E. S. *Pure Appl. Chem.* **2006**, *78*, 2067–2074.
2. Lyklema, J. *Fundamentals of Interface and Colloid Science*, Ed. Elsevier: 2005, Vol. V, Chapter II.
3. Kotz, J.; Kosmella, S.; Beitz, T. *Prog. Polym. Sci.* **2001**, *26*, 1199-1232.
4. Bungenberg de Jong, H. G.; Kruyt H. R. *Proceedings of the Koninklijke Nederlandse Akademie van Wetenschappen* **1929**, *32*, 849-856.
5. Bungenberg de Jong, H. G. Complex colloid systems. In *Colloid Science*, Ed. Elsevier: Amsterdam, 1949; Vol. II, Chapter X.
6. Overbeek, J. Th. G.; Voorn, M. J. *Journal of Cellular and Comparative Physiology* **1957**, *49*(S1), 7-26.
7. Veis, A.; Aranyi, C. *J. Phys. Chem.* **1960**, *64*, 1203-1210.
8. Nakajima, A.; Sato, H. *Biopolymers* **1972**, *10*, 1345-1355.
9. Tainaka, K. *J. Phys. Soc. Jpn.* **1979**, *64*, 1899-1906.
10. Tainaka, K. *Biopolymers* **1980**, *19*, 1289-1298.
11. Cooper, C. L.; Dubin, P. L.; Kayitmazer, A. B.; Turksen, S. *Curr. Opin. Colloid Interface Sci.* **2005**, *10*, 52-78.
12. Thunemann, A. F. *Prog. Polym. Sci.* **2002**, *27*, 1473-1572.
13. Willerich, I.; Schindler, T.; Grohn, F. *J. Phys. Chem. B* **2011**, *115*, 9710-9719.
14. Voets, I. K.; de Keizer A.; Cohen Stuart, M. A. *Adv. Colloid Interface Sci.* **2009**, *147-148*, 300-318.
15. Reinhold, F.; Kolb, U.; Lieberwirth, I. Grohn, F. *Langmuir* **2009**, *25*, 1345-1351.
16. Pergushov, D. V.; Borisov, O. V.; Zezin, A. B.; Muller, A. H. E. *Adv. Polym. Sci.* **2011**, *241*, 131-161.
17. Lee, H.; Jeong, J. H.; Park, T. G. *J. Control. Release* **2001**, *76*, 183-192.

18. Lemmers, M.; Sprakel, J.; Voets, I. K.; van der Gucht, J.; Cohen Stuart, M. A. *Angew. Chem., Int. Ed.* **2010**, *49*, 708-711.
19. Tong, W.; Gao, C. Y. *J. Mater. Chem.* **2008**, *18*, 3799-3812.
20. Harada, A.; Kataoka, K. *Macromolecules*, **1995**, *28*, 5294-5299.
21. Kabanov, A. V.; Bronich, T. K.; Kabanov, V. A.; Yu, K.; Eisenberg, A. *Macromolecules*, **1996**, *29*, 6797-6802.
22. van der Burgh, S.; de Keizer, A.; Cohen Stuart, M. A. *Langmuir* **2004**, *20*, 1073-1084.
23. Gohy, J. F.; Varshney, S. K.; Antoun, S.; Jerome, R. *Macromolecules* **2000**, *33*, 9398-9305.
24. Voets, I. K.; de Keizer, A. Cohen Stuart, M. A. *Advances in Colloid and Interface Science* **2009**, *147–148*, 300–318.
25. Yuan, X. F.; Harada, A.; Yamasaki, Y.; Kataoka, K. *Langmuir* **2005**, *21*, 2668-2674.
26. Matsuda, T.; Annaka, M. *Langmuir* **2008**, *24*, 5707-5713.
27. Bakeev, K. N.; Izumrudov, V. A.; Kuchanov, S. I. ;Zezin, A. B.; Kabanov, V. A. *Macromolecules* **1992**, *17*, 4249–4254.
28. Solomatin, S. V.; Bronich, T. K.; Bargar, T. W.; Eisenberg, A.; Kabanov, V. A.; Kabanov, A. V. *Langmuir* **2003**, *19*, 8069-8076.
29. Gohy, J. F.; Varshney, S. K.; Antoun, S.; Jerome, R. *Macromolecules* **2000**, *33*, 9298-9305.
30. Gohy, J. F.; Varshney, S. K.; Jerome, R. *Macromolecules* **2001**, *34*, 3361-3366.
31. Spruijt. E.; Westphal, A. H.; Borst, J. W.; Cohen Stuart, M. A.; van der Gucht, J. *Macromolecules* **2010**, *43*, 6476-6484.
32. Harada, A.; Kataoka, K. *Prog. Polym. Sci.* **2006**, *31*, 949–982.
33. Kataoka, K.; Harada, A.; Nagasaki, Y. *Adv. Drug Deliv. Rev.* **2001**, *47*, 113–131.
34. Voets, I. K.; de Vos, W. M.; Hofs, B.; de Keizer, A.; Cohen Stuart, M. A.; Steitz, R.; Lott, D. *J. Phys. Chem. B* **2008**, *112*, 6937-6945.
35. Duxin, N.; Liu, F. T.; Vali, H.; Eisenberg, A. *J Am Chem Soc* **2005**, *127*, 10063–10069.
36. Voets, I. K.; de Keizer, A.; Frederik, P. M.; Jellema, R.; Cohen Stuart, M. A. *J. Colloid Interface Sci.* **2009**, *339*, 317–324.
37. Moughton, A. O., O'Reilly, R. K. *Macromol. Rapid Commun.* **2010**, *31*, 37–52.
38. Friese, F. A.; Kurth, D. G. *Curr. Opin. Colloid Interface Sci.* **2009**, *14*, 81-93.
39. Yan, Y.; Huang, J. B. *Coord. Chem. Rev.* **2010**, *254*, 1072-1080.
40. Yan, Y.; de Keizer, A.; Cohen Stuart, M. A.; Besseling, N. A. M. *Adv. Polym. Sci.* **2011**, *242*, 91-115.
41. Schwarz, G.; Bodenthin, Y.; Geue, T.; Koetz, J. Kurth, D. G. *Macromolecules* **2010**, *43*, 494-500.
42. Vermonden, T.; van der Gucht, J.; De Waard, P.; Marcelis, A. T. M.; Besseling, N. A. M.; Sudholter, E. J. R.; Fleer, G. J.; Cohen Stuart, M. A. *Macromolecule* **2003**, *36*, 7035-7044;
43. Vermonden, T.; De Vos, W. M.; Marcelis, A. T. M.; Sudholter, E. J. R. *Eur. J. Inorg. Chem.* **2004**, 2847-2852.
44. Yan, Y.; Besseling, N. A. M.; de Keizer, A.; Marcelis, A. T. M.; Drechsler, M.; Cohen Stuart, M. A. *Angew. Chem. Int. Ed.* **2007**, *46*, 1807-1809.
45. Yan, Y.; Besseling, N. A. M.; de Keizer, A.; Cohen Stuart, M. A. *J. Phys. Chem. B* **2007**, *111*, 5811-5818.

46. Yan, Y.; de Keizer, A.; Cohen Stuart, M. A.; Drechsler, M.; Besseling; N. A. M. *J. Phys. Chem. B* **2008**, *112*, 10908-10914.
47. Yan, Y.; Besseling, N. A. M.; de Keizer, A.; Drechsler, M.; Fokkink, R.; Cohen Stuart, M. A. *J. Phys. Chem. B* **2007**, *111*, 11662-11669.
48. Yang, L.; Ding, Y.; Yang Y.; Yan, Y.; Huang, J. B.; de Keizer, A.; Cohen Stuart, M. A. *Soft Matter* **2011**, *7*, 2720-2724.
49. Yan, Y.; Lan, Y.; de Keizer, A.; Drechsler, M.; Van As, H.; Cohen Stuart, M. A.; Besseling, N. A. M. *Soft Matter* **2010**, *6*, 3244-3248.
50. Bunzli, J. C. G. *Chem. Rev.* **2010**, *110*, 2729-2755.

# Chapter 2

## Complex Coacervate Core Micelles from Iron-based Coordination Polymers

Abstract

Complex coacervate core micelles (C3Ms) from cationic poly (N-methyl-2-vinyl-pyridinium iodide)-*b*-poly (ethylene oxide) ($P2MVP_{41}$-*b*-$PEO_{205}$) and anionic iron coordination polymers are investigated in this chapter. Micelle formation is studied by light scattering for both Fe(II) and Fe(III) containing C3Ms. At the stoichiometric charge ratio, both Fe(II)-C3Ms and Fe(III)-C3Ms are stable for at least one week at room temperature. Excess of iron coordination polymers has almost no effect on the formed Fe(II)-C3Ms and Fe(III)-C3Ms while excess of $P2MVP_{41}$-*b*-$PEO_{205}$ copolymers in the solution can dissociate the formed micelles. Upon increasing salt concentration, the scattering intensity decreases. This decrease is due to both a decrease in the number of micelles (or an increase in CMC) and a decrease in aggregation number. The salt dependence of the CMC and the aggregation number is explained using a scaling argument for C3M formation. Compared to Fe(II)-C3Ms, Fe(III)-C3Ms have a lower CMC and a higher stability against dissociation by added salt.

Slightly modified from publication: Wang, J. Y.; de Keizer, A.; Fokkink, R.; Yan, Y. Cohen Stuart, M. A.; van der Gucht, J. *J. Phys. Chem. B* **2010**, *114*, 8313-8319

## 2.1 Introduction

Complex coacervate core micelles are self-assembled nanoparticles formed by mixing aqueous solutions of a polyion-neutral diblock copolymer and an oppositely charged polyelectrolyte.[1] This class of micelles, also known as "polyion complex micelles" (PIC micelles)[2] or "block ionomer complex micelles" (BICs) ,[3] has attracted increasing attention in recent years, because of their previewed potential as carriers for drugs, enzymes, or DNA.[4-6]

In the past few years, the formation of C3Ms from different components of oppositely charged polyelectrolytes has been investigated systematically.[7-9] It has been found that a minimum length of the charged blocks and stoichiometric charge mixing ratio are required to form C3Ms efficiently.[10,11] Recently, our research group reported on a new kind of C3Ms with metal ions in the core. It consists of a cationic-neutral diblock copolymer ($P2MVP_{41}$-*b*-$PEO_{205}$) and an oppositely charged reversible supramolecular polymer, with a backbone consisting of zinc ions coordinated by ditopic ligands ($L_2EO_4$) based on pyridine-2,6-dicarboxylic acid groups.[12] These bisligands form negatively charged coordination polymers with metal ions, with a distribution that responds to changes in concentration or temperature. At low concentration and at a 1:1 metal to ligand ratio, small rings consisting of only two monomers are predominant in solution.[13] Interestingly, these oligomers could still form C3Ms in the presence of oppositely charged diblock copolymers, indicating that confinement in the micellar core leads to a strong growth of the coordination polymers.[12] Note that C3Ms could only be formed in the presence of all three components ($L_2EO_4$, metal ions, and oppositely charged diblock copolymers); no C3Ms were formed in the absence of metal ions.[12]

The presence of metal ions in the micellar core brings up high electron density which results in a strong contrast between the particle and the environment or background in electron microscopy. This offers a convenient way to study the core structure of these micelles in detail.[14] Moreover, by varying the metal ions in the core, novel properties can be introduced, which may lead to applications in catalysis, magnetic resonance imaging, targeting, and optoelectronic devices.[15,16] Yan et al. have explored various properties of C3Ms containing zinc ions.[12,14,17,18] In this chapter, we focus on iron-containing micelles. We prepare C3Ms containing iron coordination polymers in the core, which are self-assembled from a bisligand ($L_2EO_4$) and $Fe^{2+}$ or $Fe^{3+}$ ions. For convenience, we will call

them Fe(II)-C3Ms and Fe(III)-C3Ms, respectively. Due to the presence of iron in the core, these micelles may have potential for use in MRI and biomedical applications, where they could serve as an alternative for iron oxide particles.[19,20] Recently, the redox responsiveness of such iron-containing micelles was investigated.[21] However, the stability of this kind of micelles has not yet been studied. Here, we compare Fe(II)-C3Ms and Fe(III)-C3Ms: the characteristic differences in formation, stability and salt effect are investigated in detail using light scattering. The effect of salt on C3M formation is interpreted using a simple model for electrostatically-driven micelle formation.

## 2.2 Experimental section

**Materials**

The diblock copolymer used in this study, poly (N-methyl-2-vinyl-pyridinium iodide)-b-poly(ethylene oxide) ($P2MVP_{41}$-*b*-$PEO_{205}$), was obtained by quaternization of poly(2-vinylpyridine)-*b*-poly(ethylene oxide) ($P2VP_{41}$-*b*-$PEO_{205}$) (Polymer Source, $M_w/M_n$= 1.03, $M_w$= 13.3 K) following a procedure described elsewhere.[22] The degree of quaternization is about 90%. The bisligand compound 1,11-bis(2,6-dicarboxypyridin-4-yloxy)-3,6,9-trioxaundecane ($L_2EO_4$) was prepared according to literature.[23] Chemical structures of the polymer and the bisligand are shown in Scheme 2.1. Analytical grade $FeCl_2{\cdot}4H_2O$, $FeCl_3{\cdot}6H_2O$, and $NaNO_3$ were purchased from Aldrich. Acetate buffer was prepared by mixing acetic acid and sodium hydroxide. All stock solutions were made in acetate buffer at pH 5. Fe-$L_2EO_4$ coordination polymers were prepared by mixing solutions of $FeCl_2{\cdot}4H_2O$ or $FeCl_3{\cdot}6H_2O$, and $L_2EO_4$ at a molar ratio 1:1 in 20 mM acetate buffer. Each coordination center has one ($Fe^{3+}$) or two ($Fe^{2+}$) negative charges, as illustrated in Scheme 2.1.

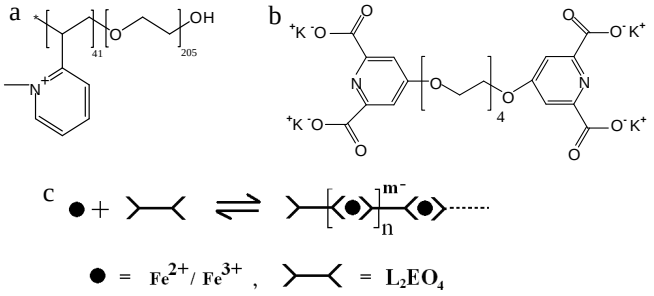


Scheme 2.1 a: Structure of $P2MVP_{41}$-*b*-$PEO_{205}$. b: Structure of $L_2EO_4$. c: Linear coordination complex of Fe(II)-$L_2EO_4$ and Fe(III)-$L_2EO_4$.

**Methods**

Dynamic Light-Scattering (DLS) Titration

Light scattering at an angle of 90 degrees was performed with an ALV light scattering-apparatus, equipped with a 400mW argon ion laser operating at a wavelength of 532.0 nm. All measurements were performed at room temperature. Titrations were carried out using a Schott-Geräte computer-controlled titration setup to control sequential addition of titrant and cell stirring. After every dosage, the laser light-scattering intensity ($I$) and the correlation function were recorded.

The CUMULANT method[24,25] was used to analyze the mean apparent hydrodynamic radius ($R_h$) and the polydispersity index *(PDI)*. $R_h$ is calculated from the average decay rate $\Gamma$ and *PDI* from the second moment $\mu_2$, according to the following formulas:

$$R_h = kTq^2 / 6\pi\eta\Gamma \quad (1)$$

$$PDI = \mu_2 / \Gamma^2 \quad (2)$$

where $q$ is the scattering vector, $k$ is the Boltzmann constant, $T$ is the absolute temperature, and $\eta$ is the viscosity of the solvent. Moreover, the CONTIN method[26,27] is used to analyze the distribution of particle (C3Ms) radius. The data is analyzed with AfterALV program (AfterALV 1.0d, Dullware), which provides $\Gamma_i W_i$ as default output for each size fraction. Here, the intensity weighted contribution $W_i$ is multiplied by Gamma, as suggested by Petr Stepanek for the "equal-area representation".[28] The absolute values of $\Gamma_i W_i$ vary a lot from different samples, which makes it difficult to compare the results directly. Therefore, we normalized $\Gamma_i W_i$ with the highest value of $\Gamma_i W_i$ for each sample, and we call this probability in the CONTIN result.

Static Light Scattering

From the measured scattering intensity we obtain the excess Rayleigh ratio $R_\theta$, using toluene as a reference:

$$R_\theta = \frac{I_{\text{sample}} - I_{\text{solvent}}}{I_{\text{toluene}}} \times R_{\text{toluene}} \times \frac{n^2_{\text{solvent}}}{n^2_{\text{toluene}}} \quad (3)$$

where $I_{sample}$ is the scattering intensity of the micellar solution and $I_{solvent}$ is the intensity of the solvent. $I_{toluene}$ is the scattering intensity of toluene, and $R_{toluene}$ is the known Rayleigh ratio of toluene ($2.1 \cdot 10^{-2}$ $m^{-1}$). The Rayleigh ratio can be linked to the concentration and mass of the scattering objects:

$$R_\theta = K_R C_{particle} M_{particle} P(qR) S(q) \quad (4)$$

where $C_{particle}$ is the weight concentration of micelles, $M_{particle}$ is their molecular mass, $R$ is the radius of the object that contribute to scatter light. For C3Ms, $R$ is closed to the core radius. $P(qR)$ and $S(q)$ are the form factor and the structure factor, respectively. In our experiments, the scattering vector $q = (4\pi n/\lambda_0) sin(\theta/2)$ is approximately 0.023 $nm^{-1}$ ($\theta$=90°), so that $qR$ is small for the micelles (which have a radius on the order of 20 nm). We therefore assume that $P(qR)$=1. We also assume that $S(q)$=1, because all experiments are carried out at low concentrations. $K_R$ is the optical constant defined as:

$$K_R = \frac{4\pi^2 n^2}{N_{Av}\lambda_0^4}\left(\frac{dn}{dc}\right)^2 \quad (5)$$

where $n$ is the refractive index of solvent, $N_{Av}$ is Avogadro's number, $\lambda_0$ is the wavelength of the incoming beam (532 nm), and $dn/dc$ is the refractive index increment of the C3Ms. We measured $dn/dc$ of the micellar solutions using a differential refractive index detector (Shodex RI-71). A value of 0.17 $cm^3/g$ was obtained for the Fe(II)-C3Ms and a value of 0.20 $cm^3/g$ for the Fe(III)-C3Ms.

The hydrodynamic radius and the scattered intensity are studied as a function of the mole fraction of positive charge ratio, $f+$, which is defined as follows:

$$f+ = \frac{[+]}{[-]+[+]} \quad (6)$$

where [-] and [+] are the molar charge concentrations of each polymer chain. The effect of salt on the C3Ms is studied by titrating 0.5 M $NaNO_3$ into the micellar solution.

## 2.3 Results and discussion

### Formation of iron C3Ms

Complex coacervate core micelles are novel nanostructures formed by electrostatically driven assembly of two oppositely charged components. One of them is the polyion-neutral diblock copolymer, which introduces a neutral block serving as the corona to stabilize the coacervate core. In this chapter, iron-based coordination polymers, Fe(II)-$L_2EO_4$ and Fe(III)-$L_2EO_4$, are used as homopolyelectrolytes and mixed with the diblock copolymer $P2MVP_{41}$-*b*-$PEO_{205}$ (Scheme 2.2). The mixing ratio between the metal ions and the ligand $L_2EO_4$ is fixed at 1:1 for all experiments (Scheme 2.1c). As stated above, depending on whether $Fe^{2+}$ or $Fe^{3+}$ is used, the coordination center carries a net -2 or -1

elementary charge for the Fe(II)-$L_2EO_4$ and Fe(III)-$L_2EO_4$ complexes, respectively. This is accounted for in the value of $f$ +. Upon neutralization of the negative charges by the positive charges of the diblock copolymer $P2MVP_{41}$-*b*-$PEO_{205}$, micelles are formed in both the Fe(II) and the Fe(III) systems.

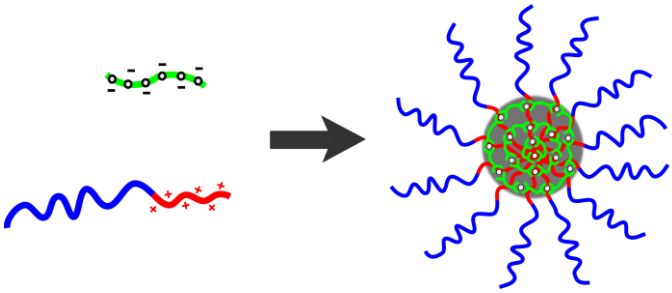

Scheme 2.2 Iron containing C3Ms are obtained by mixing anionic iron coordination polymer Fe-$L_2EO_4$ and cationic-neutral diblock copolymer $P2MVP_{41}$-*b*-$PEO_{205}$. Small circles represent iron ions.

First, we consider the effect of the mixing ratio $f$ +. Figure 2.1a shows the scattered intensity, expressed as the excess Rayleigh ratio of the sample, normalized by the total concentration $C_t$, as a function of the mixing ratio. At $f$ + = 0, the intensity is very low, but it increases immediately after the first addition of $P2MVP_{41}$-*b*-$PEO_{205}$ copolymers to the solution of the iron coordination complexes, indicating the formation of micelles. Upon adding the positively charged $P2MVP_{41}$-*b*-$PEO_{205}$ copolymers step by step, the intensity increases gradually and shows a maximum at $f$ + ≈ 0.5 for Fe(III)-C3Ms and at $f$ + ≈ 0.45 for Fe(II)-C3Ms. These maxima correspond to the preferred micellar composition (PMC) where charge stoichiometry is satisfied. Surprisingly, the scattering intensity of Fe(III)-C3Ms is about 2 times higher than that of Fe(II)-C3Ms, which may be due to a difference in core structure and size between the Fe(III)-C3Ms and Fe(II)-C3Ms, or a difference in CMC. Indeed, it was found previously that the core of Fe(III)-C3Ms is larger and denser than that of Fe(II)-C3Ms: the average radius for the former is about 13 nm and for the latter it is about 10 nm[21]. The refractive index increment of Fe(III)-C3Ms is also slightly larger than that of Fe(II)-C3Ms (see Methods). The small shift of the maximum in the Fe(II) system is probably due to oxidation of $Fe^{2+}$ ions. Since oxidation cannot be avoided completely during the experimental process, some $Fe^{2+}$ (~ 20%) are inevitably oxidized

into $Fe^{3+}$. This means that some of the coordination centers lose one negative charge, which induces a stoichiometry shift to lower *f* + values.

Figure 2.1b shows the hydrodynamic radius and PDI as a function of the positive charge fraction *f* +. The CONTIN method is also used to analyze changes in particle size and polydispersity, as shown in Figure 2.1c for Fe(II)-C3Ms and Figure 1d for Fe(III)-C3Ms. Both Fe(II)-C3Ms and Fe(III)-C3Ms have a constant size and relatively narrow size distribution before the PMC, which means that there is only one dominant kind of particles in solution and the excess of iron coordination polymers has no effect on the formed micelles. Similar results were found for the zinc system.[17,18] This behavior is different from that of C3Ms formed by covalent polyelectrolytes, which can only be formed around the stoichiometric charge ratio.[9,10,29] This difference is probably due to the reversible structure of the coordination complexes. The excess of coordination polymer is present as small rings and oligomers.[12] Apparently, these smaller complexes cannot destroy the formed micelles.

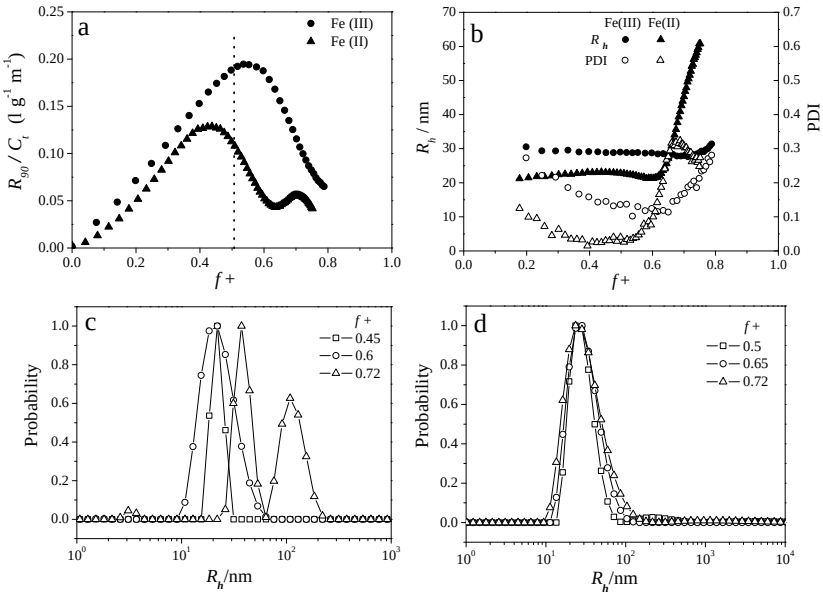


Figure 2.1 Light scattering titration of Fe(II)-$L_2EO_4$ and Fe(III)-$L_2EO_4$ coordination polymers with $P2MVP_{41}$-*b*-$PEO_{205}$ solution. a: The scattering intensity (Rayleigh ratio divided by the total concentration $C_t$) upon adding $P2MVP_{41}$-*b*-$PEO_{205}$ (1.32 g/l) to 0.14 g/l Fe(II)-$L_2EO_4$ solution (triangles) and 0.14 g/l Fe(III)-$L_2EO_4$ solution (circles). b: Changes in hydrodynamic radius and polydispersity index as a function of positive charge fraction *f* +. c, d: CONTIN analysis of Fe(II)-C3Ms (c) and Fe(III)-C3Ms (d) at different *f* +.

However, the situation is different when there is excess P2MVP$_{41}$-*b*-PEO$_{205}$ copolymer in the system. Beyond the PMC, the scattering intensity decreases gradually for both Fe(II)-C3Ms and Fe(III)-C3Ms, indicating that the micelles dissociate at $f_+ > 0.5$ (Figure 2.1a). For Fe(II)-C3Ms, we observe a strong increase in the average hydrodynamic radius of the particles and in their polydispersity (Figure 2.1b), which is due to formation of a small amount of large aggregates. Above $f_+ = 0.6$, large aggregates start to form and coexist with the small micelles in the solution. As a result, the intensity shows a second peak (Figure 2.1a) and CONTIN analysis clearly gives a bimodal distribution (Figure 2.1c). These large clusters, could be wormlike micelles or aggregates of small micelles, similar to the structures obtained in the zinc system for $f_- \leq 0.4$.[18] Such a strong increase in radius and polydispersity is not observed for the Fe(III)-C3Ms (Figure 2.1d).

**Time dependence of formed iron C3Ms**

An important aspect of C3Ms for application is their stability.[11,30] In this chapter, we study the stability of iron C3Ms at stoichiometric charge ratio at long time scale. Fe(III)-C3Ms are prepared at the preferred micellar composition, $f_+ = 0.5$ with a charge concentration [+] = [-] = 1 mM. As shown in Figure 2.2a, the intensity shows a weak minimum and becomes stable after 5 days. The hydrodynamic radius does not vary in time. CONTIN analysis (Figure 2.2c) shows no difference in size and size distribution of Fe(III)-C3Ms between 1h and 8 days. All of these results indicate that at room temperature the formed Fe(III)-C3Ms are very stable in time.

For Fe(II)-C3Ms, the time dependence was measured both at $f_+ = 0.45$, the observed optimal micellar composition, and at $f_+ = 0.5$. Assuming that indeed part of the $Fe^{2+}$ was oxidized to $Fe^{3+}$, the latter composition corresponds to a slight excess of block copolymer. The scattering intensity and hydrodynamic radius as a function of time are presented in Figures 2.2b and the size distributions at different times are presented in Figure 2.2d. At the observed optimal charge ratio, $f_+ = 0.45$, the intensity, hydrodynamic radius, and size distribution of Fe(II)-C3Ms are constant for at least 8 days. However, the size of Fe(II)-C3Ms at $f_+ = 0.5$ increases gradually in time, which is accompanied by an increase of the intensity and a shift of the CONTIN size distribution to larger values. If Fe(II)-C3Ms at $f_+ = 0.5$ are kept under argon atmosphere, a similar increase in intensity and hydrodynamic radius is observed. This means that the increase is not due to further oxidation but a direct result of the excess of diblock polymers in the system.

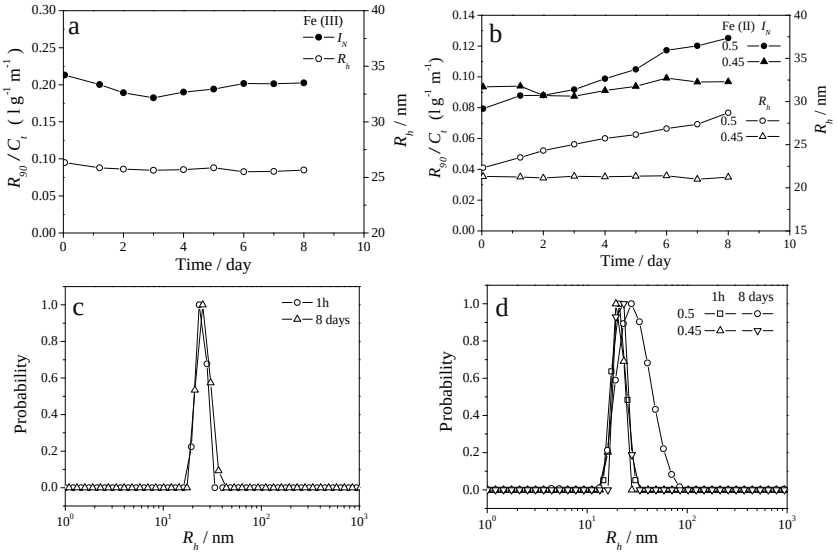


Figure 2.2 Time dependence of formed iron C3Ms. a: Intensity and hydrodynamic radius for Fe(III)-C3Ms as a function of time ($f$ + = 0.5, $C_t$ = 0.72 g/l). b: Variations of the intensity and hydrodynamic radius for Fe(II)-C3Ms at $f$ + = 0.5 ($C_t$ = 0.79 g/l) and $f$ + = 0.45 ($C_t$ = 0.68 g/l). c, d: CONTIN analysis of Fe(III)-C3Ms (c) and Fe(II)-C3Ms (d) after 1h and 8 days.

## Salt effect on iron C3Ms

### *Salt effect on scattering intensity and micellar size*

It is well-known that complex coacervate core micelles are sensitive to ionic strength, and dissociate above a critical salt concentration.[31,32] In Figure 2.3, we present the variation of the scattering intensity with ionic strength for both Fe(II)-C3Ms and Fe(III)-C3Ms at different micellar concentrations.

For both Fe(II)-C3Ms and Fe(III)-C3Ms, the intensity decreases with increasing salt concentration $C_s$, which is the sum of the added $NaNO_3$ concentration and the concentration of the buffer viewed as 1-1 type electrolyte. The scattering intensity levels off at a critical value, which was called the critical salt concentration (CSC) by Kabanov et al..[31] It is clear that this CSC depends not only on the total concentration of the micelles, but also on the nature of the coordination polymer. As shown in Figure 2.3a, Fe(III)-C3Ms at 0.72 g/l dissociate completely around a $C_s$ of 150 mM, while the micelles at 0.36 g/l and 0.18 g/l disintegrate around $C_s$ of 105 mM and 62 mM respectively. For Fe(II)-C3Ms, the CSCs at the same polymer concentrations are lower than those for Fe(III)-C3Ms: 105, 62,

and 40 mM, respectively (Figure 2.3b). This means that the Fe(III)-C3Ms are more stable than Fe(II)-C3Ms against salt, which agrees with our finding above that Fe (III)-C3Ms have a higher scattering intensity, due to a larger and more compact core than that of Fe(II)-C3Ms.

CONTIN analysis in Figure 2.3 (c and d) indicates that both Fe(III)-C3Ms and Fe(II)-C3Ms have a narrow size distribution at low salt concentration. Upon adding more $NaNO_3$ to the micellar solution, the micelles grow gradually and become more polydisperse. A similar salt-induced swelling was observed for various other C3Ms.[33,34] Probably the micelles form loose clusters, which disintegrate completely once the salt concentration exceeds the CSC. Since the driving force for micellization for C3Ms is electrostatic interaction between oppositely charged components, an increase in salt concentration will diminish the driving force for micellization. As discussed below, this affects both the CMC and the aggregation number. Note that addition of salt may also decrease the solubility of PEO in water, favoring formation of large aggregates.[35]

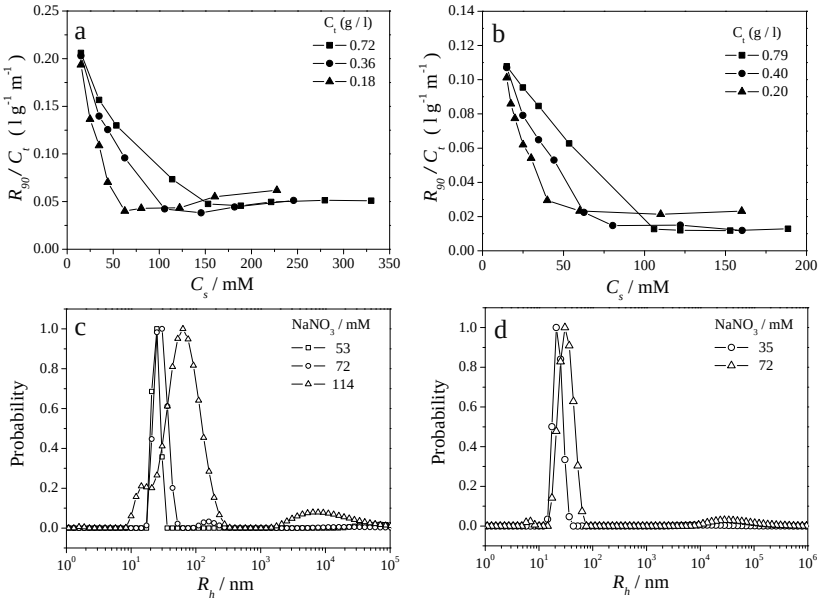


Figure 2.3 Effect of salt on the scattering intensity and micellar size. a, b: Scattering intensity for Fe(III)-C3Ms (a) and Fe(II)-C3Ms (b) at different concentrations with increasing $C_s$. c, d: CONTIN analysis of Fe(III)-C3Ms (c) and Fe(II)-C3Ms (d) at different $C_s$.

***Salt effect on CMC***

Micelle formation generally occurs once the concentration of aggregating monomers exceeds a critical value, the so-called critical micelle concentration, CMC (also called "critical association concentration" (CAC) by some authors). [32,36] It has been reported that the CMC of C3Ms is low and is sensitive to the presence of salt.[33,34] In the present work, the CMC is determined as a function of salt concentration $C_s$ by adding $NaNO_3$ to the iron C3Ms solutions with a given concentration until the micelles completely dissociate.

The CMC of spherical micelles is determined by the strength of the association mechanism. It can be expressed as:

$$CMC = \exp(-\Delta G / RT) \sim \exp(-\chi) \tag{7}$$

where $\Delta G$ is the standard free enthalpy of micellization and $\chi$ is an effective interaction parameter.[37] In case of simple surfactants, $\chi$ is the Flory–Huggins parameter that gives the energy of transfer of a hydrophobic segment from the hydrophobic core to the water phase. In case of C3Ms, the effective interaction is determined by electrostatic interaction. A simple mean-field model for complex coacervation of polyelectrolytes was developed by Voorn and Overbeek,[38] which estimates the total free energy of mixing as a sum of mixing entropy and electrostatic interaction, based on the Flory-Huggins expression and the Debye and Huckel theory respectively. For a stoichiometric charge ratio between the two polyelectrolytes in the presence of monovalent salt, the phase diagram of the complex coacervate can be mapped onto a segregative polymer-solvent mixture, with an effective interaction parameter:[39]

$$\chi_{\text{eff}} = \chi + \frac{2\pi}{3}\frac{l_B^2 \kappa^{-1} \sigma^2}{l^3} \tag{8}$$

where $l_B = e^2/4\pi\varepsilon kT$ is the Bjerrum length, $\sigma$ is the charge density on the polymer, $l$ is the Kuhn length and $\kappa^{-1}$ is the Debye length, which is inversely proportional to the square root of the salt concentration. Combining Eqn.7 and 8, we find the following relation between the CMC and the salt concentration:

$$\ln CMC = a + bC_s^{1/2} \tag{9}$$

where $a$ and $b$ are constants for a given polyelectrolyte pair. In Figure 2.4, we compare this prediction to our experimental data. Both for Fe(II)-C3Ms and Fe(III)-C3Ms, ln *CMC* increases proportionally to the square root of the salt concentration, in good agreement with Eqn.9. By extrapolation to zero salt concentration, we obtain values of CMC ≈ 0.2 g/l

(total polymer concentration) for Fe(II)-C3Ms and CMC ≈ 0.16 g/l for Fe(III)-C3Ms in the absence of salt, which are in the same range as found earlier for zinc C3Ms.[34]

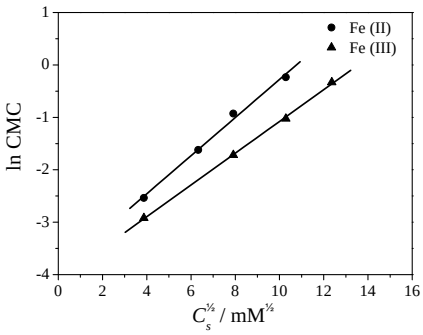


Figure 2.4 Linear relation between ln *CMC* and the square root of salt concentration for both Fe(II)-C3Ms and Fe(III)-C3Ms.

***Salt effect on aggregation number***

The decrease in association strength upon adding salt affects not only the critical micelle concentration, but also the aggregation number $N_{agg}$. This effect can be estimated from our light scattering data. From Eqn.4, we obtain with $P(qR)=S(q)=1$:

$$R_\theta = K_R C_{particle} M_{particle} = K(C_t - CMC) N_{agg}\, m_{bb} \qquad (10)$$

where $m_{bb}$ is the molecular weight of one building block (a pair of oppositely charged block) and the optical constant $K_R$ is given by Eqn.5 with $dn/dc$=0.17 cm$^3$/g for Fe(II)-C3Ms and $dn/dc$=0.20 cm$^3$/g for Fe(III)-C3Ms (see Methods). Above, we have found a relation between the CMC and the salt concentration (Figure 2.4). A fit to Eqn.9 gives ln $CMC = 0.30 C_s^{1/2} - 4.1$ for Fe(III)-C3Ms and ln $CMC = 0.36\, C_s^{1/2} - 3.9$ for Fe(II)-C3Ms. Using these equations, we obtain a rough estimate for the aggregation number $N_{agg}$ from the scattering data in Figures 2.3a and b. The resulting plot in Figure 2.5 suggests that the aggregation number decreases approximately linearly with increasing salt concentration for both Fe(II)-C3Ms and Fe(III)-C3Ms. It seems that Fe(II)-C3Ms have a slightly larger aggregation number than that of Fe(III)-C3Ms.

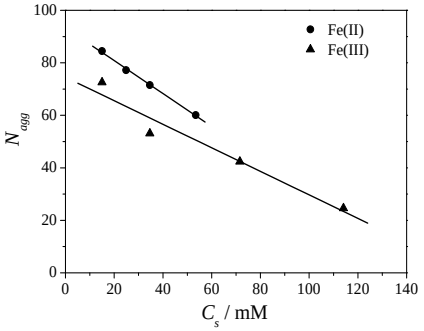


Figure 2.5 The aggregation number as a function of salt concentration. Micellar concentrations are 0.79 g/l for Fe(II)-C3Ms and 0.72 g/l for Fe(III)-C3Ms.

To explain the close-to-linear decrease of the aggregation number with increasing salt concentration, we use a simple scaling argument for micellization. According to Kramarenko et al,[40] the aggregation number of C3Ms depends on the interfacial tension $\gamma$ between the complex coacervate core and the water phase, the length $N$ of the polyelectrolyte blocks, and the volume fraction $\varphi_0$ of polymer inside the core:

$$N_{\text{agg}} \sim \gamma^{6/5} N^{4/5} \varphi_0^{-4/5} \tag{11}$$

The interfacial tension of a collapsed polymer phase is related to its density. Assuming $\gamma \sim \varphi_0^2$,[41] we expect the following relation between the aggregation number and the interfacial tension:

$$N_{\text{agg}} \sim \gamma^{4/5} \tag{12}$$

In the case of a complex coacervate core, the interfacial tension is a function of the salt concentration. Recently, Spruijt et al[42] have found that the interfacial tension of a complex coacervate phase decreases with increasing salt concentration ($C_s$) and vanishes at a critical salt concentration ($C_c$). The following relation was found experimentally:

$$\gamma \sim (C_{\text{c}} - C_{\text{s}})^{3/2} \tag{13}$$

and explained using the theory of Voorn and Overbeek for complex coacervate formation. Combining Eqn.12 and 13, we expect the following relation between the aggregation number and the salt concentration:

$$N_{\text{agg}} \sim (C_{\text{c}} - C_{\text{s}})^{6/5} \tag{14}$$

As $C_c$ is a constant for a given system, this expression predicts that the aggregation number decreases almost linearly with increasing salt concentration, in good agreement with the experimental results in Figure 2.5.

## 2.4 Conclusion

Using light scattering measurements, we have shown that micelles can be formed in aqueous solutions of cationic poly (N-methyl-2-vinyl-pyridinium iodide)-*b*-poly (ethylene oxide) ($P2MVP_{41}$-*b*-$PEO_{205}$) and anionic iron coordination polymers, from both Fe(II)-$L_2EO_4$ and Fe(III)-$L_2EO_4$. Fe(II)-C3Ms and Fe(III)-C3Ms are formed efficiently near charge stoichiometry and are very stable in time at room temperature. Excess of iron coordination polymers ($f$ + < 0.5) has almost no effect on the formed Fe(II)-C3Ms and Fe(III)-C3Ms while excess of $P2MVP_{41}$-*b*-$PEO_{205}$ copolymers in the system ($f$ + > 0.5) leads to a gradual dissociation of the micelles. Both Fe(II)-C3Ms and Fe(III)-C3Ms show the typical salt response: increasing the salt concentration results in an almost linear decrease of the scattering intensity, an increase of the CMC, a linear decrease of the aggregation number, and swelling of micelles followed by full dissociation at the critical salt concentration. Fe(III)-C3Ms are more stable against salt than Fe(II)-C3Ms. In other words, Fe(III)-C3Ms are preferred above Fe(II)-C3Ms due to the high stability, especially, in developing novel properties and potential applications.

## References


1. Cohen Stuart, M. A.; Hofs, B.; Voets, I. K.; de Keizer, A. *Curr. Opin. Colloid Interface Sci.* **2005**, *10*, 30-36.
2. Harada, A.; Kataoka, K. *Science* **1999**, *283*, 65-67.
3. Kabanov, A. V.; Bronich, T. K.; Kabanov, V. A.; Yu, K.; Eisenberg, A. *J. Am. Chem. Soc.* **1998**, *120*, 9941-9942.
4. Kataoka, K.; Harada, A.; Nagasaki, Y. *Adv. Drug Deliv. Rev.* **2001**, *47*, 113-131.
5. Harada, A.; Kataoka, K. *Macromolecules* **1998**, *31*, 288-294.
6. Kabanov, A. V.; Vinogradov, S. V.; Suzdaltseva, Y. G.; Alakhov, V. Y. *Bioconjugate Chem.* **1995**, *6*, 639-643.
7. Voets, I. K.; de Keizer, A.; Cohen Stuart, M. A.; de Waard, P. *Macromolecules* **2006**, *39*, 5952-5955.
8. Voets, I. K.; de Keizer, A.; de Waard, P.; Frederik, P. M.; Bomans, P. H. H.; Schmalz, H.; Walther, A.; King, S. M.; Leermakers, F. A. M.; Cohen Stuart, M. A. *Angew. Chem. Int. Ed.* **2006**, *45*, 6673-6676.

9. Hofs, B.; Voets, I. K.; de Keizer, A.; Cohen Stuart, M. A. *Phys. Chem. Chem. Phys.* **2006**, *8*, 4242-4251.
10. van der Burgh, S.; de Keizer, A.; Cohen Stuart, M. A. *Langmuir* **2004**, *20*, 1073-1084.
11. Stuart, M. A. C.; Besseling, N. A. M.; Fokkink, R. G. *Langmuir* **1998**, *14*, 6846-6846.
12. Yan, Y.; Besseling, N. A. M.; de Keizer, A.; Marcelis, A. T. M.; Drechsler, M.; Cohen Stuart, M. A. *Angew. Chem. Int. Ed.* **2007**, *46*, 1807-1809.
13. Vermonden, T.; van der Gucht, J.; de Waard, P.; Marcelis, A. T. M.; Besseling, N. A. M.; Sudholter, E. J. R.; Fleer, G. J.; Cohen Stuart, M. A. *Macromolecules* **2003**, 36, 7035-7044.
14. Yan, Y.; de Keizer, A.; Cohen Stuart, M. A.; Besseling, N. A. M. *Soft Matter* **2009**, *5*, 790-796.
15. Berret, J. F.; Schonbeck, N.; Gazeau, F.; El Kharrat, D.; Sandre, O.; Vacher, A.; Airiau, M. *J. Am. Chem. Soc.* **2006**, *128*, 1755-1761.
16. Bronstein, L. H.; Sidorov, S. N.; Valetsky, P. M.; Hartmann, J.; Colfen, H.; Antonietti, M. *Langmuir* **1999**, *15*, 6256-6262.
17. Yan, Y.; Besseling, N. A. M.; de Keizer, A.; Cohen Stuart, M. A. *J. Phys. Chem. B* **2007**, *111*, 5811-5818.
18. Yan, Y.; Besseling, N. A. M.; de Keizer, A.; Drechsler, M.; Fokkink, R.; Cohen Stuart, M. A. *J. Phys. Chem. B* **2007**, *111*, 11662-11669.
19. Huber, D. L. *Small* **2005**, *1*, 482-501.
20. Weissleder, R.; Stark, D. D.; Engelstad, B. L.; Bacon, B. R.; Compton, C. C.; White, D. L.; Jacobs, P.; Lewis, J. *American Journal of Roentgenology* **1989**, *152*, 167-173.
21. Yan, Y.; Lan, Y.; de Keizer, A.; Drechsler, M.; Van As, H.; Cohen Stuart, M. A.; Besseling, N. A. M. *Soft Matter* **2010**, *6*, 3244-3248.
22. Biesalski, M.; Johannsmann, D.; Ruhe, J. *J. Chem. Phys.* **2004**, *120*, 8807-8814.
23. Vermonden, T.; Branowska, D.; Marcelis, A. T. M.; Sudholter, E. J. R. *Tetrahedron* **2003**, *59*, 5039-5045.
24. Koppel, D. *J. Chem. Phys.* **1972**, 57, 4814-4820.
25. Berne, B. J.; Percora, R. *Dynamic Light Scattering: with applications to chemistry, biology and physics; 2000*, Dover Publications.
26. Provencher, S. W. *Comp. Phys. Commun.* **1982**, *27*, 213-227.
27. Provencher, S. W. *Comp. Phys. Commun.* **1982**, *27*, 229-242.
28. Stepanek, P. In Dynamic Light Scattering: the method and some applications; Brown, W., Ed.; Clarendon Press: Oxford, U.K., 1993; Chapter 4, p 177-241.
29. Voets, I. K.; van der Burgh, S.; Farago, B.; Fokkink, R.; Kovacevic, D.; Hellweg, T.; de Keizer, A.; Cohen Stuart, M. A. *Macromolecules* **2007**, 40, 8476-8482.
30. Hofs, B.; de Keizer, A.; Cohen Stuart, M. A. *J. Phys. Chem. B* **2007**, *111*, 5621-5627.
31. Kabanov, A. V.; Bronich, T. K.; Kabanov, V. A.; Yu, K.; Eisenberg, A. *Macromolecules* **1996**, *29*, 6797-6802.
32. Yuan, X. F.; Harada, A.; Yamasaki, Y.; Kataoka, K. *Langmuir* **2005**, *21*, 2668-2674.
33. Solomatin, S. V.; Bronich, T. K.; Bargar, T. W.; Eisenberg, A.; Kabanov, V. A.; Kabanov, A. V. *Langmuir* **2003**, *19*, 8069-8076.
34. Yan, Y.; de Keizer, A.; Cohen Stuart, M. A.; Drechsler, M.; Besseling, N. A. M. *J. Phys. Chem. B* **2008**, *112*, 10908-10914.
35. Bailey, F. I. Jr.; Gallard, R. W. *J. Appl. Polym. Sci.* **1959**, *1*, 56-62.

36. Harada, A.; Kataoka, K. *Macromolecules* **2003**, *36*, 4995-5001.
37. Tanford, C. *The Hydrophobic Effect: Formation of Micelles and Biological Membranes* 2nd ed.; Wiley; New York, 1980
38. Overbeek. J. T. G.; Voorn, M. J. *Journal of Cellular and Comparative Physiology* **1957,** *49***,** 7-26.
39. de Vries, R.; Cohen Stuart, M. A. In: *Fundamentals of Interface and Colloid* Science, vol. 5, J. Lyklema ed.; Academic Press London, 1991.
40. Kramarenko, E. Y.; Khokhlov, A. R.; Reineker, P. *J. Chem. Phys.* **2006**, *125*, 194902.
41. Grosberg, A. Y.; Khokhlov, A. R. *Statistical Physics of Macromolecules* AIP, New York, 1994
42. Spruijt. E.; Sprakel, J.; Cohen Stuart, M. A.; van der Gucht, J. *Soft Matter* **2010**, *6*, 172-178.

# Chapter 3

# The Effect of pH on Complex Coacervate Core Micelles from Fe(III)-based Coordination Polymer

Abstract

In this chapter, we study the effect of pH on iron containing complex coacervate core micelles Fe(III)-C3Ms. The Fe(III)-C3Ms are formed by mixing cationic poly (N-methyl-2-vinyl-pyridinium iodide)-*b*-poly (ethylene oxide) ($P2MVP_{41}$-*b*-$PEO_{205}$) and anionic iron coordination polymers [Fe(III)-$L_2EO_4$] at stoichiometric charge ratio. Light scattering and Cryo-TEM have been performed to study the variations of hydrodynamic radius and core structure with changing pH. The hydrodynamic radius of Fe(III)-C3Ms is determined mainly by the corona and does not change very much in a broad pH range. However, Cryo-TEM pictures and magnetic relaxation measurements indicate that the structure of the micellar cores changes upon changing the pH, with a more crystalline, elongated shape and lower relaxivity at high pH. We attribute this to the formation of mixed iron complexes in the core, involving both the bisligand and hydroxide ions. These complexes are stabilized towards precipitation by the diblock copolymer.

Slightly modified from publication: Wang, J. Y.; de Keizer, A.; van Leeuwen, H. P.; Yan, Y.; Vergeldt, F.; van As, H.; Bomans, P. H. H.; Sommerdijk, N. A. J. M.; Cohen Stuart, M. A.; van der Gucht, J. *Langmuir* **2011**, *27*, 14776-14782

## 3.1 Introduction

Complex coacervate core micelles (C3Ms) are novel nanostructures formed by the electrostatically driven assembly of oppositely charged components. Such micelles are also called "polyion complex micelles" (PIC micelles)[1] or "block ionomer complex micelles" (BICs).[2] One of the components must be a polyion-neutral diblock copolymer, ensuring a neutral corona to stabilize the coacervate core. The other component could be oppositely charged homopolymer,[3,4] another polyion-neutral diblock copolymer,[5,6] or reversible coordination polymer.[7] The latter has a backbone consisting of metal ions coordinated by ditopic ligands ($L_2EO_4$) which can form C3Ms with metal ions in the core.[8] The chemical structure of the polymer and the bisligand are shown in Scheme 3.1. Depending on the charge of the metal ions, each coordination center in the polymer carries a net -2 or -1 elementary charge. These negatively charged coordination polymers show a distribution that responds to changes in concentration or temperature. At low concentration and at a 1:1 metal to $L_2EO_4$ ratio, small rings consisting of only two monomers are predominant in solution.[9] Interestingly, these oligomers could still form C3Ms in the presence of oppositely charged diblock copolymers, indicating that confinement in the micellar core leads to a strong growth of the coordination polymers. C3Ms could only be formed in the presence of all three components ($L_2EO_4$, metal ions, and oppositely charged diblock copolymers); no C3Ms were formed in the absence of metal ions.[7]

Iron containing C3Ms (Fe-C3Ms) were studied in chapter 2. Such micelles are of interest, because the paramagnetic properties of the iron nuclei could make them suitable for MRI contrast agents, as an alternative for iron oxide particles. From the application point of view, stability is a very crucial aspect of C3Ms. C3Ms from covalent polyelectrolytes are sensitive to ionic strength and dissociate completely above a critical salt concentration (CSC); in the case of weak polyelectrolytes, the structure and size also depend on the pH.[10-14] For metal containing C3Ms, we have found that they were formed efficiently near charge stoichiometry and were very stable in time. An increase in salt concentration resulted in an increase of the CMC, a decrease in aggregation number, and swelling of the micelles followed by full dissociation at the CSC.[15] However, the effect of pH on this kind of micelles has not been investigated. Since the diblock copolymer $P2MVP_{41}$-*b*-$PEO_{205}$ does not respond to pH, the pH response of the C3Ms is determined completely by the variation of coordination complexes with changing pH. At low pH, the ligand becomes protonated,

destabilizing the coordination polymer. In the case of Fe(III) as metal ion, hydroxide complexes can be formed at high pH, and these may be expected to affect the micellar structure and stability. In this chapter, we focus on the effect of pH on Fe(III)-C3Ms.

## 3.2 Experimental section

### Materials

The diblock copolymer, poly(N-methyl-2-vinyl-pyridinium iodide)-*b*-poly(ethylene oxide) ($P2MVP_{41}$-*b*-$PEO_{205}$), was obtained by quaternization of poly(2-vinylpyridine)-b-poly(ethylene oxide) ($P2VP_{41}$-*b*-$PEO_{205}$) (Polymer Source, $M_w/M_n$= 1.03, $M_w$= 13.3 k) following a procedure described elsewhere.[16] The degree of quaternization is about 90%. The bisligand compound 1,11-bis(2,6-dicarboxypyridin-4-yloxy)-3,6,9-trioxaundecane ($L_2EO_4$) was prepared according to literature.[17] Iron chloride, $FeCl_3{\cdot}6H_2O$ (analytical grade) and sodium nitrate $NaNO_3$ (analytical grade) were purchased from Aldrich and used without further purification. Fe(III)-$L_2EO_4$ coordination polymers were prepared by mixing solutions of $FeCl_3{\cdot}6H_2O$ and $L_2EO_4$ at molar ratio 1:1. The coordination center has one negative charge, as illustrated in Scheme 3.1. All samples were prepared in water with 10 mM NaCl, HCl and NaOH were used to adjust the solution pH.

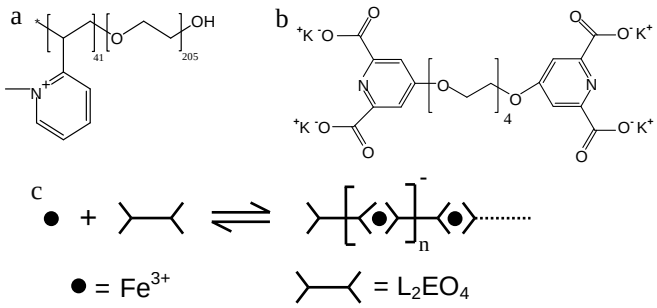


Scheme 3.1 a: Structure of $P2MVP_{41}$-*b*-$PEO_{205}$. b: Structure of $L_2EO_4$. c: Linear structure of coordination complex Fe(III)-$L_2EO_4$.

### Methods

Light Scattering

Light scattering at an angle of 90 degrees was performed with an ALV light scattering-apparatus, equipped with a 400mW argon ion laser operating at a wavelength of 532.0 nm. All the measurements were performed at room temperature.

The light scattering intensity is expressed as the excess Rayleigh ratio $R_\theta$ divided by the total polymer concentration. $R_\theta$ is obtained as

$$R_\theta = \frac{I_{\text{sample}} - I_{\text{solvent}}}{I_{\text{toluene}}} \times R_{\text{toluene}} \times \frac{n^2_{\text{solvent}}}{n^2_{\text{toluene}}} \quad (1)$$

where $I_{\text{sample}}$ is the scattering intensity of the micellar solution and $I_{\text{solvent}}$ is the intensity of the solvent. $I_{\text{toluene}}$ is the scattering intensity of toluene, and $R_{\text{toluene}}$ is the known Rayleigh ratio of toluene ($2.1 \cdot 10^{-2}$ $m^{-1}$). The total polymer concentration is the sum of the concentrations of all components contributing to micelles formation. The CUMULANT method was used to analyze the mean apparent hydrodynamic radius ($R_h$), which is

$$R_h = kTq^2 / 6\pi\eta\Gamma \quad (2)$$

where $q$ is the scattering vector (~ 0.023 $nm^{-1}$ at 90º), $k$ is the Boltzman constant, $T$ is the absolute temperature, $\eta$ is the viscosity of the solvent, and $\Gamma$ is the measured average decay rate of the correlation function. The CONTIN method is used to analyze the distribution of particle (C3Ms) radii.

Cryogenic Transmission Electronic Microscopy (Cryo-TEM)

The TEM-grids were surface plasma treated using a Cressington 208 carbon coater operating at 5 mA for 40 s prior to the sample preparation. A few microliters of sample were placed on a TEM grid and the excess of liquid was removed with filter paper, followed by shooting the grid into liquid ethane cooled to -170 ºC. The sample vitrification procedure was carried out using an automated vitrification robot (FEI Vitrobot Mark III) equipped with humidity and temperature chamber. Samples were studied on a CryoTitan microscope (FEI) equipped with a field emission gun (FEG) operating at 300 kV and a post column Gatan Energy Filter (GIF). Images were recorded using a post-GIF 2k x 2k Gatan CCD camera. For each sample, images were collected for a number of different regions in the sample.

NMR-Relaxation Time Measurement

The longitudinal relaxation times $T_1$ of aqueous solutions of Fe(III)-C3Ms were measured using a Maran Ultra spectrometer (Resonance Instruments, Abingdon, U.K.) operating at 30.9 MHz proton resonance frequency. A combined Inversion Recovery Carr–Purcell–Meiboom–Gill (IR-CPMG) pulse sequence was used to measure $T_1$. Data were analyzed using a home-written IDL program (Research Systems Inc., Boulder, CO, USA) and

expressed as the relaxivity $r_1=[(1/T_1)-(1/T_{1,0})]/C_{Fe(III)}$, with $T_{1,0}$ the relaxation time in pure water.

## 3.3 Results and discussion

### The effect of pH on coordination complex Fe(III)-$L_2EO_4$

Before discussing the effect of pH on the Fe-C3Ms, we first consider the pH dependence of the iron coordination polymer in the absence of the diblock copolymer. The stability of the coordination polymer is determined by the strength of the $FeL_2^-$ complexes (iron ions bound to two ligand groups), as these complexes form the backbone of the coordination polymer (see Scheme 3.1c).

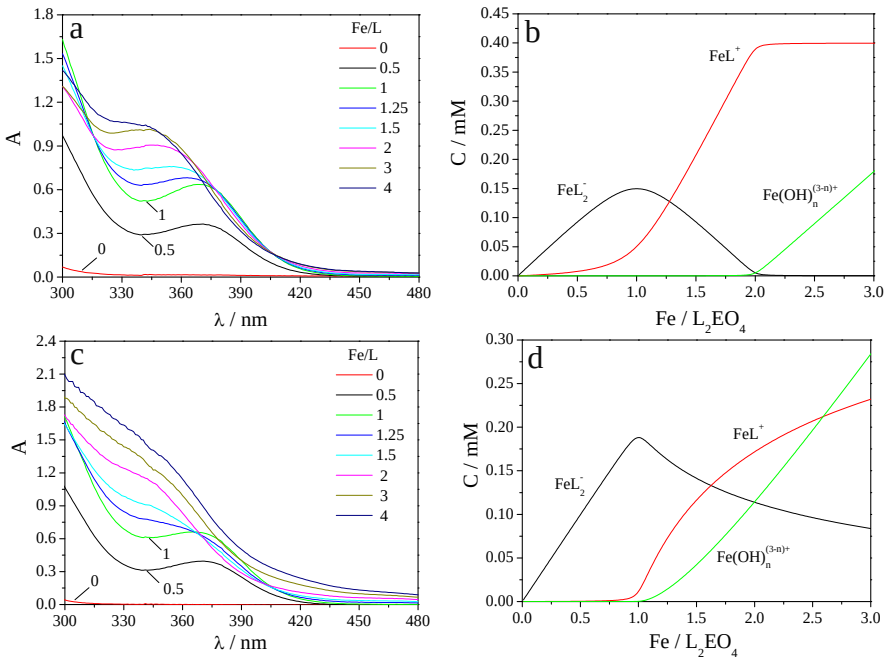


Figure 3.1 UV-vis spectra of titration of $L_2EO_4$ (0.2 mM) solution with $Fe^{3+}$ for different metal to ligand ratios at pH 3 (a) and pH 5 (c). Calculated equilibrium speciation as a function of Fe/L ratio at pH 3 (b) and pH 5 (d). Values for the various equilibrium constants, obtained from literature, are reported in the text. $FeL^+$ is 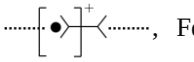 , $FeL_2^-$ represents 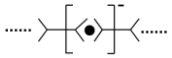 and $Fe(OH)_n^{(3-n)+}$ is the sum of all soluble iron hydroxides ($Fe(OH)^{2+}$, $Fe(OH)_2^+$, $Fe(OH)_3$, $Fe(OH)_4^{-1}$).

The speciation of $Fe^{3+}$ is rather complex and involves, besides the $FeL^+$ and $FeL_2^-$ species, also various hydroxide complexes and mineral phases, depending on the pH. Here we discuss the distribution of the various species in solutions of $Fe^{3+}$ and $L_2EO_4$ by combining UV/vis spectroscopy and equilibrium speciation calculations. Only the $FeL^+$, $FeL_2^-$ and soluble iron hydroxide species are taken into account. All the equilibrium constants are available in literature:[18,19] log $Ka1_{(HL)}$ = 2.1, log $Ka2_{(HL)}$ = 4.383; log $\beta_{(FeL)}$ = 10.91, log $\beta_{(FeL2)}$ = 17.13; $Fe(OH)_n^{(3-n)+}$(aq): log $\beta_{11}$ = 11.81, log $\beta_{12}$= 22.31, log $\beta_{13}$ = 28.91, log $\beta_{14}$ = 34.4.

In figure 3.1a, we show absorbance spectra for solutions at different $Fe/L_2EO_4$ ratios at pH 3, where iron hydroxide complexes are insignificant. In figure 3.1b, we show the expected equilibrium distribution as a function of the metal to ligand ratio calculated using the equilibrium constant listed in the text above. When the ligand is in excess, an absorbance peak is observed around 370 nm. This peak can be attributed to $FeL_2^-$ complexes that form predominantly under these conditions.[20,21] Under excess metal conditions, the peak gradually disappears, while a new peak appears around 350 nm, which is ascribed to the formation of $FeL^+$ complexes, as can be seen from figure 3.1b. We conclude from this that the absorbance peak at 370 nm can be used to identify the presence of $FeL_2^-$ complexes.

Figures 3.1 c and d show the absorbance spectra and calculated species distributions for various $Fe/L_2EO_4$ ratios at pH 5. Under excess ligand conditions, $FeL_2^-$ is still the dominant species as indicated by the absorbance peak. However, in the excess metal regime this peak disappears more rapidly than at pH 3. The speciation diagram suggests that this is related to the formation of iron hydroxide complexes.

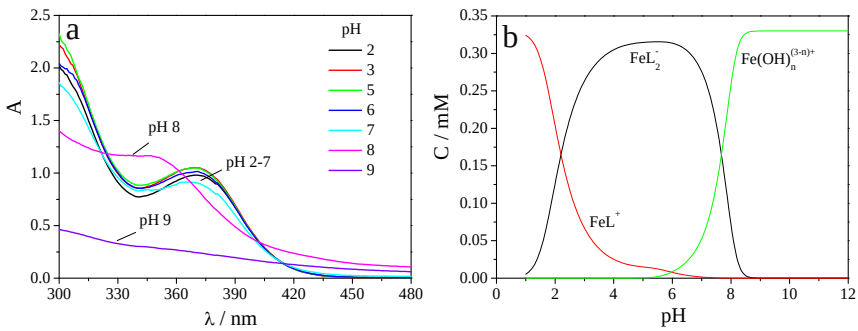


Figure 3.2 UV-vis spectra of Fe(III)-$L_2EO_4$ (1:1) complexes (a) and calculated curve of equilibrium speciation at different pH (b).

Figure 3.2a shows absorbance spectra at a 1:1 Fe(III)/$L_2EO_4$ ratio for different pH and figure 3.2b shows the corresponding species distributions obtained from the equilibrium calculation. $FeL^+$ is dominant in solution when pH < 2, because part of the ligand groups are protonated at low pH, making them less available for complexation with iron. Above this pH, anionic 1:2 complexes $FeL_2^-$ become the main complexes in solution. With further increasing pH, more and more iron hydroxide complexes form, leading to dissociation of the coordination polymer. Indeed, the absorbance peak decreases between pH 6 and 7 and disappears near pH 8. A peak around 350 nm appears at pH 8. However, it can not be due to $FeL^+$ complexes, because their concentration is very low at this high pH (Figure 3.2b). We suppose that it is due to mixed FeLOH complexes, which are not taken into account in the calculations. We can conclude from this that $FeL_2^-$ complexes are the dominant species between pH 2 and 7. Coordination polymers should therefore be stable at 1:1 Fe/$L_2EO_4$ ratio in this pH range.

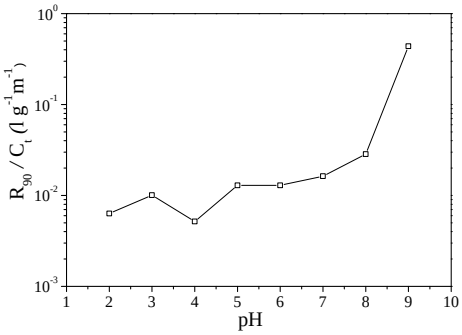


Figure 3.3 Light scattering intensity of Fe(III)-$L_2EO_4$ coordination complexes without diblock copolymer at different pH.

Bombi *et al*[19] have studied iron coordination complexes with the mono-ligand (L), and found a brown precipitate at pH above 5 (depending on metal and ligand concentrations). They attributed this to the formation of insoluble $Fe(OH)_3$. In our system, a brown precipitate can be found above pH 6 only at high ionic strength (1 M NaCl). At lower ionic strength (10 Mm NaCl), the solution of Fe(III)-$L_2EO_4$ is transparent until pH 9. However, light scattering performed at different pH clearly shows that aggregates are formed at pH > 7, as can be seen from an increase in light scattering intensity at low ionic strength (Figure 3.3). These aggregates are probably stabilized against further association by a surface charge leading to repulsion. At pH 9, precipitation occurs already at low ionic strength, and

the scattering intensity increases strongly. In order to characterize the precipitation that was observed after adding salt, we collected the precipitate formed at pH 6 (1M NaCl) and redispersed it in water by decreasing salt concentration. When measuring the absorbance spectrum, we found the characteristic peak at 370 nm, indicating that the precipitate in our system contains $FeL_2^-$ complexes and is not just $Fe(OH)_3$ as found by Bombi *et al*. for iron in the presence of the mono-ligand. We presume that the precipitate contains a mixture of iron complexes involving both ligand groups and hydroxide ions. Mixed complexes, such as FeLOH have indeed been reported.[19] At pH > 8, where the characteristic absorption peak has disappeared, the precipitate is probably dominated by $Fe(OH)_3$. To confirm this, we redissolved the precipitate formed at pH 9 by adding HCl. The resulting solution did not show the absorbance around 370 nm in UV/vis spectrum, showing that there was indeed no ligand in the precipitate.

**The effect of pH on Fe(III)-C3Ms**

We have seen that iron-hydroxide formation leads to disruption of the coordination polymers at pH > 8. Now we investigate what happens if the coordination polymer is confined to the core of a C3M. The formation of Fe(III)-C3Ms has been studied in detail in chapter 2. Micelles in this study are prepared following the same strategy, by mixing cationic-neutral diblock copolymers $P2MVP_{41}$-*b*-$PEO_{205}$ and anionic iron coordination polymers Fe(III)-$L_2EO_4$ at stoichiometric charge ratio.

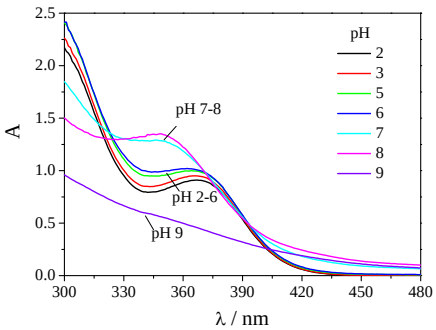


Figure 3.4 UV-vis spectra of Fe(III)-C3Ms at different pH.

To see whether the micellization induced by the diblock copolymer has an effect on the speciation, we show in Figure 3.4 absorbance spectra of Fe(III)-C3Ms at different pH. The characteristic absorption peak for the $FeL_2^-$ complexes can be seen at low pH. However,

compared to coordination complexes without diblock copolymer (Figure 3.2a), the absorbance peak disappears already at pH 7 instead of 8. This means that confinement of the coordination polymer in the core of a micelle facilitates hydroxide formation. This could be due to a locally higher concentration of $FeL_2^-$ complexes in the core. Additionally, the cationic block of the copolymer could locally create a positively charged domain, where the pH is higher than that in the bulk solution. This would cause the disruption of the coordination polymer already at lower bulk pH.

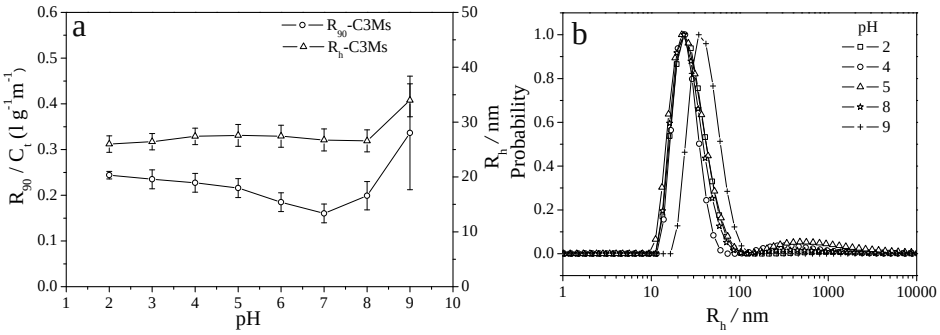


Figure 3.5 a: Variations of light scattering intensity and hydrodynamic radius at different pH. b: CONTIN analysis of particle size and size distribution ($\Gamma$ weighted) at different pH.

Figure 3.5 shows the light scattering data of Fe(III)-C3Ms as a function of pH. Both the light scattering intensity and the hydrodynamic radius obtained from the cumulant analysis do not change very much from pH 2 to pH 8. Larger aggregates form at pH 9, leading to an increase of the light scattering intensity. However, these aggregates are still stable structures. We did not find any brown precipitate even after several weeks in the micellar solution. Hence, the block copolymer stabilizes the iron complexes against continued aggregation. When either the block copolymer or the ligand are left out, a brown precipitation was observed after several hours at pH 9, which means that the ligand and diblock copolymer are both needed to stabilize the structures. CONTIN analysis in Figure 3.5b confirms the result from cumulant analysis. The micellar size and size distribution do not change very much from pH 2 to pH 8. The peak at pH 9 shifts to a bigger size and a broader distribution.

**pH-dependent core structure of Fe(III)-C3Ms**

Cryo-TEM pictures in Figure 3.6 show the micellar core structure at different pH. A striped core structure is observed with different shapes in a broad pH range (4-8). A similar

structure has been found in previous work.[20] At pH 4, the stripes in the core have a length of 20 - 30 nm and a space between them of 1 - 2 nm. This spacing is comparable to the size of the Fe(III)-$L_2EO_4$ complex, which is the dominant coordination complex in the system at this pH, as shown above. We therefore believe that the stripes are formed by aligned coordination polymers, probably associated with the cationic blocks of the diblock copolymer (Scheme 3.2). The neutral corona from the copolymer stops continuous growth and irregular aggregation, leading to mono-dispersed spherical particles. We note that rodlike coordination polymers were observed recently by Kurth et al.[22,23] for solutions containing iron and a rigid bisligand, 1,4-bis(2,2':6',2"-terpyridin-4'-yl)benzene. In our system, the Fe(III)-$L_2EO_4$ complexes do not form rod-like structures in solution due to the flexible EO-linker between the ligand groups. Probably, the diblock copolymer assists by aligning the Fe(III)-$L_2EO_4$ coordination polymer along the charged block by electrostatic coacervation.

Rod-like structures have also been observed for iron hydroxide in the presence of a polymer network.[24,25] However, the absorbance spectra discussed above (Figure 3.2) show that at pH 4 the coordination polymer is the dominant species in the system, while there is very little iron hydroxide. Nevertheless, hydroxide ions probably do play a role, since similar structures were never observed with less acidic metal ions, such as $Zn^{2+}$ and $Nd^{3+}$. Moreover, changing the pH clearly has an effect on the shape of the micellar cores. At low pH (pH 2), where hydroxide ions do not play a role, the regular striped structure in the core is absent and instead irregular aggregates are formed that contain small dark particles. Protonation of the ligands, leading to weakening of the electrostatic interaction, may also disrupt the core structure at low pH. Above pH 4, the striped structures are formed and at higher pH these structures become more asymmetric. The width of the stripe does not change but the length goes up to 25 - 40 nm upon changing pH from 5 to 7, leading to an elongated core shape. At pH 7, some branched or star like shapes appear in solution, which are more numerous at pH 8. The high concentration of hydroxide ions at this pH may induce a multi-directional growth of iron complexes, leading to these special structures. At pH 9, more irregular particles are observed containing small dots, similar to the structures observed at pH 2. From the absorbance spectra, however, we can see that these particles must be very different from the particles observed at pH 9. At this high pH, the coordination polymer is disrupted, so that these particles are probably iron hydroxide particles that are stabilized against precipitation by the diblock copolymer.

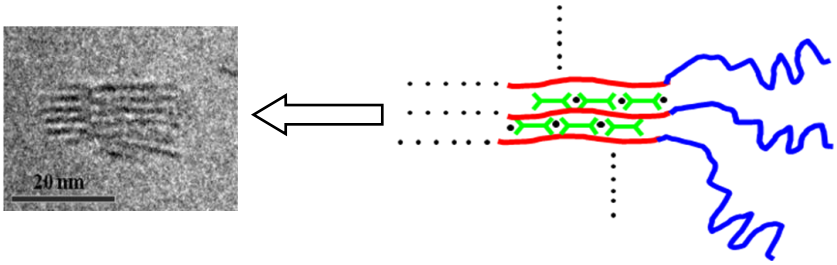


Scheme 3.2 Illustration of the formation of the striped core structure of Fe(III)-C3Ms.

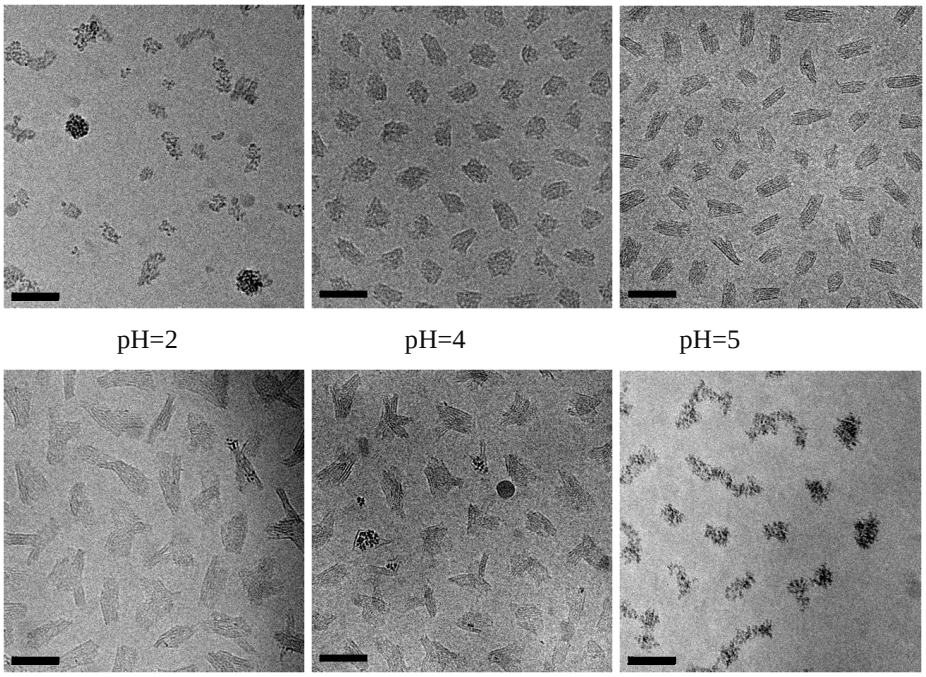


Figure 3.6 Cryo-TEM pictures of Fe(III)-C3Ms at different pH, every bar represents 50 nm.

Although the structure of the core was observed to change between pH 2 and pH 8 from UV/vis spectroscopy and Cryo-TEM images, light scattering did not show any significant changes. This means that the contrast and the mass of the scattering objects hardly changes. Also dynamic light scattering did not show any changes in hydrodynamic radius, probably because this is determined mainly by the large corona. We tried depolarized dynamic light

scattering[26] to check the elongated structure at pH 5, but unfortunately, no significant depolarization signal could be detected due to the small aspect ratio L/d.

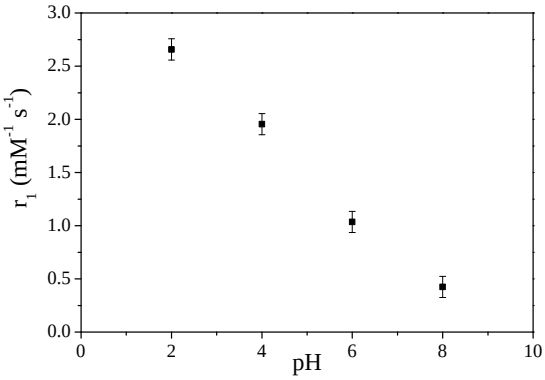


Figure 3.7 The effect of pH on the relaxivity $r_1$ of Fe(III)-C3Ms solution. $r_1$ is the molar longitudinal relaxation rate of water protons in the presence of Fe(III)-C3Ms.

## The effect of pH on NMR relaxivity of Fe(III)-C3Ms

A potential application of the Fe(III)-C3Ms studied in this chapter is as MRI contrast agents. It is therefore important to investigate how the relaxivity depends on the pH. The relaxivity $r_1$ (molar longitudinal relaxation rate) of Fe(III)-C3M solutions is shown as a function of pH in Figure 3.7. We find that the relaxivity $r_1$ is low (1 - 2.5 $mM^{-1}$ $s^{-1}$), which is in the same range as that of Fe-EDTA complexes reported by Bloch *et al.*[27] The relaxivity decreases almost linearly with increasing pH. Above pH 8, the relaxivity of the micellar solution is almost the same as that of pure water. The low relaxivity is due to the strong binding between the ligand and $Fe^{3+}$ ions, which induces a strong crystal field around the metal ions and forces them into a low spin state.[19, 28,29] The strong effect of pH must be due to the binding of hydroxide ions.[30] This is quite surprising as the absorbance spectrum shows that the $FeL_2^-$ complex is the dominating species at pH < 6, suggesting that iron hydroxides do not yet form. A similar decrease of $r_1$ with pH was also observed for Fe(III)-EDTA complexes.[27] It was argued that the iron in this complex is seven-coordinated with a water molecule occupying the seventh coordination site. Deprotonation of this coordinated water molecule leads to a strongly reduced proton exchange rate and thereby to a lower relaxivity. Moreover, dinuclear Fe(III) complexes can be formed at high

pH that are diamagnetic and have almost no effect on proton relaxation[32]. Similar mechanisms could explain the decrease of the relaxivity observed for the Fe(III)-$L_2EO_4$ complexes studied here. Such a pH-dependent iron coordination is also suggested by the changes observed in the core structure of the micelles.

## 3.4 Conclusion

The effect of pH on Fe(III)-C3Ms has been studied by UV-vis spectroscopy, light scattering, Cryo-TEM and magnetic relaxation measurements. The core of the micelles consists of a coacervate of the anionic iron coordination polymer and a cationic polyelectrolyte block, which is stabilized by a neutral corona. The Fe(III)-$L_2EO_4$ complexes in the micellar core form striped structures. The coordination polymer in the micellar core is stable in a broad pH range, from 2 to 7. However, the coordination of the metal does change with pH as observed from a decrease of the proton relaxivity and changes in the internal structure and the shape of the core, which changes from spherical shape (pH 4) to elongated shape (pH 5-7), and a mixture of elongated and branched structures (pH 8). Probably, mixed complexes are formed, in which the iron is coordinated to both the ligand groups and hydroxide ions.

## References


1. Harada, A.; Kataoka, K. *Science* **1999**, *283*, 65-67.
2. Kabanov, A. V.; Bronich, T. K.; Kabanov, V. A.; Yu, K.; Eisenberg, A. *J. Am. Chem. Soc.* **1998**, *120*, 9941-9942.
3. van der Burgh, S.; de Keizer, A.; Cohen Stuart, M. A. *Langmuir* **2004**, *20*, 1073-1084.
4. Kabanov, A. V.; Bronich, T. K.; Kabanov, V. A.; Yu, K.; Eisenberg, A. *Macromolecules*, **1996**, *29*, 6797-6802.
5. Voets, I. K.; de Keizer, A.; de Waard, P.; Frederik, P. M.; Bomans, P. H. H.; Schmalz, H.; Walther, A.; King, S. M.; Leermakers, F. A. M.; Cohen Stuart, M. A. *Angew. Chem. Int. Ed.* **2006**, *45*, 6673-6676.
6. Voets, I. K.; de Keizer, A.; Cohen Stuart, M. A.; de Waard, P. *Macromolecules* **2006**, *39*, 5952-5955.
7. Yan, Y.; Besseling, N. A. M.; de Keizer, A.; Marcelis, A. T. M.; Drechsler, M.; Cohen Stuart, M. A. *Angew. Chem. Int. Ed.* **2007**, *46*, 1807-1809.
8. Yan, Y.; Besseling, N. A. M.; de Keizer, A.; Cohen Stuart, M. A. *J. Phys. Chem. B* **2007**, *111*, 5811-5818.
9. Vermonden, T.; van der Gucht, J.; de Waard, P.; Marcelis, A. T. M.; Besseling, N. A. M.; Sudholter, E. J. R.; Fleer, G. J.; Cohen Stuart, M. A. *Macromolecules* **2003**, 36, 7035-7044.

10. Kabanov, A. V.; Bronich, T. K.; Kabanov, V. A.; Yu, K.; Eisenberg, A. *Macromolecules* **1996**, *29*, 6797-6802.
11. Solomatin, S. V.; Bronich, T. K.; Bargar, T. W.; Eisenberg, A.; Kabanov, V. A.; Kabanov, A. V. *Langmuir* **2003**, *19*, 8069-8076.
12. Gohy, J. F.; Varshney, S. K.; Antoun, S.; Jerome, R. *Macromolecules* **2000**, *33*, 9298-9305.
13. Yuan, X. F.; Harada, A.; Yamasaki, Y.; Kataoka, K. *Langmuir* **2005**, *21*, 2668-2674.
14. Gohy, J. F.; Varshney, S. K.; Jerome, R. *Macromolecules* **2001**, *34*, 3361-3366.
15. Yan, Y.; de Keizer, A.; Cohen Stuart, M. A.; Drechsler, M.; Besseling, N. A. M. *J. Phys. Chem. B* **2008**, *112*, 10908-10914.
16. Biesalski, M.; Johannsmann, D.; Ruhe, J. *J. Chem. Phys.* **2004**, *120*, 8807-8814.
17. Vermonden, T.; Branowska, D.; Marcelis, A. T. M.; Sudholter, E. J. R. *Tetrahedron* **2003**, *59*, 5039-5045.
18. Anderegg, G. *Helv. Chim. Acta* **1960**, *43*, 1530-1545.
19. Bombi, G. G.; Aikebaier R.; Dean, A.; Marco, V. B. D.; Marton, D.; Tapparo, A. *Polyhedron* **2009**, *28*, 327-335.
20. Yan, Y.; Lan, Y.; de Keizer, A.; Drechsler, M.; Van As, H.; Cohen Stuart, M. A.; Besseling, N. A. M. *Soft Matter* **2010**, *6*, 3244-3248.
21. Ding, Y.; Fu, Z. B.; Hu, X. L.; Xia, C. F. *J. Inorg. Organomet. Polym.* **2010**, *20*, 642-648.
22. Schwarz, G.; Bodenthin, Y.; Geue, T.; Koetz, J.; Kurth, D. G. *Macromolecules* **2010**, *43*, 494-500.
23. Meister, A.; Forster, G.; Thunemann, A. F.; Kurth, D. G. *Chem-PhysChem* **2003**, *43*, 1095-1100.
24. Haas, W.; Zrinyi, M.; Kilian, H. G.; Heise, B. *Colloid Polym. Sci.* **1993**, *4*, 1024-1034.
25. Brunner, R.; Gall, S.; Wilke, W.; Zrinyi, M. *Physical A* **1995**, *214*, 153-161.
26. Lehner, D.; Lindner, H.; Glatter, O. *Langmuir* **2000**, *16*, 1689-1695.
27. Bloch, J.; Navon, G. *J. Inorg. Nucl. Chem.* **1979**, *42*, 693-699.
28. Bodenthin,Y.; Pietsch,U.; Mohwald, H.; Kurth, D. G. *J. Am. Chem. Soc.* **2005**, *127*, 3110-3114.
29. Bodenthin, Y.; Schwarz, G.; Tomkowicz, Z.; Geue, T.; Haase, W.; Pietsch, U.; Kurth, D. G. *J. Am. Chem. Soc.* **2009**, *131*, 2934-2941.
30. Koenig, S. H.; Baglin, C. M.; Brown III, R. D. *Magn. Reson. Med.* **1985**, *2*, 283-288.
31. Schugar, H. J.; Rossman, G. R.; Barraclough, C. G.; Gray, H. B. *J. Am. Chem. Soc.* **1972**, *94*, 2683-2690.

# Chapter 4

## Stable Polymer Micelles Formed by Metal Coordination

Abstract

In this chapter, we develop a method to prepare stable metal-containing polymer micelles. A diblock copolymer poly(4-vinylpyridine)-*b*-poly(ethylene oxide) ($P4VP_{48}$-*b*-$PEO_{193}$) with terdentate ligand groups grafted to the PVP block is synthesized. Added metal ions cross-link the ligand-carrying blocks together, while the hydrophilic block stabilizes the formed coordination complex, leading to the formation of micelles. The structure and stability of the formed micelles are investigated by light scattering and Cryo-TEM. The strong coordination bonds provide high stability of the micelles: adding salt or EDTA hardly affects the formed micelles.

Slightly modified from publication: Wang, J. Y.; Cohen Stuart, M. A.; Marcelis, A. T. M.; Colomb-Delsuc, M.; Otto, S.; van der Gucht, J. *Macromolecules* **2012**, *45*, 7179-7185

## 4.1 Introduction

Self-assembly based on coordination interaction is a very promising strategy for the preparation of organic-inorganic hybrid functional materials.[1-3] Metal-ligand coordination bonds have been used to build supramolecular polymers, micelles, vesicles, dendrimers and cross-linked hydrogels.[4-6] In particular, metal-containing polymer micelles have attracted much attention because of their potential for medical or nanotechnological applications. In recent years, ingenious strategies have been developed to make such metal containing polymer micelles. In most cases, a hydrophobic polymer is modified with a ligand group at one side of the chain. The hydrophobic parts form the micellar core, while the hydrophilic ligand groups and the coordinated metal ions are exposed to the aqueous solution.[7-9] These micelles are stabilized by the net charge of the metal-ligand complexes, which makes them rather sensitive to added salt. Schubert and coworkers have used diblock copolymers in which a hydrophilic and a hydrophobic polymer were connected by a metal coordination complex to make micelles or vesicles.[10-12] A similar strategy was followed by other groups.[13-15] More recently, Yan *et al.* reported a novel type of self-assembled metal-containing micelles,[16] based on the electrostatic interaction between a polycationic-neutral diblock copolymer and an anionic reversible coordination polymer consisting of metal ions coordinated by a ditopic ligand. Such metal-containing complex coacervate micelles can accommodate a large number of metal ions in the micellar core. However, the electrostatic driving force limits their stability at high ionic strength: typically they dissociate around 200 mM salt.[17] In these examples, micellization is driven by either hydrophobic or ionic interactions; the metal-ligand coordination is just an assistant driving force. As an alternative strategy, the coordination interaction can also act as the direct driving force for micellization. To achieve this, a diblock copolymer consisting of a neutral hydrophilic block and a block with ligand groups is required. Added metal ions cross-link the ligand-carrying blocks together, and the formed complex is stabilized by the hydrophilic block, leading to the formation of micelles. Indeed, diblock copolymers with carboxylic groups or pyridine groups in one of the blocks were reported to form micelles with $Ca^{2+}$ and $Pt^{2+}$ metal ions.[18-20] However, both carboxylic and pyridine groups are monodentate ligands and only give weak coordination bonds. Here, we develop a diblock copolymer where one block carries terdendate ligand groups, which provide strong coordination bonds for micellization. The metal binding constants of the ligand groups used here are about a factor

of $10^5$ larger than those of pyridine or carboxylic acid groups.[21-23] The formed micelles are therefore expected to be much more stable than micelles based on either electrostatic interaction or weak coordination.

## 4.2 Experimental section

### Materials

4-Hydroxypyridine-2,6-dicarboxylic acid (chelidamic acid) and 1,2-dibromoethane are obtained from Aldrich and used without further purification. The diblock copolymer, poly(4-vinylpyridine)-*b*-poly(ethylene oxide) ($P4VP_{48}$-*b*-$PEO_{193}$, $M_w/M_n$= 1.10, $M_n$= 13.5 k) is purchased from Polymer Source. All stock solutions are prepared in MES (2-(*N*-morpholino) ethanesulfonic acid) buffer (20 mM, pH 6) with 0.1 M NaCl. The Zn containing micelles are made by direct mixing the aqueous solutions of modified polymer and $Zn(NO_4)_2 \cdot 4H_2O$ (analytical grade).

**Synthesis and characterization of the modified diblock copolymer**

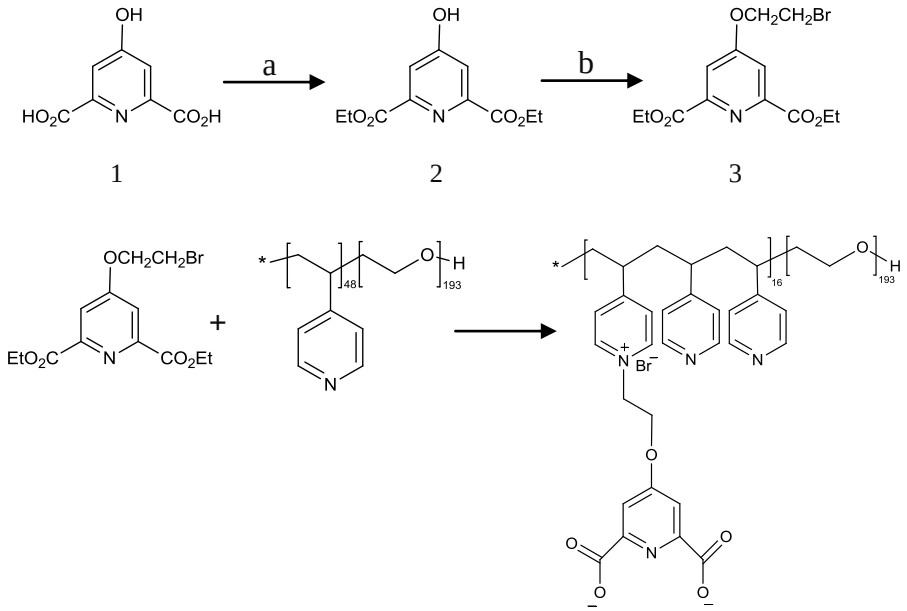


Synthesis of the chelidamic acid derivatives and modification of the diblock copolymer $P4MVP_{48}$-*b*-$PEO_{193}$. (a): $SOCl_2$, $CH_3CH_2OH$, 80℃, reflux 20 h, (67%); (b): $BrCH_2CH_2Br$, $CH_3CN$, 80℃ (76%).

4-Hydroxypyridine-2,6-dicarboxylic acid (chelidamic acid, 1) is esterified with ethanol to diethyl 4-hydroxypyridine-2,6-dicarboxylate (2).[24] Diethyl 4-(2-bromoethoxy)pyridine-2,6-dicarboxylate (3) is then synthesized following a published procedure.[25] The modification of the diblock copolymer $P4VP_{48}$-*b*-$PEO_{193}$ is carried out as follows: Diethyl 4-(2-bromoethoxy)pyridine-2,6-dicarboxylate (5.35 g, 15.5 mmol) and $P4VP_{48}$-*b*-$PEO_{193}$ polymer (1.0 g, 3.5 mmol pyridine groups) were dissolved in 60 ml methanol. The solution was heated at 60℃ and refluxed for 3 days under $N_2$ atmosphere. The methanol was evaporated afterwards and 5 g $K_2CO_3$ and 90 ml $H_2O$ were then added to the residual powder and the mixture was stirred at 70℃ for 24 h. The resulting solution was transferred to a dialysis tube and dialyzed against water for one week to remove all low molecular mass molecules. After the dialysis, the solution was filtrated (450 nm filter) and concentrated to a viscous phase, followed by freeze-drying from water to provide a brown product 4 (1.0 g). The structure of the modified polymer was confirmed by $^1$H NRM and $^{13}$C NMR spectra and FT-IR. The degree of quaternization of the pyridine groups on the side chain was about 34% as determined from UV-vis titration.

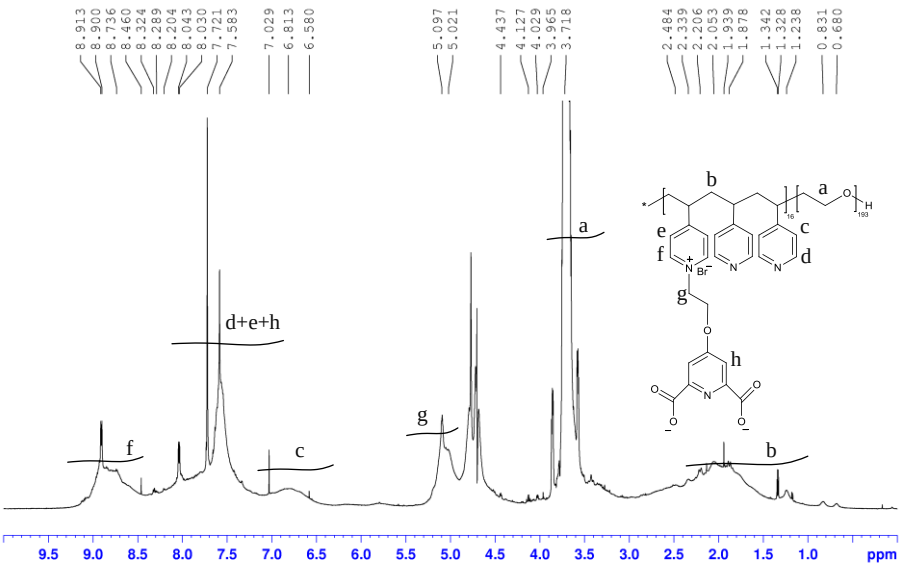


$^1$H-NMR spectrum of the modified polymer. Polymer was dissolved in $D_2O$ and measured at 298 K on Bruker AMX-500 spectrometer (500 MHz).

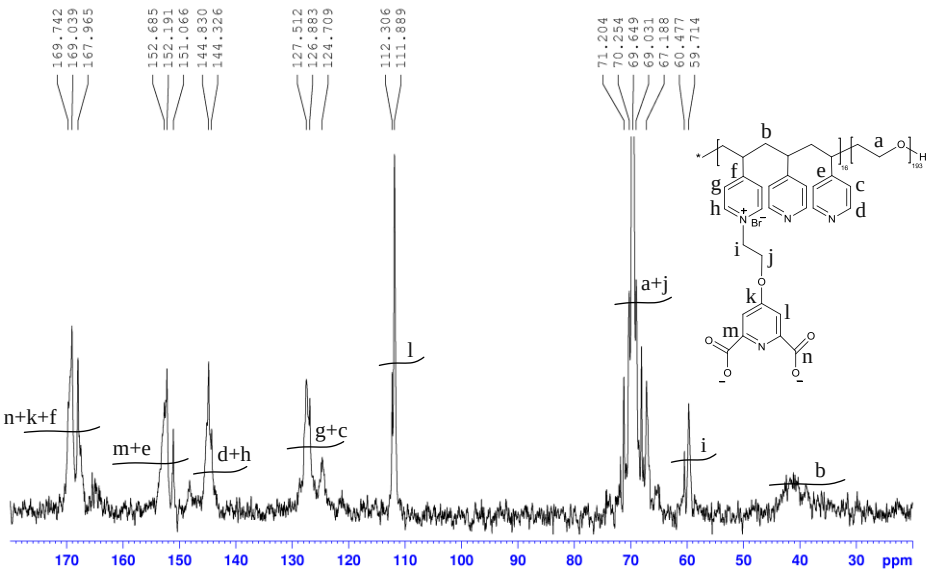


$^{13}$C-NMR spectrum of the modified polymer.

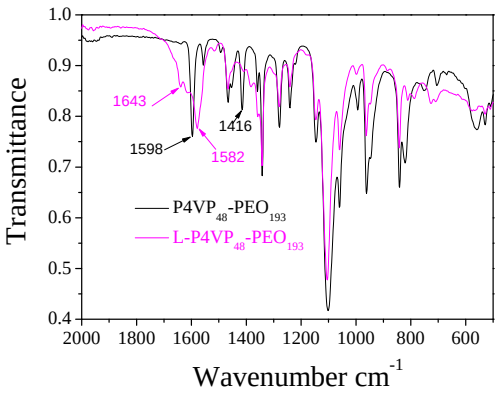


FT-IR spectra were recorded with a Bruker Tensor 27 spectrophotometer operated with Bruker's OPUS software. The quaternization is confirmed by the decay of the peaks at 1416 cm$^{-1}$ and 1598 cm$^{-1}$ (pyridine ring) and the appearance of new peaks at 1643 cm$^{-1}$ and 1582 cm$^{-1}$ (pyridinium group).[26, 27]

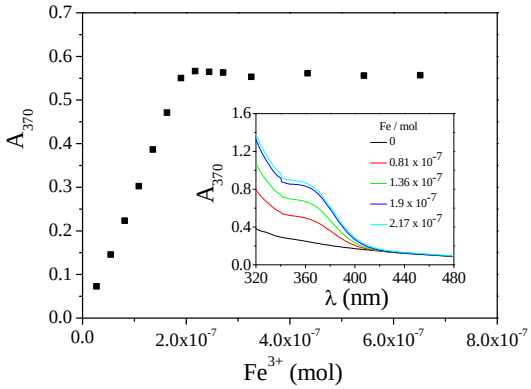


Fe(III)-ligand coordination complexes formed at M/L ratio of 1/2 (one iron binds with two ligand groups) show a typical absorbance at 370 nm in UV-vis spectroscopy.[28] By titrating the polymer solution (0.505 g/l, 0.8 ml, pH 3, 0.8 M NaCl) with $Fe^{3+}$, we find that the solution contains $3.9\times10^{-7}$ mol ligand groups, from which we find that the molecular weight $M_n$ of the polymer is 17.23 k and the degree of the quaternization is about 34%.

## Methods

### Light Scattering

Light scattering at an angle of 90 degrees was performed with an ALV light scattering-apparatus, equipped with a 400 mW argon ion laser operating at a wavelength of 532.0 nm. All the measurements were performed at room temperature. The light scattering intensity is expressed as the excess Rayleigh ratio $R_\theta$ divided by the polymer concentration. $R_\theta$ is obtained as

$$R_\theta = \frac{I_{\text{sample}} - I_{\text{solvent}}}{I_{\text{toluene}}} \times R_{\text{toluene}} \times \frac{n^2_{\text{solvent}}}{n^2_{\text{toluene}}} \tag{1}$$

where $I_{\text{sample}}$ is the scattering intensity of the micellar solution and $I_{\text{solvent}}$ is the intensity of the solvent. $I_{\text{toluene}}$ is the scattering intensity of toluene, and $R_{\text{toluene}}$ is the known Rayleigh ratio of toluene ($2.1 \cdot 10^{-2}$ $m^{-1}$). The CUMULANT method was used to analyze the mean apparent hydrodynamic radius ($R_h$), which is

$$R_h = kTq^2 / 6\pi\eta\Gamma \tag{2}$$

where $q$ is scattering vector, $k$ is the Boltzman constant, $T$ is the absolute temperature, $\eta$ is the viscosity of the solvent, and $\Gamma$ is the measured average decay rate of the correlation function. The CONTIN method is used to analyze the distribution of particle radius.

The Rayleigh ratio can be linked to the concentration and mass of the scattering objects:

$$\frac{K_R C}{R_\theta} = \frac{1}{M} \times \frac{1}{P(qR)} \times \frac{1}{S(q)} \tag{3}$$

where $C$ is the weight concentration of micelles, $M$ is their molecular mass and $R$ is the radius of the object that contribute to scatter light. $P(qR)$ and $S(q)$ are the form factor and the structure factor, respectively. $K_R$ is an optical constant defined as:

$$K_R = \frac{4\pi^2 n^2}{N_{Av}\lambda_0^4}\left(\frac{dn}{dc}\right)^2 \tag{4}$$

where $n$ is the refractive index of solvent, $N_{Av}$ is Avogadro's number, $\lambda_0$ is the wavelength of the incoming beam (532.0 nm), and $dn/dc$ is the refractive index increment of the Zn-L-P4VP$_{48}$-*b*-PEO$_{193}$ micelles. We measured $dn/dc$ of the micellar solutions using a differential refractive index detector (Shodex RI-71).

In our experiments, the scattering vector $q = (4\pi n/\lambda_0)sin(\theta/2)$ is approximately 0.023 nm$^{-1}$ ($\theta$=90°), so that $qR$ is small for the micelles (which have a radius on the order of 15 nm). We therefore assume that $P(qR)$=1. At low concentrations, the structure factor can be approximated as

$$\frac{1}{S(q)} = 1 + 2B_2\frac{C}{M} \tag{5}$$

Substitution into equation 3, we get

$$\frac{K_R C}{R_\theta} = \frac{1}{M} + 2B_2\frac{C}{M^2} \tag{6}$$

By plotting $K_R C/R_\theta$ versus C, we can obtain the molar mass of the micelles from the intercept, from which we can obtain the aggregation number of the micelles. The second virial coefficient $B_2$ obtained from the slope of the curve is used to calculate the effective excluded volume ($V_{eff}$) and radius ($R_{eff}$): $B_2 = \frac{1}{2}N_{AV}V_{eff}$ , $V_{eff} = \frac{4}{3}\pi R_{eff}^3$

Cryogenic Transmission Electronic Microscopy (Cryo-TEM)

A few microliters of sample were placed on a Quantifoil 3.5/1 holey carbon coated grid and the excess of liquid was removed with filter paper, followed by shooting the grid into

liquid ethane cooled to -170 ºC. The sample vitrification procedure was carried out using Vitrobot (FEI, Eindhoven, The Netherlands) equipped with humidity and temperature chamber. Samples were studied in a Philips CM12 Cryo-electron microscope operating at 120 kV with a Gatan model 626 cryo-stage. Images were recorded under low-dose conditions with a slow-scan CCD camera (Gatan, model 794). For each sample, images were collected for a number of different regions in the sample.

## 4.3 Results and discussion

The terdentate ligand group chosen in this work is chelidamic acid (also known as dipicolinic acid), a widely studied chelate group for building coordination structures.[29] NMR and FT-IR spectra confirm that the ligand groups are attached on the PVP block successfully. The degree of quaternization of pyridine groups is determined by a UV-vis titration with $Fe^{3+}$ and was found to be around 34 %.

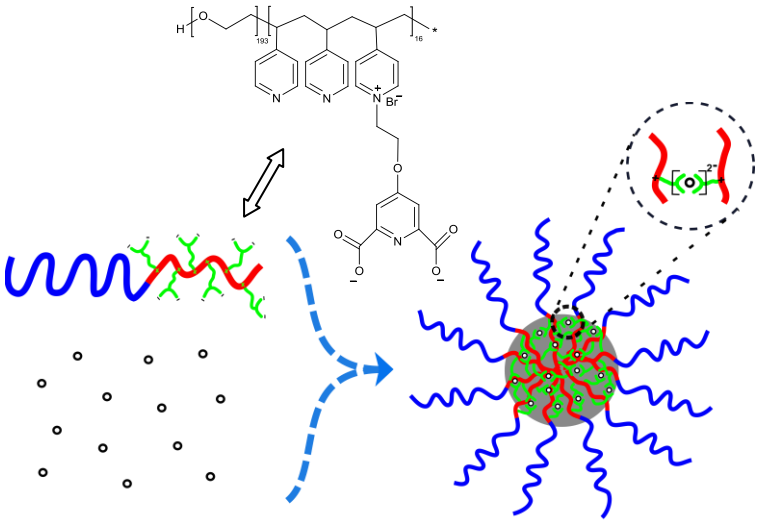

Scheme 4.1 Structure of L-P4VP$_{48}$-*b*-PEO$_{193}$ polymers (top) and illustration of the formation of Zn-L-P4VP$_{48}$-*b*-PEO$_{193}$ micelles (bottom). Small dots represent the $Zn^{2+}$ ions.

As shown in Scheme 4.1, the modified copolymer L-P4VP$_{48}$-*b*-PEO$_{193}$ has both positive charge on the quaternized pyridinium group and negative charges on the carboxylic groups. Hence, we first studied the self-assembly of this diblock copolymer as a function of pH in the absence of metal ions. The L-P4VP$_{48}$-*b*-PEO$_{193}$ becomes soluble in water above pH 6

(Figure 4.1a), where most of the carboxylic groups dissociate and the net charge of the polymer is negative. Decreasing the pH below 6 leads to the partial protonation of the carboxylic groups and a decrease of the overall net charge of the polymer. We find that the diblock copolymers start to aggregate below pH 6, initially forming nanoparticles with a hydrodynamic radius around 90 nm. These particles are not stable and a precipitate is formed after a few hours. However, the white precipitation can be dissolved completely by adding salt (Figure 4.1b). This strongly suggests that the aggregates are formed by electrostatic interaction between the positive charges on the pyridinium group and the negative charges of the carboxylic group. The pH-dependent aggregation behavior of L-P4VP$_{48}$-*b*-PEO$_{193}$ is completely different from that of unmodified P4VP$_{48}$-*b*-PEO$_{193}$ copolymer. The latter is soluble in water at low pH (< 5) and forms micelles above pH 5, based on hydrophobic interaction between the PVP blocks.[30] The light scattering intensity in Figure 4.1a shows a maximum around pH 4, which is likely to be the isoelectric point of L-P4VP$_{48}$-*b*-PEO$_{193}$. Below pH 4, also the second carboxylic group of the ligand becomes protonated and the polymer acquires an overall positive charge, leading to the redissolution of the polymer.

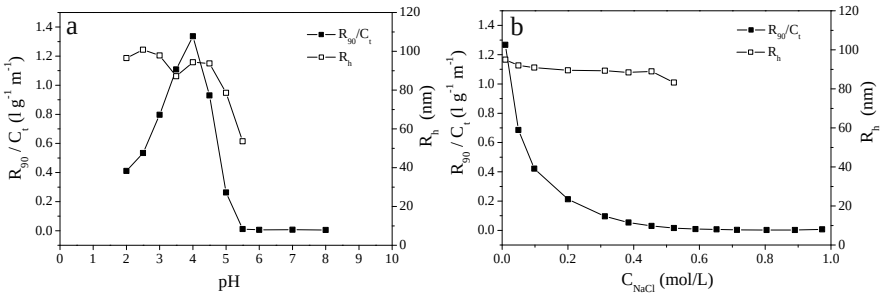


Figure 4.1 a: Light scattering intensity (expressed by the excess Rayleigh ratio $R_{90}$ divided by the total polymer concentration) and hydrodynamic radius of aggregates from L-P4VP$_{48}$-*b*-PEO$_{193}$ polymers in the absence of metal salt at different pH (0.64 g/l polymer). b: The effect of salt on the intensity and size of aggregates from L-P4VP$_{48}$-*b*-PEO$_{193}$ formed at pH 4.

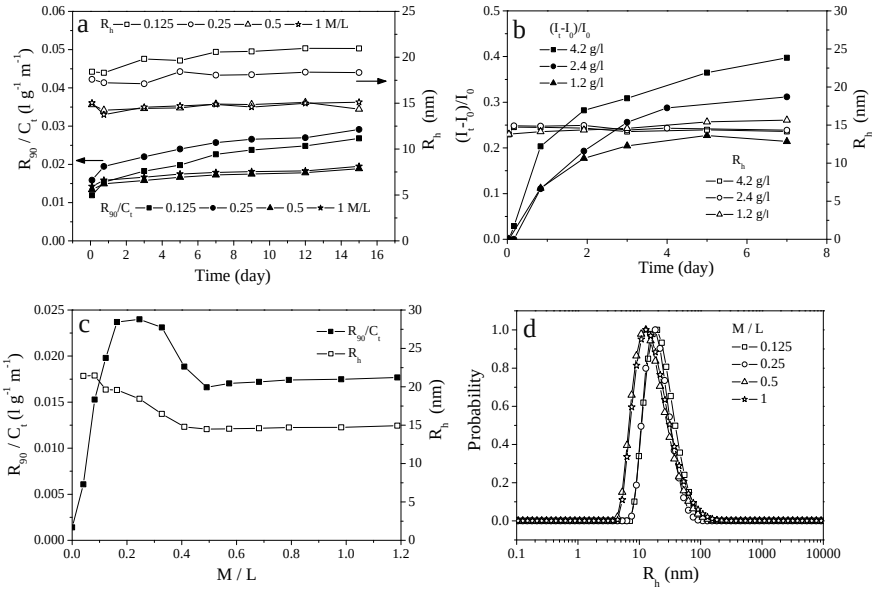


Figure 4.2 a, b: Variations of light scattering intensity and hydrodynamic radius of Zn-L-P4VP$_{48}$-*b*-PEO$_{193}$ micelles formed at different M/L ratios (a) and different polymer concentrations (b). c: Light scattering intensity and hydrodynamic radius as a function of the M/L ratio. d: CONTIN analysis of particle size and size distribution of Zn-L-P4VP$_{48}$-*b*-PEO$_{193}$ micelles formed at different M/L ratios (measured after 5 days). For a, c, d, polymer concentration is fixed at 1.2 g/l.

To study micelle formation with metal ions ($Zn^{2+}$, added in the form of a $Zn(NO_3)_2$ solution), we choose conditions (pH 6, 0.1 M NaCl) where the L-P4VP$_{48}$-*b*-PEO$_{193}$ polymer dissolves completely, so that any aggregate formation can be ascribed to the action of the metal ions. Indeed, the scattering intensity of the L-P4VP$_{48}$-*b*-PEO$_{193}$ solution in the absence of metal salt is very low, but it increases strongly when $Zn^{2+}$ is added to the solution. Figure 4.2a shows the light scattering intensity and hydrodynamic radius of Zn-L-P4VP$_{48}$-*b*-PEO$_{193}$ micelles formed at different metal ion to ligand ratios M/L as a function of time. While the size of the scattering objects remains more or less constant in time, the intensity first increases rapidly, followed by a more gradual increase over several days. To explain this, we hypothesize that upon adding $Zn^{2+}$ to the block copolymer solution, we do not only obtain micellar aggregates, but also smaller intramolecular complexes, where one $Zn^{2+}$ ion binds with two ligands from the same polymer chain. The latter do not contribute much to the scattering intensity compared to the micelles. Our

observation that the intensity keeps increasing slowly after the initial rapid increase must then imply that some of the intramolecular complexes convert into intermolecular complexes to form more micelles. Apparently, there is an energy barrier associated with this reorganization, which makes further aggregation a slow process, leading to a slow increase of the intensity. This two-step scenario must imply that intermolecular complexes are more favorable than intramolecular complexes. Probably, the polymer chain must bend or twist slightly in order to form an intramolecular complex, leading to a strained or low entropy conformation. This strain is released when intermolecular complexes are formed. To test this two-step hypothesis, we measured the increase of light scattering intensity of Zn-L-P4VP$_{48}$-*b*-PEO$_{193}$ micelles at different polymer concentrations with M/L fixed at 0.5. Both the probabilities of inter- and intramolecular complex formation and the rate of reorganization should depend on the polymer concentration, so we expect a faster increase of the micelle formation at higher polymer concentration. As shown in Figure 4.2b, the intensity of micelles at higher polymer concentration indeed shows a faster increase than that of micelles at lower polymer concentration, while the micelle size at all polymer concentrations hardly changes over time.

Figure 4.2c shows the light scattering intensity and hydrodynamic radius of Zn-L-P4VP$_{48}$-*b*-PEO$_{193}$ micelles as a function of the ratio between metal ion and ligand group concentration, M/L. All data points in this figure correspond to the light scattering intensity after an equilibration time of 5 days after mixing the components directly at the desired ratio. Surprisingly, the intensity varies non-monotonically with M/L ratio. Around M/L equal to 0.3, the intensity goes through a maximum and then decreases until it reaches a constant value around M/L 0.5, where every $Zn^{2+}$ ion can coordinate two ligand groups. Adding more metal ions (up to a ratio M/L of 1.2) does not lead to a decrease in intensity, indicating that an excess of $Zn^{2+}$ ions does not disrupt the formed micelles. The hydrodynamic radius decreases monotonically from 21 nm at M/L 0.1 to 15 nm at M/L 0.5 and then becomes constant for M/L > 0.5. However, additional experiments indicate that the micellar objects are not equilibrium structures, even after several days. Adding additional $Zn^{2+}$ to a one-day old micelle solution prepared at M/L 0.25 did not lead to a decrease in size. Likewise, adding additional polymer to a solution prepared initially at M/L 0.5 did not give the same size as for a solution which is prepared directly at M/L 0.25. This means that the coordination interaction is quite strong in this system and the formed micelles are non-equilibrium structures. The CONTIN results (Figure 4.2d) confirm the

micellar size and indicate that there is one dominant kind of particle in solution at all M/L ratios. We also characterized the micelles with Cryo-TEM. As shown in Figure 4.3, at M/L=0.25, we see objects with radii of 5 - 10 nm. We presume that these structures are the micellar cores, where the metal ions reside. The corona of the PEO blocks provides insufficient contrast to be visible. Comparing the size of the core to the hydrodynamic radius (20 nm at this ratio), we find that the corona has a thickness around 10 nm, in agreement with values found for other micelles.[16] At M/L ratios of 0.5 and 1 the micellar core is smaller, around 3 - 6 nm. Hence, the decrease in light scattering intensity and hydrodynamic radius seem to be caused by a decrease in size of the core.

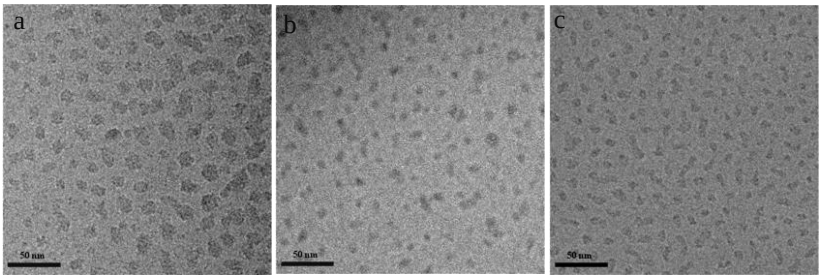


Figure 4.3 Cryo-TEM images of Zn-L-P4VP$_{48}$-*b*-PEO$_{193}$ micelles at different M/L a: 0.25; b: 0.5; c: 1 (polymer concentration is fixed at 2.53 g/l, MES buffer, pH 6, 0.1 M NaCl, measured after 5 days).

What causes this decrease in core size upon increasing the metal concentration? One possible explanation is the repulsion between the un-occupied ligands. When a $Zn^{2+}$ ion binds to two ligand groups, the overall charge of the L-Zn-L complex is -2, which just compensates the two positive charges of the pyridine groups to which the ligands are attached (see Scheme 4.1). This means that at a M/L ratio of 0.5, where all the ligand groups are involved in a L-M-L complex, the overall charge of the polymer approaches zero. The attraction between the negative L-M-L complexes and the positive pyridine groups may then lead to a compaction of the micellar core. At M/L ratios below 0.5, there are still unoccupied ligand groups on the polymer chain. The overall negative charge of the polymers then probably prevents compaction of the core, resulting in the larger sizes seen with Cryo-TEM and light scattering. We tried to measure zeta potentials of the Zn-L-P4VP$_{48}$-*b*-PEO$_{193}$ micelles in the solution, but unfortunately we could not obtain reliable data due to the electrostatic screening of the background electrolyte (0.1 M NaCl). Note

that the electrostatic screening length does not vary significantly in our experiments, because the salt concentration changes by at most a few percent upon adding metal due to the relatively high concentration of background electrolyte.

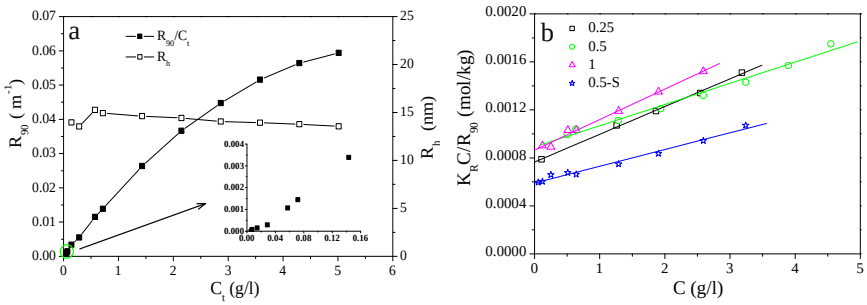


Figure 4.4 a: Light scattering intensity and hydrodynamic radius versus total concentration of polymer and $Zn^{2+}$. Inset shows a zoom in for low concentrations. b: $K_RC/R_{90}$ is plotted as a function of C (C = $C_t$ – CMC, $C_t$ is the total concentration of polymer and $Zn^{2+}$). Zn-L-P4VP$_{48}$-*b*-PEO$_{193}$ micelles are prepared at M/L 0.25, 0.5 and 1 in 20 mM MES buffer, pH 6, 0.1 M NaCl; 0.5-S sample is prepared at M/L 0.5, in 20 mM MES buffer, pH 6, 0.8 M NaCl.

| M/L | CMC (g/l) | dn/dc ($m^3$/kg) | $N_{agg}$ | $B_2$ ($m^3$/mol) | $V_{eff}$ ($m^3$) | $R_{eff}$ (nm) |
|---|---|---|---|---|---|---|
| 0.25 | 0.019 | 1.34 x $10^{-4}$ | 71 | 198 | 6.58 x $10^{-22}$ | 54 |
| 0.5 | 0.020 | 1.25 x $10^{-4}$ | 60 | 111 | 3.68 x $10^{-22}$ | 44 |
| 1 | 0.010 | 1.25 x $10^{-4}$ | 62 | 171 | 5.68 x $10^{-22}$ | 51 |
| 0.5-S | 0.010 | 1.25 x $10^{-4}$ | 91 | 202 | 6.70 x $10^{-22}$ | 54 |

Table 4.1 Critical micelle concentration (CMC), aggregation number ($N_{agg}$), second virial coefficient $B_2$, and effective excluded volume $V_{eff}$ and corresponding radius $R_{eff}$ of the micelles as a function of the M/L ratio and the salt concentration. Values were obtained by analyzing the light scattering data shown in Figures 4.4.

An alternative explanation for the decrease in size upon increasing M/L ratio may also be due to a decrease of the aggregation number of micelles from low M/L to higher ratio. In Figure 4.4a, we plot the changes of light scattering intensity and hydrodynamic radius of Zn-L-P4VP$_{48}$-*b*-PEO$_{193}$ micelles upon diluting with buffer solution. By extrapolating the

intensity to the baseline, we found that the critical micelle concentration (CMC) is about 0.02 g/l. The aggregation number of micelles formed at different M/L ratios is obtained by plotting $K_RC/R_{90}$ as a function of the concentration C (Figure 4.4b) and using equation 6. The results are summarized in Table 4.1. We found that the aggregation number of the micelles is larger at M/L < 0.5 than at M/L > 0.5, while the CMC does not depend strongly on the M/L ratio. The second virial coefficient $B_2$ has a minimum at M/L 0.5, where the micelles are most compact.

At first sight, it seems surprising that the aggregation number is larger at low M/L ratios, where the electrostatic repulsion between the unoccupied ligand groups is stronger. However, it must be kept in mind that the micelles are not equilibrium structures, so that the aggregation number is determined largely by kinetic effects. Probably, at M/L < 0.5 the metal ions have more opportunities to crosslink a larger number of polymer chains, leading to larger aggregation numbers at smaller M/L ratios.

As mentioned in the introduction, Zn-L-P4VP$_{48}$-*b*-PEO$_{193}$ micelles are formed based on the strong coordination between ligand and metal ions. One of the advantages of using coordination bonds as the direct driving force for micellization is that coordination bonds are not very sensitive to added salt. To test whether this reduced sensitivity indeed leads to more stable micelles, we investigated the effect of the salt concentration on the Zn-L-P4VP$_{48}$-*b*-PEO$_{193}$ micelles (M/L 0.5). Figure 4.5a shows that the light scattering intensity and hydrodynamic radius of Zn-L-P4VP$_{48}$-*b*-PEO$_{193}$ micelles do not change up to salt concentration as high as 0.4 M NaCl and then even go up as the salt concentration increases further to 1 M. The increase in intensity at high salt concentration can be explained by the screening effect of the salt ions that weakens the electrostatic interaction between the positively charged pyridine groups and the negatively charged metal complexes, leading to swelling of the core (without disrupting it). This also leads to an increase of the aggregation number of the micelles, and an increase of the excluded volume, as shown by the light scattering results (Table 4.1). Our results contrast strongly with previous observations for metal-containing complex coacervate core micelles based on electrostatic co-assembly, where the scattering intensity decreased strongly upon adding salt,[17] and confirms that the micelles do not dissociate at high ionic strength. The high stability of the micelles is due to the strong coordination bonds between the chelidamic acid ligand groups and $Zn^{2+}$ ions. To test how strong these bonds are, we added EDTA to the micellar solution as a competing ligand. We did not notice any change in the light

scattering intensity and hydrodynamic radius of the micellar solution after adding EDTA over a period of 8 days (Figure 4.5c), indicating that the coordination bonds that keep the micelles together are indeed very strong. Probably, the cross-linked micellar structure and the favorable electrostatic interaction with the pyridinium groups make the coordination bonds even stronger than for free chelidamic acid.

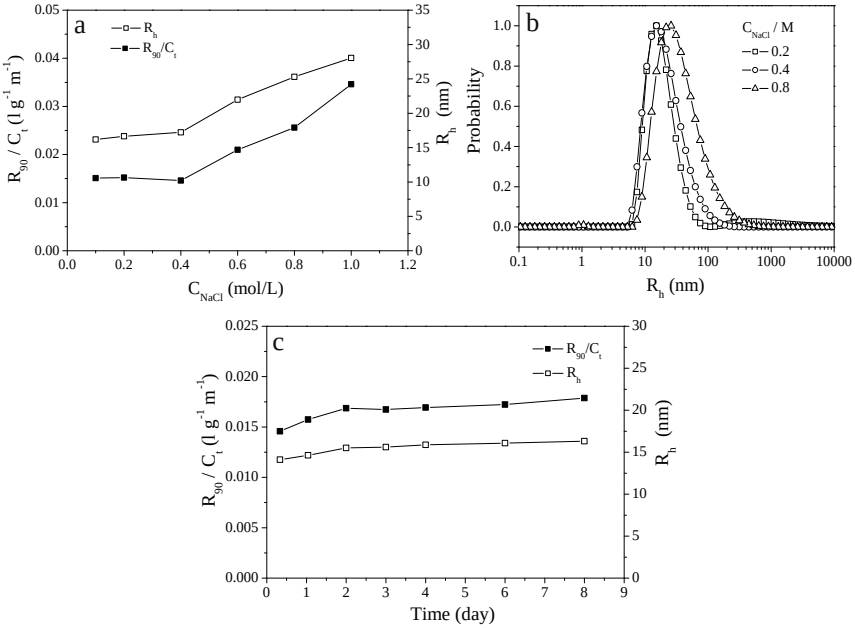


Figure 4.5 a: The effect of salt on the scattering intensity and hydrodynamic radius of Zn-L-P4VP$_{48}$-*b*-PEO$_{193}$ micelles; b: CONTIN analysis of particle size and size distribution at different salt concentration; c: Variations of intensity and radius of micelles with EDTA in solution (same amount with chelidamic acid groups).

## 4.4 Conclusion

A stable metal containing polymer micelle system is studied. A diblock copolymer P4VP$_{48}$-*b*-PEO$_{193}$ is modified with a terdentate ligand grafted to the PVP block. Upon mixing with metal ions, micelles are formed, directly driven by the metal-ligand coordination interaction. The formed Zn-L-P4VP$_{48}$-*b*-PEO$_{193}$ micelles have a hydrodynamic radius of about 15 nm, while the radius of the micellar core is around 5 nm. Adding salt and EDTA hardly affects the Zn-L-P4VP$_{48}$-*b*-PEO$_{193}$ micelles, confirming the high stability of the structures. Preliminary results show that micelles can also be made with other metal ions

than $Zn^{2+}$ ($Ni^{2+}$, $Mn^{2+}$, $Gd^{3+}$), demonstrating the general applicability of this strategy for making stable metal-containing micelles.

## References


1. Wang, X.; McHale, R. *Macromol. Rapid Commun.* **2010**, *31*, 331–350.
2. Paz, F. A. A.; Klinowski, J.; Vilela, S. M. F.; Tome, J. P. C.; Cavaleiro, J. A. S.; Rocha, J. *Chem. Soc. Rev.* **2012**, *41*, 1088–1110.
3. Winter, A.; Hager, M. D.; Newkome, G. R.; Schubert, U. S. *Adv. Mater.* **2011**, *23*, 5728–5748.
4. Kurth, D. G., Higuchi, M. *Soft Matter* **2006**, *2*, 915–927.
5. Moughton, A. O.; O'Reilly, R. K. *Macromol. Rapid Commun.* **2010**, *31*, 37–52.
6. Schubert, U. S.; Eschbaumer, C. *Angew.Chem. Int. Ed.* **2002**, *41*, 2892-2926.
7. Kimpe, K.; Parac-Vogt, T. N.; Laurent, S.; Pierart, C.; Elst, L. V.; Muller, R. N.; Binnemans, K. *Eur. J. Inorg. Chem.* **2003**, 3021-3027.
8. Gianolio, E.; Giovenzana, G. B.; Longo, D.; Longo, I.; Menegotto, I.; Aime, S. *Chem. Eur. J.* **2007**, *13*, 5785-5797.
9. Owen1, T.; Butler, A. *Coord. Chem. Rev.* **2011**, *255*, 678-687.
10. Gohy, J. F.; Lohmeijer, B. G. G.; Schubert, U. S. *Macromolecules* **2002**, *35*, 4560-4563.
11. Gohy, J. F.; Lohmeijer, B. G. G.; Schubert, U. S. *Macromol. Rapid Commun.* **2002**, *23*, 555–560.
12. Ott, C.; Hoogenhoom, R.; Hoeppener, S.; Wouters, D.; Gohy, J. F.; Schubert, U. S. *Soft Matter* **2009**, *5*, 84–91.
13. Zhou, G.; He, J.; Harruna, I. I. *J. Polym. Sci., Part A: Polym. Chem.* **2007**, *45*, 4204-4210.
14. Moughton, A. O.; O'Reilly, R. K. *J. A. Chem. Soc.* **2008**, *130*, 8714-8725.
15. Joubert, M.; In, M. *ChemPhysChem* **2008**, *9*, 1010–1019.
16. Yan, Y.; Besseling, N. A. M.; de Keizer, A.; Marcelis, A. T. M.; Drechsler, M.; Cohen Stuart, M. A. *Angew. Chem. Int. Ed.* **2007**, *46*, 1807-1809.
17. Yan, Y.; de Keizer, A.; Cohen Stuart, M. A.; Drechsler, M.; Besseling, N. A. M. *J. Phys. Chem. B* **2008**, *112*, 10908-10914.
18. Bronich, T. K.; Keifer, P. A.; Shlyakhtenko, L. S.; Kavanov, A. V. *J. Am. Chem. Soc.* **2005**, *127*, 8236-8237.
19. Bronstein, L. M.; Sidorov, S. N.; Zhirov, V.; Zhirov, D.; Kabachii, Y. A.; Kochev, S. Y.; Valetsky, P. M.; Stein, B.; Kiseleva, O. I.; Polyakov, S. N.; Shtykova, E. V.; Nikulina, E. V.; Svergun, D. I.; Khokhlov, A. R. *J. Phys. Chem. B* **2005**, *109*, 18786-18798.
20. Bronstein, L. M.; Sidorov, S. N.; Valetsky, P. M. *Langmuir* **1999**, *15*, 6256-6262.
21. Nyman, C. J. *J. Am. Chem. Soc.* **1953**, *75*, 3575-3576.
22. Bunting, J. W.; Thong, K. M. *Can. J. Chem.* **1970**, *48*, 1654-1656.
23. Vermonden, T.; van der Gucht, J.; de Waard, P.; Marcelis, A. T. M.; Besseling, N. A. M.; Sudholter, E. J. R.; Fleer, G. J.; Cohen Stuart, M. A. *Macromolecules* **2003**, 36, 7035-7044.
24. Vermonden, T.; Branowska, D.; Marcelis, A. T. M.; Sudholter, E. J. R. *Tetrahedron* **2003**, *59*, 5039-5045.
25. Froidevaux, P.; Harrowfield, J. M.; Sobolev, A. N. *Inorg. Chem.* **2000**, *39*, 4678-4687.
26. Wang, J. Y.; Yang, X. L. *Langmuir* **2008**, *24*, 3358-3364.

27. Zhang, B. Q.; Chen, G. D.; Pan, C. Y.; Luan, B.; Hong, C. Y. *J. Appl. Polym. Sci.* **2006**, *102*, 1950-1958.
28. Yan, Y.; Lan, Y.; de Keizer, A.; Drechsler, M.; Van As, H.; Cohen Stuart, M. A.; Besseling, N. A. M. *Soft Matter* **2010**, *6*, 3244-3248.
29. Yan, Y.; de Keizer, A.; Cohen Stuart, M. A.; Besseling, N. A. M. A*dv. Polym. Sci.* **2011**, *242*, 91-115.
30. Ma, L.; Kang, H. L.; Liu, R. G.; Huang, Y. *Langmuir* **2010**, *26*, 18519-18525.

# Chapter 5

## Controlled Mixing of Lanthanide(III) Ions in Coacervate Core Micelles

Abstract

Combined Eu/Gd-C3Ms are studied in this chapter. The formed coacervate core micelles contain a few hundred $Eu^{3+}$ and $Gd^{3+}$ ions in the core at a composition ratio between $Eu^{3+}$ and $Gd^{3+}$ that can be adjusted between 0 – 100%, resulting in a corresponding linear respons of the luminescence and magnetic relaxation properties of the micelles. Light scattering, Cryo-TEM, luminescence spectroscopy and magnetic relaxation measurements indicate that the micelles are very stable under physiological conditions, in different buffer solutions, in presence of high salt concentrations, and in the presence of scavenging ligands like EDTA, showing great potential for use as bimodal imaging probes.

Submitted for publication in a slightly modified form as: Wang, J. Y.; Velders, A. H.; Gianolio, E.; Aime, S.; Vergeldt, F. J.; Van As, H.; Yan, Y.; Drechsler, M.; De Keizer A.; Cohen Stuart, M. A.; van der Gucht, J. *Controlled Mixing Lanthanide(III) Ions in Coacervate Core Micelles*

## 5.1 Introduction

Complexes of lanthanide(III) ions have attracted considerable interest for their unique optical and magnetic properties, arising from their partially filled f-shell.[1,2] For example, gadolinium(III) complexes, with their seven unpaired electron spins, strongly decrease the spin-lattice relaxation time (T1) of nearby water molecules in a magnetic field, which has led to their wide-spread application in contrast agents for magnetic resonance imaging (MRI) in medical diagnosis.[3,4] Other lanthanide complexes are known for their luminescent characters and, in particular, complexes containing europium(III), terbium(III) and erbium(III) are used as optical imaging probes with high resistance to photo-bleaching, long luminescent lifetimes, and sharp emission bands.[5,6] In biomedical diagnostics each imaging modality has its specific advantages and drawbacks, and for example MRI has high resolution but low sensitivity, while optical imaging has high sensitivity but limited resolution.[7,8] A recent trend is therefore to develop bimodal probe systems, where, e.g., the high resolution of MRI and the high sensitivity of optical imaging can be combined.[9,10] To achieve this, different lanthanides, such as gadolinium(III) and europium(III), must be incorporated into one probe particle; a good control of the mixing ratio between the different lanthanides is essential for this.[11-13] For solid particles, however, this control has proven to be a difficult task, because there usually is a preference for one lanthanide ion over another for specific crystal lattices, preventing a statistical distribution of a mixture of lanthanide ions in the particles.[14-16] Moreover, investigations of lanthanide-doped nanoparticles have shown that the doped ions in the core of the nanoparticle have different properties than the ones closer to the surface.[17] In this chapter, we develop a solid and straightforward approach to incorporate different lanthanide ions, i.e. europium and gadolinium, in a 20 nanometer (radius) coacervate micellar structure in a controlled and statistical manner. The luminescence and the effect on magnetic relaxation rate of these bimodal probes containing several hundreds of lanthanide ions in the core have been studied and their stability against salt and competing ligands has been investigated.

## 5.2 Experimental section

### Materials

The diblock copolymer, poly(N-methyl-2-vinyl-pyridinium iodide)-*b*-poly(ethylene oxide) ($P2MVP_{41}$-*b*-$PEO_{205}$), was obtained by quaternization of poly(2-vinylpyridine)-*b*-

poly(ethylene oxide) ($P2VP_{41}$-*b*-$PEO_{205}$) (Polymer Source, $M_w/M_n$= 1.03, $M_w$= 13.3 k) following a procedure described elsewhere.[18] The degree of quaternization is about 90%. The bisligand compound 1,11-bis(2,6-dicarboxypyridin-4-yloxy)-3,6,9-trioxaundecane ($L_2EO_4$) was prepared according to literature.[19] Gadolinium chloride $GdCl_3{\cdot}6H_2O$, europium nitrate $Eu(NO_3)_3{\cdot}5H_2O$ and sodium chloride NaCl (analytical grade) were purchased from Aldrich and used without further purification. All stock solutions were made in acetate buffer at pH 5.

**Methods**

Light Scattering

Light scattering at an angle of 90 degrees was performed with an ALV light scattering-apparatus, equipped with a 400mW argon ion laser operating at a wavelength of 532.0 nm. All measurements were performed at room temperature. Titrations were carried out using a Schott-Geräte computer-controlled titration setup to control sequential addition of titrant and cell stirring. After every dosage, the laser light-scattering intensity (*I*) and the correlation function were recorded. The hydrodynamic radius and the scattered intensity are studied as a function of the mole fraction of positive charge, *f* +, which is defined as follows:

$$f+ = \frac{[+]}{[-]+[+]} \tag{1}$$

where [-] and [+] are the molar charge concentrations of charged units on each polymer chain.

The light scattering intensity is expressed as the excess Rayleigh ratio $R_\theta$ divided by the total polymer concentration. $R_\theta$ is obtained as

$$R_\theta = \frac{I_{\text{sample}} - I_{\text{solvent}}}{I_{\text{toluene}}} \times R_{\text{toluene}} \times \frac{n^2_{\text{solvent}}}{n^2_{\text{toluene}}} \tag{2}$$

where $I_{\text{sample}}$ is the scattering intensity of the micellar solution and $I_{\text{solvent}}$ is the intensity of the solvent. $I_{\text{toluene}}$ is the scattering intensity of toluene, and $R_{\text{toluene}}$ is the known Rayleigh ratio of toluene ($2.1 \cdot 10^{-2}$ $m^{-1}$). The total polymer concentration is the sum of the concentrations of all components contributing to micelle formation. The CUMULANT method was used to analyze the mean apparent hydrodynamic radius ($R_h$) as

$$R_h = kTq^2 / 6\pi\eta\Gamma \tag{3}$$

where $q$ is scattering vector, $k$ is the Boltzman constant, $T$ is the absolute temperature, $\eta$ is the viscosity of the solvent, and $\Gamma$ is the measured average decay rate of the correlation function. The CONTIN method is used to analyze the distribution of particle (C3Ms) radii. The Rayleigh ratio can be linked to the concentration and mass of the scattering objects:

$$\frac{K_R C}{R_\theta} = \frac{1}{M} \times \frac{1}{P(qR)} \times \frac{1}{S(q)} \tag{4}$$

where $C$ is the weight concentration of micelles, $M$ is their molecular mass and $R$ is the radius of the object that contribute to scatter light. For C3Ms, the $R$ is closed to the core radius. $P(qR)$ and $S(q)$ are the form factor and the structure factor, respectively. $K_R$ is an optical constant defined as:

$$K_R = \frac{4\pi^2 n^2}{N_{Av}\lambda_0^4}\left(\frac{dn}{dc}\right)^2 \tag{5}$$

where $n$ is the refractive index of solvent, $N_{Av}$ is Avogadro's number, $\lambda_0$ is the wavelength of the incoming beam (532.0 nm), and $dn/dc$ is the refractive index increment of the Gd-C3Ms. We measured $dn/dc$ of the micellar solutions using a differential refractive index detector (Shodex RI-71) and found a value of $1.58 \cdot 10^{-4}$ $m^3/kg$ for Gd-C3Ms.

In our experiments, the scattering vector $q = (4\pi n/\lambda_0)sin(\theta/2)$ is approximately 0.023 $nm^{-1}$ ($\theta$=90°), so that $qR$ is small for the micelles (which have a radius on the order of 20 nm). We therefore assume that $P(qR)$=1. At low concentrations, the structure factor can be approximated as

$$\frac{1}{S(q)} = 1 + 2B_2\frac{C}{M} \tag{6}$$

where $B_2$ is the second virial coefficient. Substitution into equation 4, we get

$$\frac{K_R C}{R_\theta} = \frac{1}{M} + 2B_2\frac{C}{M^2} \tag{7}$$

By plotting $K_R C/R_\theta$ versus C, we can obtain the molar mass of the micelles from the intercept, from which we can obtain the aggregation number of the micelles.

Relaxometric Measurements

The longitudinal water proton relaxation rate as a function of pH was measured at 25°C by using a Stelar Spinmaster (Stelar, Mede, Pavia, Italy) spectrometer operating at 20 MHz, by means of the standard inversion-recovery technique. The temperature was controlled with a Stelar VTC-91 air-flow heater equipped with a copper constantan thermocouple

(uncertainty 0.1°C). The relaxometric characterization of the field-dependent relaxometry of the paramagnetic Gd(III)-probes solutions was carried out through the acquisition of the NMRD profiles. The proton $1/T_1$ NMRD profiles were measured at 25°C on a fast field-cycling Stelar relaxometer over a continuum of magnetic field strengths from 0.00024 to 0.47 T (corresponding to 0.01 - 20 MHz proton Larmor frequencies). The relaxometer operates under computer control with an absolute uncertainty in $1/T_1$ of ± 1%. Additional data points in the range 20 - 70 MHz were obtained on the Stelar Spinmaster spectrometer. The concentration of the solutions used for the relaxometric characterization was determined according to a previously reported relaxometric method.[20]

Cryogenic Transmission Electronic Microscopy (Cryo-TEM)

A few microliters of sample were placed on a bare copper TEM grid (Plano, 600 mesh) and the excess of liquid was removed with filter paper, followed by shooting the grid into liquid ethane cooled to -170 ºC. The sample vitrification procedure was carried out using a cryo-box (Carl Zeiss NTS GmbH, Oberkochen, Germany) equipped with humidity and temperature chamber. Samples were studied at an acceleration voltage of 120 kV. Images were recorded under low-dose conditions with a bottom-mounted CCD camera (UltraScan 1000, Gatan). For each sample, images were collected for a number of different regions in the sample.

## 5.3 Results and discussion

The Eu/Gd micelles are formed based on the electrostatic interaction between an anionic coordination complex with both $Eu^{3+}$ and $Gd^{3+}$, and a cationic-neutral diblock copolymer. The chemical structures of the ligand 1,11-bis(2,6-dicarboxypyridin-4-yloxy)-3,6,9-trioxaundecane ($L_2EO_4$) and the diblock copolymer poly(N-methyl-2-vinyl-pyridinium iodide)-*b*-poly(ethylene oxide) ($P2MVP_{41}$-*b*-$PEO_{205}$) are shown in Scheme 5.1. $Eu^{3+}$ and $Gd^{3+}$ ions with the $L_2EO_4$ ligand at a metal to ligand ratio M/L of 2/3, where branched structures are formed with net three negative charges per coordination "$LnL_3$" unit (Scheme 5.1c).[21,22] Upon mixing with $P2MVP_{41}$-*b*-$PEO_{205}$ copolymer, Eu/Gd-$L_2EO_4$ coordination structures quickly aggregate with the cationic block and the formed coacervate aggregates are stabilized by the neutral PEO chain, leading to the formation of micelles.

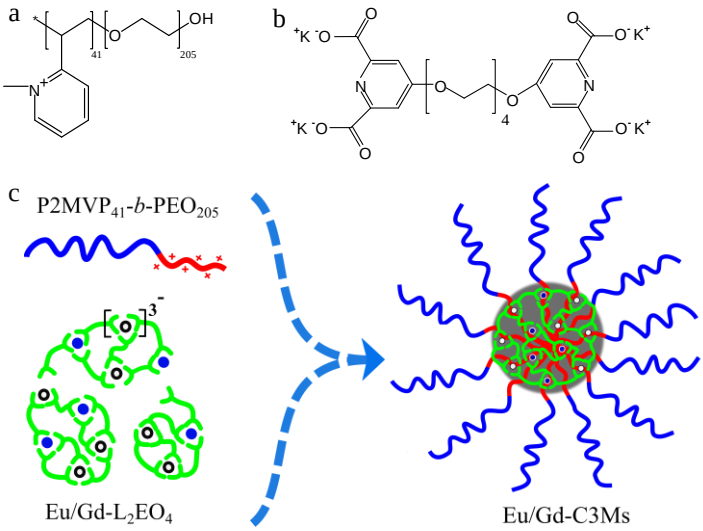


Scheme 5.1 a: Structure of $P2MVP_{41}$-*b*-$PEO_{205}$. b: Structure of $L_2EO_4$. c: Formation of Eu/Gd-C3Ms. (blue dot represents $Eu^{3+}$ ion and white dot represents $Gd^{3+}$ ion).

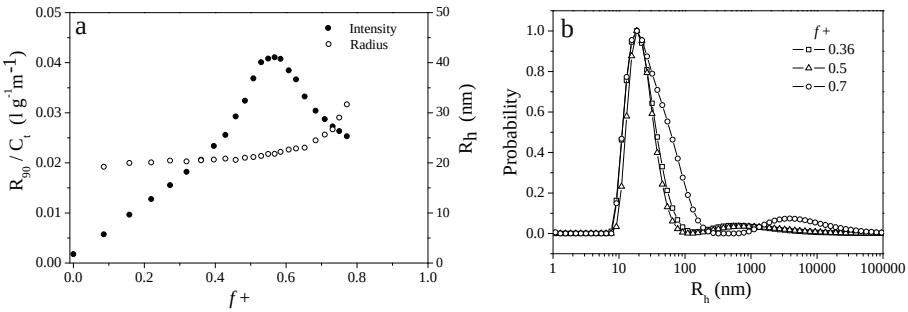


Figure 5.1 Light scattering titration of Gd-$L_2EO_4$ (Gd/L = 2/3) coordination complex with $P2MVP_{41}$-b-$PEO_{205}$. a: Variations of light scattering intensity, as expressed by the excess Rayleigh ratio, and hydrodynamic radius as a function of positive charge fraction. b: CONTIN analysis of Gd-C3Ms at different *f* +.

The preferred micellar composition (PMC) is determined by the titration process with Gd-$L_2EO_4$ coordination complexes. As shown in Figure 5.1a, the light scattering intensity of coordination complexes in the absence of cationic block is very low, indicating that the formed structures are relatively small. The light scattering intensity increases immediately after the first addition of $P2MVP_{41}$-*b*-$PEO_{205}$ copolymers and shows a maximum around *f* +

≈ 0.5. This maximum suggests the micelles are formed mostly at the stoichiometric charge ratio where the opposite charges are neutralized completely.

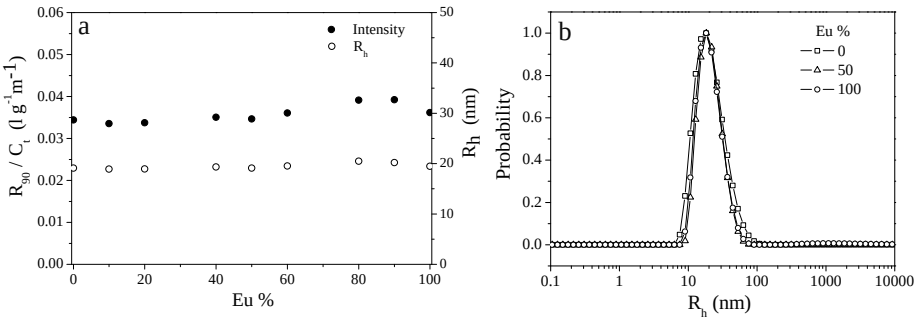


Figure 5.2 a: Light scattering intensity and hydrodynamic radius of Eu/Gd-C3Ms at different $Eu^{3+}/Gd^{3+}$ ratios. b: CONTIN analysis of the particles size and distribution (micelles are prepared in 20 mM acetate buffer, pH 5, total metal concentration is fixed at 0.5 mM/L).

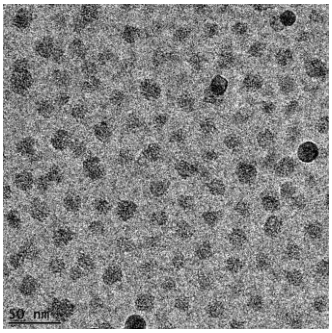


Figure 5.3 Cryo-TEM images of Gd-C3Ms prepared in 20 mM acetate buffer, pH 5.

Figure 5.2a shows the intensity of the scattered light, and the hydrodynamic radius of the micelles as a function of mixing ratio $Eu^{3+}/Gd^{3+}$. Both the intensity and hydrodynamic radius show independence on varying the $Eu^{3+}/Gd^{3+}$ ratio. The CONTIN results in Figure 5.2b confirm the micelle radius being around 20 nm and indicate that there is only one dominant kind of particle in solution at all $Eu^{3+}/Gd^{3+}$ mixing ratios. The Cryo-TEM image in Figure 5.3 indicates that the formed micelles have a core radius around 8 nm, so the thickness of the corona is about 12 nm, which fits with values found for other micelles.[23]

The critical micelle concentration (CMC) of Gd-C3Ms (100% $Gd^{3+}$) is found around 0.015 g/L (total concentration of polymer and Gd-$L_2EO_4$). The aggregation number is determined by plotting $K_RC/R_{90}$ as a function of the concentration (Figure 5.4) and calculated with equation 7. It is found around 50, which means that approximately 300 metal ions are contained in one micelle.

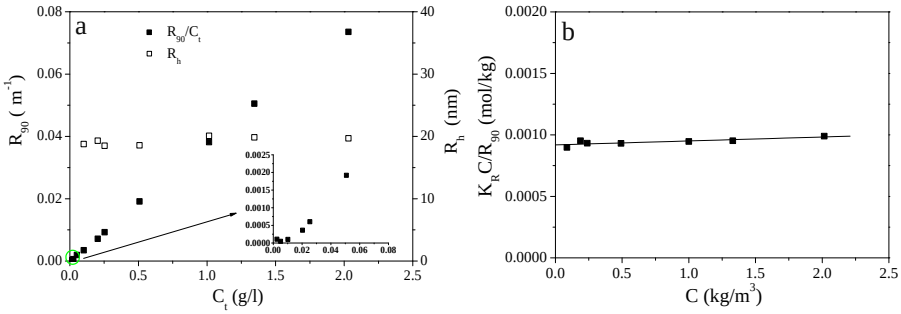


Figure 5.4 a: Light scattering intensity and hydrodynamic radius versus total concentration of components. The CMC is estimated by extrapolating the intensity to the baseline. Inset shows a zoom in for low concentrations. b: $K_RC/R_{90}$ is plotted as a function of C (C = Ct – CMC). (Gd-C3Ms are prepared in acetate 20 mM buffer, pH 5)

The bimodal functionalities of the Eu/Gd-C3Ms were further characterized by luminescence spectroscopy and magnetic relaxation measurements. For the luminescence an excitation wavelength of 284 nm was used (Figure 5.5a), with the $L_2EO_4$ ligand functioning as antenna to transfer energy to $Eu^{3+}$ ions which by itself has a negligible absorption coefficient at this wavelength.[24,25] The longitudinal relaxation rate of Eu/Gd-C3Ms was measured by recording the NMR dispersion curves (Figure 5.5b) and was found around 10 $s^{-1}$ (0.5 mM/L, 30.9 MHz). In Figure 5.5c, both the luminescence intensity at 614 nm and the relaxation rate (298 K, 30.9 MHz, total metal concentration is 0.5 mM/L) of Eu/Gd-C3Ms are plotted as a function of the $Eu^{3+}/Gd^{3+}$ ratio. We find linear dependences of both the luminescence and the relaxation rate on the amount of $Eu^{3+}$ and $Gd^{3+}$, respectively in the micelle. It is worth to mention that Gd-C3Ms show negligible luminescence compared to that of Eu-C3Ms, while Eu-C3Ms does not contribute to the relaxation rate, indicating that the luminescence and relaxation are attributable to the $Eu^{3+}$ and $Gd^{3+}$ respectively. These results indicate that the $Eu^{3+}$ and $Gd^{3+}$ complexes in the

micelle do not interfere with each other and that the luminescence and relaxation can be adjusted simply by changing the $Eu^{3+}/Gd^{3+}$ composition ratio.

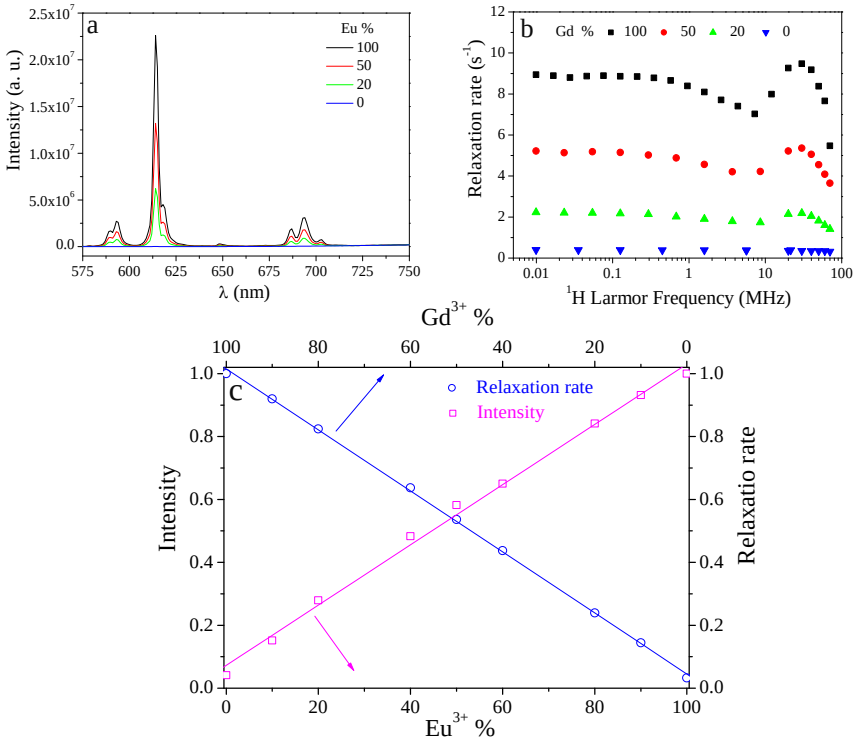


Figure 5.5 a: Luminescent emission intensity of Eu/Gd-C3Ms at different $Eu^{3+}/Gd^{3+}$ ratio. (excitation wavelength is 284 nm, total metal concentration is 0.5 mM/L). b: NMRD profiles (Nuclear Magnetic Resonance Dispersion) of Eu/Gd-C3Ms at different $Eu^{3+}/Gd^{3+}$ ratio. c: Normalized luminescent intensity and relaxation rate as a function of $Eu^{3+}/Gd^{3+}$ ratio. [Luminescent intensity and relaxation rate normalized by the values of Eu-C3Ms (100% $Eu^{3+}$) and Gd-C3Ms (100% $Gd^{3+}$), respectively. Eu/Gd-C3Ms are prepared in 20 mM acetate buffer, pH 5]

The high tunability of the physical properties of the Eu/Gd-C3Ms holds great promise from the application point of view, so we have further investigated the stability of the micelle structures at high salt concentrations and with different buffer conditions. Complex coacervate core micelles typically strongly respond to ionic strength.[26,27] Hence, we first studied the effect of salt on the micelles. Figure 5.6 shows the light scattering intensity and hydrodynamic radius of Gd-C3Ms as a function of salt concentration. Remarkably, the

intensity decreases only slightly and the radius does not change up to 500 mM NaCl. The critical salt concentration (CSC) where the Gd-C3Ms micelles dissociate completely is around 800 mM. This is significantly higher than for previously reported systems (Zn-C3Ms, Fe-C3Ms), where micelles started to dissociate immediately upon increasing the salt concentration and fell apart completely around 200 mM salt.[28] The iron(III) and zinc(II) micelles in these previous studies were formed from linear M-$L_2EO_4$ complexes (M/L = 1/1) with only one or two negative charges for each coordination center, respectively. It is thus likely that the high stability of Gd-C3Ms is due to the branched structure and the high negative charge of Gd-$L_2EO_4$ complexes formed at a 2/3 ratio with three tridentate ligand moieties coordinating to a single lanthanide ion. Both the intensity and hydrodynamic radius of Gd-C3Ms formed at ratio 2/3 show an increase followed by a sharp drop upon approaching the CSC point. A similar phenomenon has been found in other studies as well[26-28] and the recent study shows that the increase is due to the formation of worm-like structures near the CSC point.[29]

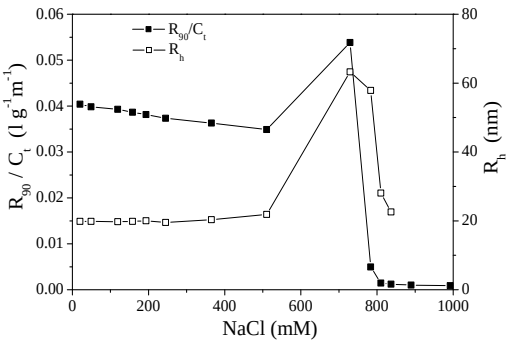


Figure 5.6 The effect of salt on scattering intensity and micellar size of Gd-C3Ms. Gd-C3Ms are formed in 20 mM acetate buffer, pH 5.

In addition, the following stability tests were carried out by putting Eu-C3Ms and Gd-C3Ms in different buffers: acetate buffer, PBS buffer and PBS buffer with added EDTA as a strong competing ligand (at the same concentration as that of the $L_2EO_4$ ligand). The variations of the luminescence intensity of Eu-C3Ms, relaxation rate of Gd-C3Ms, light scattering intensity and hydrodynamic radii of both are recorded over a period of 100 hours.

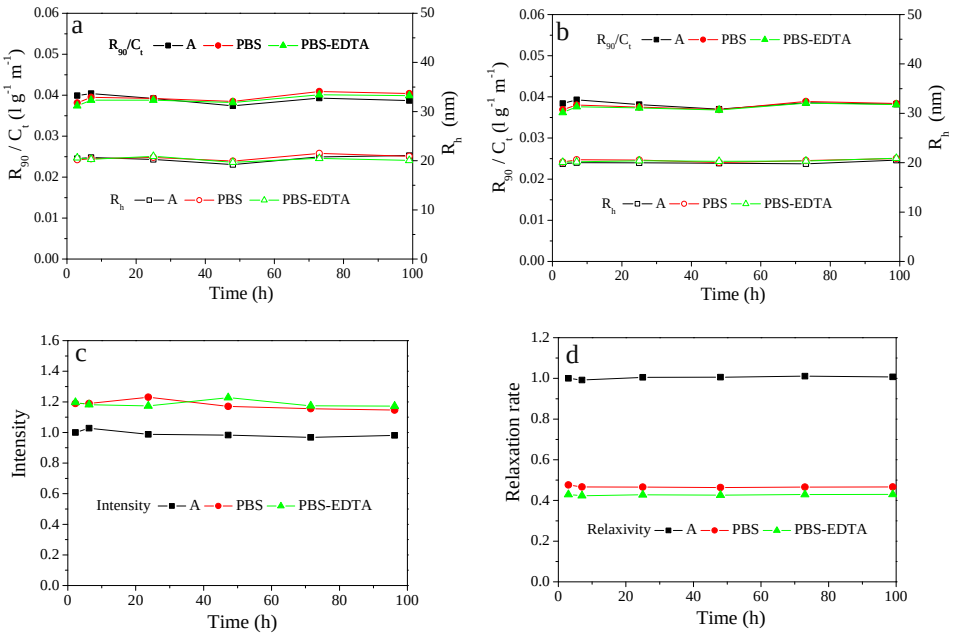


Figure 5.7 Variations of light scattering intensity and micellar size of Eu-C3Ms (a) and Gd-C3Ms (b) in different buffers and salt concentrations over time. c: Variation of the luminescent intensity of Eu-C3Ms in different buffers over time (normalized by the intensity of Eu-C3Ms in 20 mM acetate buffer, $Eu^{3+}$ concentration is 0.2 mM/L). d: Time dependence of longitudinal relaxation rate of Gd-C3Ms in different buffers (normalized by the relaxation rate of Gd-C3Ms in 20 mM acetate buffer, $Gd^{3+}$ concentration is 0.5 mM/L). A: acetate buffer, 20 mM, pH 5; PBS: phosphate buffer saline, pH 7.4; PBS-EDTA: phosphate buffer saline, pH 7.4, with added EDTA (at the same concentration as that of $L_2EO_4$) to the Ln-C3Ms solution.

First of all, Eu-C3Ms and Gd-C3Ms in different buffer solutions did not show any change in the light scattering intensity and hydrodynamic radius (Figure 5.7a,b), and Cryo-TEM images give similar size, indicating that there are no general structural changes (Figure

5.8). The luminescent intensity of Eu-C3Ms in PBS buffer is higher than that in acetate buffer (Figure 5.7c), but adding EDTA into the PBS buffer with micelles does not change the luminescent intensity, indicating that there is no leakage of $Eu^{3+}$ ions or exchange of EDTA and $L_2EO_4$ ligands,[30] confirming the high stability of the micelles. The Gd-C3Ms show opposite dependence on the two buffers used, with a higher relaxation rate in acetate buffer than in PBS buffer and PBS-EDTA solution (Figure 5.7d). Most importantly, although there are differences in luminescence and relaxation rate that depend on the buffer, under all conditions measured the luminescence and relaxation rate response remain constant over the full time scale measured of 100 hours. In particular the lack of change in response between the PBS buffer and the PBS-EDTA buffer strongly corroborates the stability of the coordinated lanthanide ions in the micellar structures.

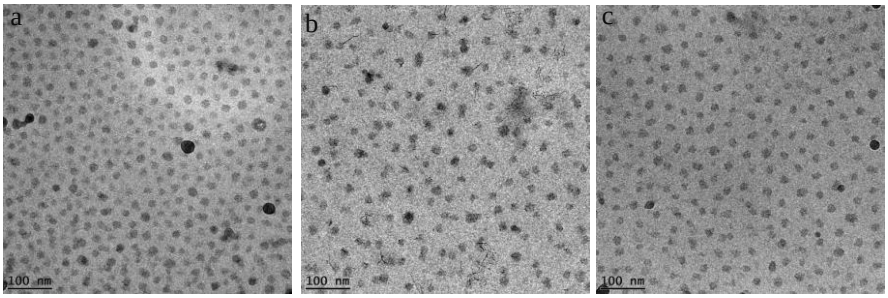


Figure 5.8 Cryo-TEM images of Gd-C3Ms in different buffer solutions. a: acetate buffer, 20 mM, pH 5; b: PBS, pH 7.4; c: PBS with EDTA(same amount with $L_2EO_4$ ligand).

## 5.4 Conclusion

In conclusion, we develop a novel $Eu^{3+}$ and $Gd^{3+}$ combined micelle system containing several hundreds of lanthanide ions in the coacervate core. The $Eu^{3+}$ and $Gd^{3+}$ amounts can be adjusted at will, leading to high tunability between luminescence and relaxation. Eu/Gd-C3Ms are very stable: the light scattering intensity and hydrodynamic radius, Cryo-TEM

images, the luminescent intensity and the relaxation rate remaining constant in acetate buffer, PBS buffer and PBS-EDTA solution over a few days. The high tunability and stability provide great potential for use in new materials or bi- or multimodal imaging probes, for material or biomedical applications, including eventually even radioisotopes for additional diagnostic modality and/or for therapeutic purposes. The excellent response of the lanthanide ions and the stability of the micelle structures, together with the observed differences under various buffer conditions, allow for further studies investigating the inner structure of coacervate micelles in detail. Particularly the dynamics of water and (buffer) ions exchange of the core with the bulk is of major interest.

## References


1. Bunzli, J. C. G.; Piguet, C. *Chem. Soc. Rev.* **2005**, *34*, 1048–1077.
2. Bunzli, J. C. G. *Chem. Rev.* **2010**, *110*, 2729-2755.
3. Castelli, D. D.; Gianolio, E.; Aime, S. *Bioinorganic Medicinal Chemistry*, chapter 8, 223-251.
4. Hermann, P.; Kotek, J.; Kubicek, V.; Lukes, I. *Dalton Trans*. **2008**, 3027-3047.
5. Ruggi, A.; Reinhoudt, D. N.; Velders, A. H. *Bioinorganic Medicinal Chemistry*, chapter 13, 383-406.
6. dos Santos, C. M. G.; A. Harte, J.; Quinn, S. J.; Gunnlaugsson, T. *Coord. Chem. Rev.* **2008**, *202*, 2512-2527.
7. Lim, Y. T.; Noh, Y. W.; Han, J. H.; Cai, Q. Y.; Yoon, K. H.; Chung, B. H. *Small* **2008**, *4*, 1640-1645.
8. Mulder, W. J.; Griffioen, A. W.; Strijkers, G. J.; Cormode, D. P.; Nicolay, K.; Fayad, Z. A. *Nanomedicine* **2007**, *2*, 307-324.
9. Frullano, L.; Meade, T. J. *J. Biol. Inorg. Chem.* **2007**, *12*, 939-949.
10. Mulder, W. J. M.; Strijkers, G. J.; Van Tilborg, G. A. F.; Cormode, D. P.; Fayad, Z. A.; Nicolay, K. *Acc.Chem. Res.* **2009**, *42*, 904-914.
11. Bonnet, C. S.; Toth, E. *C. R. Chimie* **2010**, *13*, 700-714.
12. Pellegatti, L.; Zhang, J.; Drahos, B.; Villette, S.; Suzenet, F.; Guillaumet, G.; Petoud, S.; Toth, E. *Chem. Commun*.. **2008**, 6591-6593.
13. Bonnet, C. S.; Pellegatti, L.; Buron, F.; Shade, C. M.; Villette, S.; Kubicek, V.; Guillaumet, G.; Suzenet, F.; Petoud, S.; Toth, E. *Chem. Commun.* **2010**, *46*, 6591-6593.
14. Riwotzki, K.; Haase, M. *J. Phys. Chem. B* **1998**, *102*, 10129-10135.
15. Lo, A. Y. H.; Sudarsan, V.; Sivakumar, S.; van Veggel, F. C. J. M.; Schurko, R. W. *J. Am. Chem. Soc.* **2007**, *129*, 4687-4700.
16. Dong, C.; Pichaandi, J.; Regier, T.; van Veggel, F. C. J. M. *J. Phys. Chem. C* **2011**, *115*, 15950-15958.
17. Sudarsan, V.; van Veggel, F. C. J. M.; Herringb, R. A.; Raudsepp, M. *J. Mater. Chem.* **2005**, *15*, 1332–1342.
18. Biesalski, M.; Johannsmann, D.; Rühe, J. *J. Chem. Phys*. **2004**, *120*, 8807-8814.

19. Vermonden, T.; Branowska, D.; Marcelis, A. T. M.; Sudholter, E. J. R.; *Tetrahedron* **2003**, *59*, 5039-5045.
20. Arena, F.; Singh, J. B.; Gianolio, E.; Stefanìa, R.; Aime, S. *Bioconjug. Chem.* **2011**, *22*, 2625-2635.
21. Vermonden, T.; De Vos, W. M.; Marcelis, A. T. M.; Sudholter, E. J. R. *Eur. J. Inorg. Chem.* **2004**, 2847-2852.
22. Yan, Y.; Besseling, N. A. M.; de Keizer, A.; Cohen Stuart, M. A. *J. Phys. Chem. B* **2007**, *111*, 5811-5818.
23. Yan, Y.; Besseling, N. A. M.; de Keizer, A.; Marcelis, A. T. M.; Drechsler, M.; Cohen Stuart, M. A. *Angew. Chem. Int. Ed.* **2007**, *46*, 1807-1809.
24. Yilmaz, M. D.; Hsu, S. H.; Reinhoudt, D. N.; Velders, A. H.; Huskens, J. *Angew. Chem. Int. Ed.* **2010**, *49*, 5938-5941.
25. Kirby, J. P.; Cable, M. L.; Levine, D. J.; Gray, H. B.; Ponce, A. *Anal. Chem.* **2008**, *80*, 5750-5754.
26. Solomatin, S. V.; Bronich, T. K.; Bargar, T. W.; Eisenberg, A.; Kabanov, V. A.; Kabanov, A. V. *Langmuir*, **2003**, *19*, 8069-8076.
27. Yuan, X. F.; Harada, A.; Yamasaki, Y.; Kataoka, K. *Langmuir*, **2005**, *21*, 2668-2674.
28. Yan, Y.; de Keizer, A.; Cohen Stuart, M. A.; Drechsler, M.; Besseling, N. A. M. *J. Phys. Chem. B* **2008**, *112*, 10908-10914.
29. van der Kooij, H. M.; Spruijt, E.; Voets, I. K.; Fokkink, R.; Cohen Stuart, M. A.; van der Gucht, J. *Langmuir*, **2012**, *28*, 14180-14191.
30. Eu-EDTA complexes excited at 284 nm do not show emission at 614 nm. If there is a leakage of $Eu^{3+}$ or exchange between EDTA and $L_2EO_4$ ligand, the emission intensity at 614 nm should decrease with time. But we did not find any decay of the intensity.

# Chapter 6

# Phase Diagram of Coacervate Complexes Containing Reversible Coordination Polymers

Abstract

Phase separation of coacervate complexes from cationic PDMAEMA [Poly(N,N-dimethylaminoethyl methacrylate)] and anionic reversible coordination polymers is studied in this chapter. The coordination polymers are formed from zinc and a bisligand $L_2EO_4$ [1,11-bis(2,6-dicarboxypyridin-4-yloxy)-3,6,9-trioxaundecane] and have variable chain length. The charge mixing ratio and metal to ligand ratio, M/L are varied systematically and the composition of the two coexisting phases is measured using $^1$H-NMR and ICP-AES. The resulting phase diagram is asymmetric: the coacervate complex phase tolerates an excess of coordination polymer much more than an excess of the homopolymer. Moreover, the coacervate complex tends to choose the right amount of the three components under non-stoichiometric mixing conditions. Both the metal to ligand ratio (M/L ≈ 1) and charge ratio ($f$ - ≈ 0.5) in the coacervate phase are around stoichiometry, leaving the excess components in the dilute phase.

Slightly modified form publication: Wang, J. Y.; Cohen Stuart, M. A.; van der Gucht, J. *Macromolecules*, in press (DOI: 10.1021/ma301690t)

## 6.1 Introduction

Complex coacervation refers to the phase separation that occurs upon mixing oppositely charged polyelectrolytes in aqueous solution. Generally, the dilute phase contains mainly water and released counterions, while the concentrated phase is rich in both polyelectrolytes, which can be a precipitated solid complex, or a liquid-like complex.[1,2] The latter was called a coacervate complex by Bungenberg de Jong and Kruyt, who were the first to investigate complexation in mixtures of gelatin and arabic gum.[3] The driving forces for complexation are the electrostatic attraction between polycations and polyanions and the entropy gain of the counterions that are released upon complex formation.[4,5]

In recent years, polyelectrolyte coacervates have been used to prepare nano- or micro-structures as functional materials. For example, the macroscopic phase separation can be controlled into the colloidal domain by attaching a neutral hydrophilic block to one or both of the charged polymer chains, leading to formation of micelles with a complex coacervate core.[6] These micelles have been studied systematically by our group and some other groups.[7-9] Beside micelles, vesicles, microemulsions, hydrogels, brushes and layer-by-layer structures based on coacervate complexes have been studied.[10-14] Despite this widespread use as a driving force, a fundamental understanding of complex coacervation is still lacking. The reason is that coacervate formation is a complicated process that depends on many factors, such as polymer chain length, charge density, polymer concentration, charge mixing ratio, ionic strength, pH and temperature.[1,2] Overbeek and Voorn developed the first theoretical model for complex coacervation, in which they estimated the total free energy of mixing as the sum of the mixing entropy and the electrostatic interaction free energy from a Debye-Huckel approximation.[15] Based on this model, Van der Gucht and co-workers reported a phase diagram for a system containing polycation and polyanion with equal charge and chain length.[5] Various improvements of the Voorn-Overbeek model have been reported, but a detailed comparison with experiment has not been made.[16-19]

Experimentally, a few studies have been carried out to investigate the phase diagram and the binodal compositions. Chollakup et al. determined the phase boundaries between solution, coacervate and precipitate for poly(acrylic acid) (PAA) and poly(allylamine hydrochloride) (PAH) mixtures, varying an extensive range of factors, including charge mixing ratio, polymer concentration, ionic strength, pH and temperature.[1] Spruijt and co-workers studied the binodal compositions of coacervate complexes from poly(N,N-

dimethylaminoethyl methacrylate) (PDMAEMA) and fluorescently labeled PAA.[2] The polymer chain length and salt concentration were mainly discussed in their work, but the mixing ratio was always equal to unity. All these studies are based on two oppositely charged polymers with equal chain length and charge. This makes the phase diagram symmetric with respect to an excess of either polycation or polyanion. In many cases, however, coacervate complexes from polyelectrolytes may be asymmetric in terms of chain length and charge density. Early studies on such asymmetric polyelectrolyte complexes based on a long host polymer and shorter guest polymers with opposite charges were carried out by Tsuchida and Kabanov.[20-23] The shorter polyions were found to attach to part of the long polyion chains under non-stoichiometric mixing ratios to form soluble polyelectrolyte complexes with a neutralized domain. The structure, size and kinetics, and the effect of salt thereon were studied systematically, but no phase behavior and quantitative information about binodal compositions were included in these studies. In this chapter, we make a new contribution to understand the phase separation of asymmetric polyelectrolyte mixtures. We study an extreme case, in which the polyanion is a supramolecular metal coordination polymer, which can adjust its molar weight distribution reversibly. Previously, we have shown that such coordination polymers can form complexes with polycation-neutral diblock copolymers, leading to metal-containing complex coacervate micelles. Here, we study bulk complexation with homo-polyelectrolytes. We will show that the asymmetry between the two polyelectrolytes leads to a strong asymmetry in the phase diagram.

## 6.2 Experimental section

**Materials**

Poly(N,N-dimethylaminoethyl methacrylate), PDMAEMA was obtained from Polymer Source Inc. ($M_w/M_n$= 1.06, $M_w$= 17.0 k, N = 108). The bisligand compound 1,11-bis(2,6-dicarboxypyridin-4-yloxy)-3,6,9-trioxaundecane ($L_2EO_4$) was prepared according to literature.[24] $Zn(NO_4)_2{\cdot}4H_2O$, $NiCl_2{\cdot}6H_2O$ (analytical grade), 3-(Trimethylsilyl) propanoic-2,2,3,3-$d_4$ acid sodium salt (TSP, 98% D) and deuterium oxide (99% D) were purchased from Aldrich and used without further purification.

**Preparation of the mixture**

All the stock solutions were prepared in $D_2O$ and the pH was adjusted to 5 ± 0.2 with DCl or NaOD. The PDMAEMA at pH 5 is assumed to be protonated completely.[2] The mixing

ratio between Zn-$L_2EO_4$ and PDMAEMA is presented as the mole fraction of negative charge, $f$ -, which is defined as follows:

$$f\text{-} = \frac{[\text{-}]}{[\text{-}]+[+]} \tag{1}$$

where [-] and [+] are the molar charge concentrations of charged units on Zn-$L_2EO_4$ and PDMEAEMA. The positive charge fraction is: $f + = 1 - f$ -. For mixtures at $f$ - < 0.5, the concentration of PDMAEMA is fixed at 9.0 g/L, while Zn-$L_2EO_4$ increases from 0 to the charge stoichiometry. For mixtures at $f$ - > 0.5, the coordination polymer concentration is fixed at 25.32 g/L and PDMAEMA is increased gradually. We kept the M/L at 1:1 (unless stated otherwise), the total volume at 4 ml and the salt concentration (including counter ions) at 0.1 ± 0.01 M, adjusted with NaCl. For the mixtures with varying M/L ratios, the concentration of PDMAEMA was kept constant at 9.0 g/L and either the amount of ligand or $Zn^{2+}$ were doubled.

In a typical mixing procedure, ligand and PDMAEMA are mixed first, providing a transparent solution. Upon adding $Zn^{2+}$ into the mixture, the solution becomes turbid immediately. The mixture was then shaken vigorously and sonicated for 10 minutes to mix well. After about 5 hours, the solution became transparent again and the polyelectrolyte complexes had sedimented to the bottom of the cell, either as solid precipitate or as liquid coacervate complexes. The phase separated mixture was centrifuged gently at 3000 g for 5 minutes after 3 days, then left to equilibrate further for another 3 days at room temperature. Both the dilute phase and the coacervate phase were transparent before analysis. To test whether the order in which the components are mixed plays a role, we have compared different mixing protocols for the sample prepared at $f$ - = 0.5. In all cases, we found very similar compositions of the coexisting phases.

**Analysis of the separated phases**

The mixture separated into two clear phases after a few days. The top phase was transferred carefully with a graduated pipet and its volume was determined. The concentrated phase was dissolved in $D_2O$ containing 1M NaCl. The two phases were both analyzed quantitatively with $^1$H-NMR to obtain the concentrations of PDMAEMA and $L_2EO_4$ and inductively coupled plasma atomic emission spectrometry (ICP-AES) to obtain the $Zn^{2+}$ concentration.

The chemical structures of PDMAEMA and bisligand are shown in Scheme 6.1, and the characteristic protons for tracing polymer (amino groups) and ligand (pyridine ring) in $^1$H-NMR spectra are labeled with a star. The spectrum of the mixture of PDMAEMA and Zn-$L_2EO_4$ coordination polymers shows easily distinguished peaks for polymer and ligand respectively (Appendix). With TSP [3-(Trimethylsilyl) propanoic-2,2,3,3-$d_4$ acid sodium salt, 98% D] as quantitative internal standard, we then obtain the PDMEAEMA and ligand concentrations from the peak integrals. All the $^1$H-NMR measurements were carried out at 298 K on a Bruker AMX-400 spectrometer (400 MHz). The $Zn^{2+}$ concentration in the two phases is determined by ICP-AES (Varian, Mulgrave, Australia). The complexes in solution need to be dissociated in advance. Typically, 0.5 ml solution from the dilute or concentrated phase is added into 9.5 ml 1.4 M $HNO_3$ solution, in which all the complexes in the mixture are assumed to be destroyed completely. For our method, the relative error in the calculated concentrations is estimated by summation of the relative errors from determining the volumes, weights of the components (1.6%), mixing ratio (2%), and integrals from $^1$H-NMR spectra (2%).

Dynamic light scattering (DLS) was used to characterize the coacervation process and structures of the polyelectrolyte complexes. The DLS measurement was performed at an angle of 90 degrees with an ALV light scattering-apparatus, equipped with a 400 mW argon ion laser operating at a wavelength of 532.0 nm. All measurements were performed at room temperature. The size and size distribution are presented as the diffusion coefficient obtained from both CUMULANT and CONTIN methods.

## 6.3 Results and discussion

**Observation of phase separation and coacervate complexes**

The structure of Zn-$L_2EO_4$ coordination complexes has been studied systematically previously.[25] At a metal to ligand ratio M/L 1:1, the coordination complexes form small rings and short linear oligomers coexisting in the solution (Scheme 6.1). Both these structures are reversible and can change between each other depending on the environmental factors. In general, the fraction of linear coordination polymers increases with increasing total concentration and temperature. In previous studies on complex coacervate core micelles formed with these coordination complexes, we found that micelles could be obtained even at very low concentration, where the coordination complexes in solution only form small rings and short oligomers.[26] However, in the

absence of metal ions no micelles were formed, even though the free ligand molecules have more negative charges than the oligomers formed at M/L=1.[26] This indicates that the cationic polymer chains must facilitate the growth of the coordination complexes into longer chains. The explanation that was given for this chain growth is that the coordination structures gather around the charged blocks during mixing, resulting in a high local concentration of the coordination complexes, enabling them to grow into longer linear structures.[27]

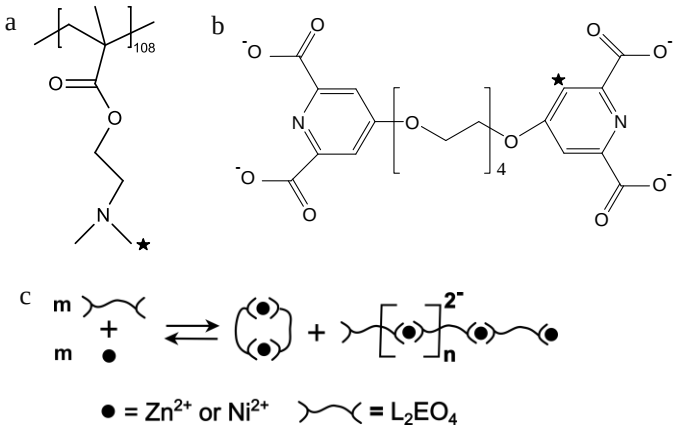


Scheme 6.1 a, b: Structure of PDMAEMA and $L_2EO_4$; the star signs represent the characteristic protons used for analyzing polymer and ligand in $^1$H-NMR spectra. c: Illustration of reversible coordination structures of M-$L_2EO_4$.

In the present study, the concentration of coordination complex is about a hundred times higher than the concentration in the micellar systems. Upon mixing with oppositely charged PDMEAEMA, the Zn-$L_2EO_4$ coordination complexes are expected to form linear coordination polymers with negative charges distributed equally on the chain (Figure 6.1). In our experiments, we found that mixing any two of the three components without the third one did not lead to phase separation, indicating that the complexation requires both electrostatic attraction and coordination.

Since $Zn^{2+}$ ions are colorless, it is difficult to visualize the coacervate phase separation with Zn-$L_2EO_4$ complexes. As an alternative, we use $Ni^{2+}$ as the metal ion, which gives the coacervate a green color. Two clear phases are shown in Figure 6.1a (M/L = 1/1, $f_-$ = 0.5). The top phase contains salt ions and a small amount of polyelectrolytes, so it is almost colorless. The bottom phase, by contrast, has a green color, indicating a high nickel

concentration in the coacervate. The coacervate complexes are transparent, liquid-like but with a high viscosity, for the complexes from both the Ni-$L_2EO_4$ (Figure 6.1c) and Zn-$L_2EO_4$ (Figure 6.1d) coordination polymers. This gel-like appearance is quite similar to that of coacervate complexes formed by pure organic polyelectrolytes.[2]

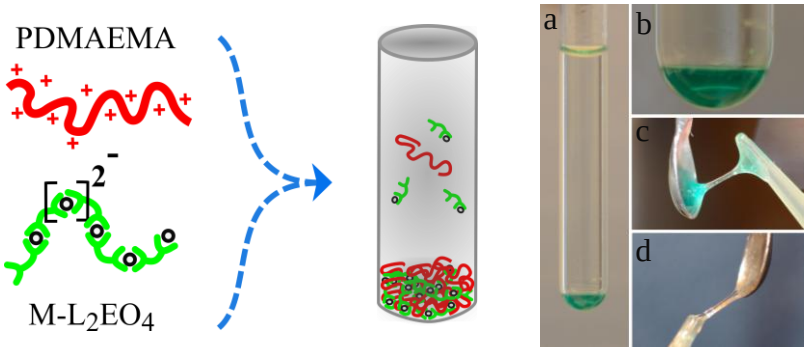


Figure 6.1 Left: Schematic illustration of the coacervate phase separation of PDMAEMA and M-$L_2EO_4$ (M = $Zn^{2+}$, $Ni^{2+}$) mixture. Right: Pictures of the phase separation and coacervate complexes with Ni-$L_2EO_4$ (a, b, c) and Zn-$L_2EO_4$ (d) coordination polymers. M/L is fixed at 1/1, and charge mixing ratio (equation 1) *f* - is 0.5.

**Phase diagram and composition of the complexes**

Figure 6.2a shows the complex coacervate phase diagram that summarizes the binodal concentrations of PDMAEMA and Zn-$L_2EO_4$ in the dilute and concentrated phase at different charge mixing ratios. The overall M/L ratio is fixed at 1/1, and the salt concentration is controlled at 0.1 ± 0.01M and assumed to be equal in both phases. The concentrations of PDMAEMA and Zn-$L_2EO_4$ polymers in the two phases are represented as the charge concentrations. Coexisting phases are connected by tie lines in the region where a liquid coacervate phase coexists with a dilute phase. Above this two-phase region, where there is an excess of polycation, there is only one phase which is a transparent solution. For excess coordination polymer, however, a solid precipitate is found when the amount of polycation is too low. Note that all these measurements are carried out for overall concentrations limited to the square area shown in Figure 6.2, since the coordination polymer is not soluble above 0.1mol/L. The phase diagram is asymmetric: the two-phase region extends further below the diagonal dash line that indicates charge stoichiometric mixing than above it. This means that the coacervate phase is more stable

towards an excess coordination polymer than towards an excess of polycation. The $Zn^{2+}$ and ligand concentrations in the two phases were measured separately, and all the Zn-$L_2EO_4$ coordination complexes in both top and coacervate phases have a M/L ratio around 1/1.

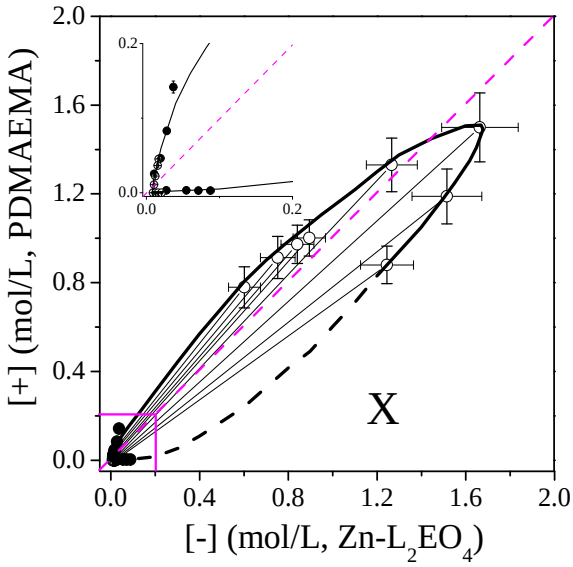


Figure 6.2 Phase diagram of the associative phase separation between PDMAEMA and Zn-$L_2EO_4$ coordination complexes. The filled dots are the phase boundaries obtained from Figure 6.3. The magenta dashed line represents the charge stoichiometry and the square indicates the range in which experiments were carried out. The inset is a magnification of the lower left region in Figure 6.2 (low concentrations in dilute phase). In the region marked X, a solid precipitate is formed due to the limited solubility of the coordination polymer.

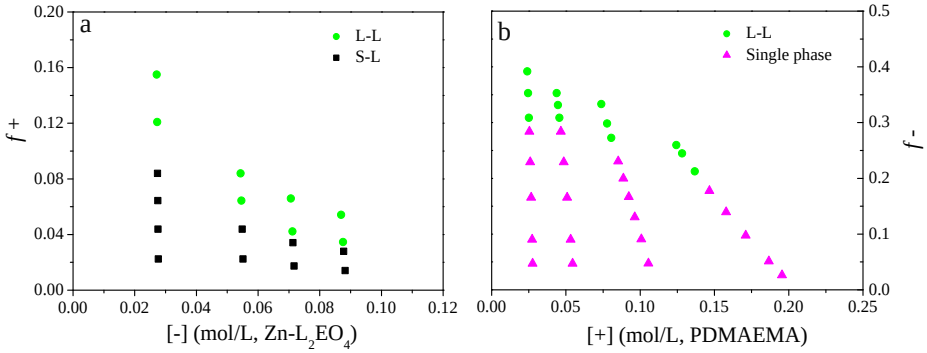


Figure 6.3 Phase boundaries determined by titration tests. a: Adding PDMAEMA to a Zn-$L_2EO_4$ solution. b: Adding Zn-$L_2EO_4$ to a PDMAEMA solution. The concentration of the component is represented as charge concentration. S-L: solid (precipitate) liquid phase separation; L-L: liquid-like coacervate complexes separated from solution.

To estimate the phase boundary in the lower-left region of the phase diagram more precisely, we carry out titrations from two sides: adding PDMAEMA to a Zn-$L_2EO_4$ solution and the other way around. We first consider adding PDMAEMA to a Zn-$L_2EO_4$ coordination polymer solution (Figure 6.3a). At all the tested concentrations, adding PDMAEMA leads to precipitation if the positive charge fraction $f$ + exceeds a certain value, which varies from 4% ~ 10% with decreasing Zn-$L_2EO_4$ concentration. This part is indicated as S-L phase separation in Figure 6.3a. Apparently, the complexes formed under conditions of excess coordination polymer are poorly soluble. However, upon increasing the PDMAEMA concentration further, the complex phase becomes liquid, and we enter the liquid-liquid phase separation region. The phase boundary between the S-L and L-L regions are shown in Figure 6.2 as filled circles.

The situation is rather different for conditions of excess polycation. Adding Zn-$L_2EO_4$ coordination polymers to a PDMAEMA solution does not lead to phase separation until the fraction of negative charges $f$ - reaches approximately 0.3. Beyond this the solution is not stable. It first becomes turbid and then separates into two liquid phases after a few hours. From Figures 6.3a and 6.3b we see that liquid-liquid phase separation occurs roughly between $f$ - values between 0.3 and 0.9. This range becomes wider as the concentration increases. This means that it is more favorable to form liquid-like coacervate complexes at higher concentrations of the components.

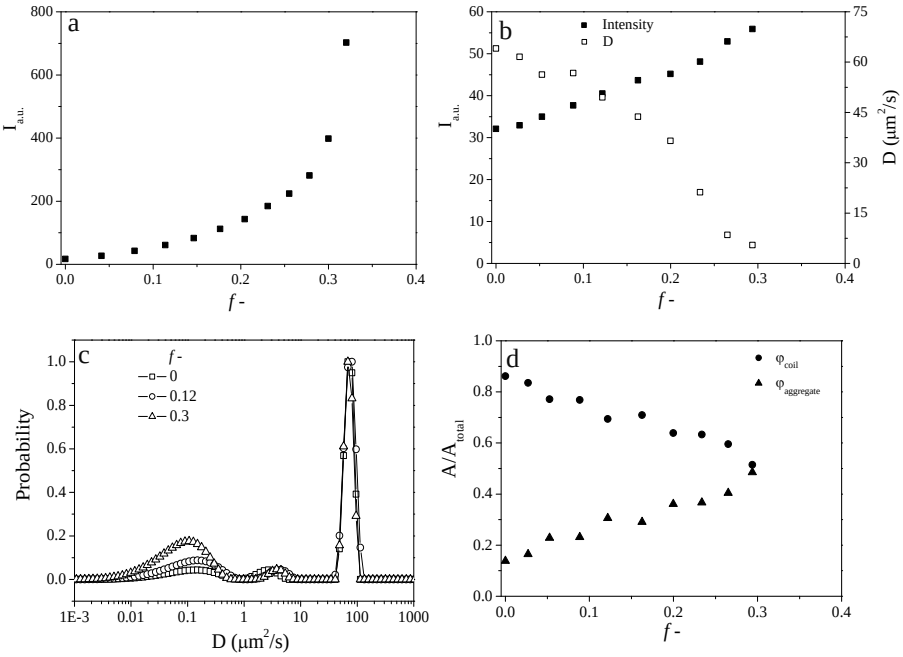


Figure 6.4 Variations of light scattering intensity and diffusion coefficient upon adding Zn-$L_2EO_4$ coordination complexes into PDMAEMA solution at $f$ - < 0.3. a: $C_{PEMAEMA}$ 9g/L. b: $C_{PEMAEMA}$ 0.9g/L. c: CONTIN analysis of the size distribution of the titration performed at $C_{PEMAEMA}$ 0.9g/L. d: Contributions of the polymer coils and coil aggregates to the light scattering intensity, represented as the relative area fraction of the CONTIN peaks attributed to coil (D: 20 - 160 $\mu m^2$/s) and aggregates (D < 10 $\mu m^2$/s).

What is the structure of the single-phase solution in the excess polycation region, at $f$ - < 0.3? We used DLS to characterize the titration process. Figure 6.4a shows the variation of the light scattering intensity upon adding Zn-$L_2EO_4$ to the PDMAEMA solution. The PDMAEMA concentration is 9 g/L. The intensity first increases gradually with increasing Zn-$L_2EO_4$ concentration and then shoots up at $f$ - ~ 0.3, confirming the phase boundary found in Figure 6.3b. At this high concentration, which is above the overlap concentration, it is not possible to determine the size of the formed complexes.[28] We therefore repeat the titration at a concentration which is 10 times lower. The polymer coils under this condition (0.9 g/L, pH 5, 0.1 ± 0.01 M) show a diffusion coefficient around 64 $\mu m^2$/s (Figure 6.4b), which corresponds to a coil size of approximately 3 nm according to the Stokes-Einstein equation. The size increases with increasing Zn-$L_2EO_4$ amount and big aggregates show up

at $f$ - ~ 0.3. At the same time the light scattering intensity increases gradually. This indicates the formation of complexes already before the binodal composition is reached. In the studies of Tsuchida and Kabanov, soluble complexes formed if the long chain partly aggregated with short guest chains under non-stoichiometric mixing condition.[20-23] Here, similar structures may be formed, in which the Zn-$L_2EO_4$ complexes partly decorate the cationic polymer chains, while the excess, uncompensated positive charges stabilize the complexes in solution. Only at higher concentrations of Zn-$L_2EO_4$, where most of the cationic charge is compensated, can the complexes aggregate to form a macroscopic coacervate phase.

CONTIN analysis shows two peaks in the distribution of diffusion coefficients (Figure 6.4c). We attribute the peak at diffusion coefficients between 20 - 160 $\mu m^2/s$ to partly decorated PDMAEMA coils and the peak at lower diffusion coefficient to large aggregates, consisting of aggregated complexes. The relative contributions to light scattering intensity of these two kinds of objects are summarized in Figure 6.4d. Clearly, the number of partly decorated coils decreases, while the contribution of large aggregates increases with increasing Zn-$L_2EO_4$ amount.

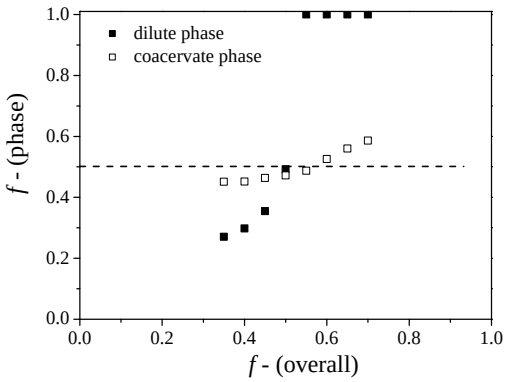


Figure 6.5 Charge fraction of Zn-$L_2EO_4$ coordination complexes in dilute phase and coacervate phase as a function of overall charge mixing ratio.

The charge stoichiometry of the two different phases is shown in Figure 6.5. It is clear from this figure that the negative charge fraction in the dilute phase varies much more with the overall mixing ratio than the charge fraction in the coacervate phase, which remains around 0.5 for all the coacervate complexes formed with overall mixing ratio varying from

0.35 to 0.7. This means that the coacervate phase has a tendency to select a matching proportion between the charged components, while most of the excess components are expelled to the dilute phase. A similar selectivity has been reported in layer-by-layer structures containing Fe-$L_2EO_4$ coordination complexes, where they found that the coacervate multilayer always chose the charged components to match stoichiometry.[29]

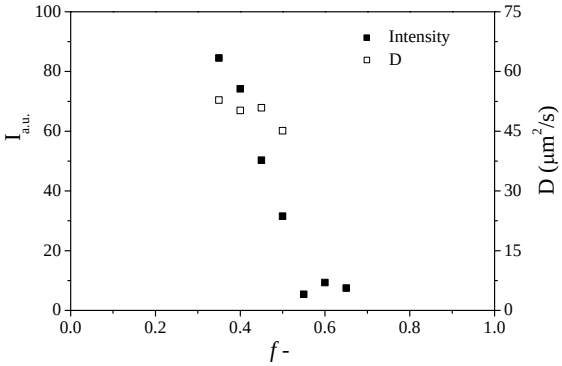


Figure 6.6 Light scattering analysis of the top solutions at different overall charge mixing ratio.

Due to the selectivity of the coacervate phase, the dilute phase contains mostly the excess charged components if the overall charge ratio is not 0.5. The dilute solutions are analyzed with DLS and the results are shown in Figure 6.6. At $f$ - > 0.5, excess of Zn-$L_2EO_4$ complexes are in the dilute solution. The light scattering intensity is very low, indicating only soluble and small structures in the solution. This is consistent with previous findings that Zn-$L_2EO_4$ only forms small rings and short oligomers at low concentration without oppositely charged blocks.[25] On the other side, with excess of PDMAEMA in the solution, we find soluble structures with a diffusion coefficient around 50 $\mu m^2$/s, which is similar to the size of PDMAEMA coils or partly decorated coils found when Zn-$L_2EO_4$ was added to the PDMAEMA solution at $f$ - < 0.3 (Figure 6.4b).

**Composition of the complexes with varying M/L ratio**

Zn-$L_2EO_4$ coordination complexes respond not only to the overall concentration, but also to the metal to ligand ratio, M/L. Long chains are only formed when the M/L ratio is close to 1. [25] At different ratios, either ligand or $Zn^{2+}$ acts as a chain growth stopper, leading to shorter structures (see Scheme 6.2). This is confirmed by viscosity measurements in

previous studis.[25] In the present system, we also varied the M/L ratio to see whether this affects the complex coacervation process.

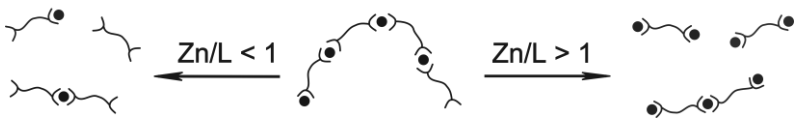


Scheme 6.2 Schematic drawing of the structure changes of Zn-$L_2EO_4$ coordination complexes with varying M/L.

The PDMAEMA concentration is still fixed at 9 g/L, and either ligand or Zn concentrations are doubled. As shown in Figure 6.7a, the M/L ratio in the two phases responds differently to the overall M/L ratio. In the coacervate phase the M/L ratio deviates only slightly from 1/1 at all overall M/L ratios. By contrast, in the dilute phase, the M/L ratio changes dramatically upon varying the overall M/L ratio. The charge ratio, shown in Figure 6.7b, shows a similar dependence. This confirms that the coacervate phase indeed selects all the components around the right stoichiometry even when the overall M/L is not optimal for forming coordination polymers.

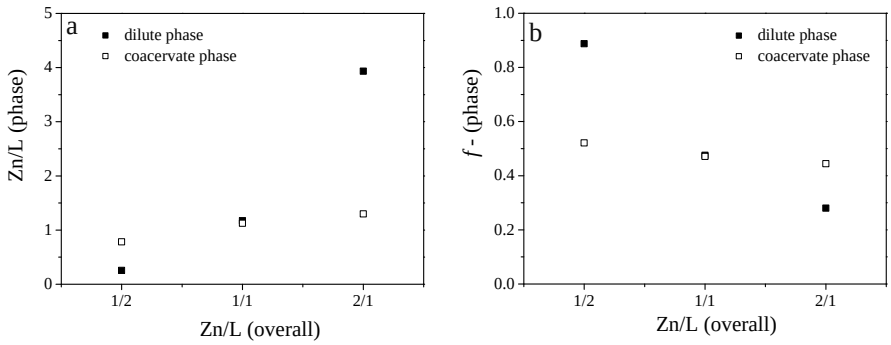


Figure 6.7 Zn/L ratio (a) and charge fraction (b) in the dilute and coacervate phases at different overall mixing M/L ratio.

**Asymmetry of the system**

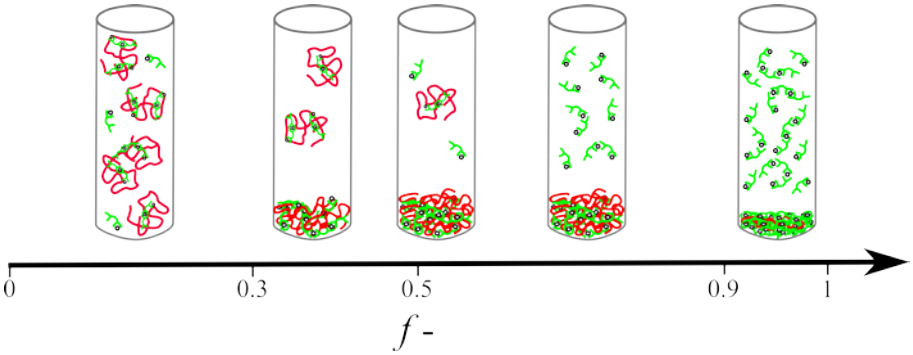


Scheme 6.3 Schematic illustration of the asymmetry of mixtures at different charge mixing ratios represented as the negative charge fractions. Counter ions and charges are not shown in the scheme.

Upon mixing PDMAEMA and reversible Zn-$L_2EO_4$ coordination polymers in solution, we have found an asymmetric phase diagram: the coacervate phase tolerates excess coordination polymer better than excess polycation. This asymmetry arises because the coordination polymer can dissociate into smaller structures in the excess phase. As shown in Scheme 6.3, the dilute phase contains only a small amount of polyelectrolytes under charge stoichiometry ($f$ - 0.5). Upon increasing the amount of polycation ($f$ - < 0.5), the excess cationic polymers in the dilute phase attract more coordination complexes from the coacervate phase, which destabilizes the complex coacervate phase. Once the amount of polycation reaches the critical amount ($f$ - ~ 0.3), the coacervate phase disappears completely and the two phases merge into one single phase, which contains soluble cationic polymer coils partly decorated with Zn-$L_2EO_4$ complexes. By contrast, an excess of coordination complexes does not affect the coacervate phase very much. The excess Zn-$L_2EO_4$ complexes in the dilute phase form only small structures in the absence of polycations. Apparently, these small structures are not strong enough to attract polycations into the dilute phase, so the coacervate phase remains stable in a wide range on this side ($f$ - 0.5 ~ 0.9). Only when the amount of coordination complexes is increased to $f$ - > 0.9 does the liquid coacervate phase destabilize, forming poorly soluble complexes that sediment as a solid precipitate.

## 6.4 Conclusion

We have seen that coacervates of a cationic polymer and a reversible anionic coordination supramolecule have an asymmetric phase diagram: the coacervate complex phase tolerates an excess of coordination polymer much more than an excess of the homopolymer. This observation is completely different from coacervates in which the polycation and polyanion have an equal chain length and also an equal effect on coacervate stability. We believe that our result helps to understand asymmetric coacervation, which is more relevant for practical situations, since most coacervations in nature and in applications are based on asymmetric polyelectrolytes. Moreover, we found that the reversible nature of the coordination polymer helps the coacervate to select the right amount of the three components under non-stoichiometric mixing. Both the metal to ligand ratio (M/L ≈ 1) and charge ratio ($f$ - ≈ 0.5) in the coacervate phase are around the stoichiometry and the excess components just stay in the dilute phase. This may help to simplify the procedure for preparing coacervate complexes, since the overall mixing ratio is not crucial anymore in asymmetric systems.

## References


1. Chollakup, R.; Smitthipong, W.; Eisenbach, C. D.; Tirrell, M. *Macromolecules* **2010**, *43*, 2518–2528.
2. Spruijt, E.; Westphal, A. H.; Borst, J. W.; Cohen Stuart, M. A.; van der Gucht, J. *Macromolecules* **2010**, *43*, 6476–6484.
3. Bungenberg-de Jong, H.; Kruyt, H. *Proc. Sect. Sci., K. Ned. Akad. Wetenschappen* **1929**, *32*, 849–856.
4. Dautzenberg H. *Macromolecules* **1997**, *30*, 7810–7815.
5. van der Gucht, J.; Spruijt, E.; Lemmers, M.; Cohen Stuart, M. A. *J. Colloid Interface Sci.* **2011**, *361*, 407–422.
6. van der Burgh, S.; Cohen Stuart, M. A. *Langmuir* **2004**, *20*, 1073–1084.
7. Voets, I. K.; de Keizer, A.; Cohen Stuart, M. A. *Adv. Colloid Interface Sci.* **2009**, *147-148*, 300–318.
8. Harada, A.; Kataoka, K. *Macromolecules* **1995**, *28*, 5294-5299.
9. Kabanov, A. V.; Bronich, T. K.; Kabanov, V. A.; Yu, K.; Eisenberg, A. *Macromolecules* **1996**, *29*, 6797-6802.
10. Imura, T.; Yanagishita, H.; Kitamoto, D. *J. Am. Chem. Soc.* **2004**, *126*, 10804–10805.
11. Hofs, B.; de Keizer, A.; van der Burgh, S.; Leermakers, F.; Cohen Stuart, M. A.; Millard, P. E.; Muller, A. *Soft Matter* **2008**, *4*, 1473–1482.

12. Lemmers, M.; Sprakel, J.; Voets, I.; van der Gucht, J.; Cohen Stuart, M. A. *Angew. Chem., Int. Ed.* **2010**, *49*, 708–711.
13. de Vos, W. M.; Kleijn, J. M.; de Keizer, A.; Cohen Stuart, M. A. *Angew. Chem., Int. Ed.* **2009**, *48*, 5369–5371.
14. Tong, W.; Gao, C. Y. *J. Mater. Chem.* **2008**, *18*, 3799–3812.
15. Overbeek, J.; Voorn, M. *J. Cell. Comp. Phys.* **1957**, *49*, 7–26.
16. Borue,V.; Erukhimovich, I.Y. *Macromolecules* **1990**, *23*, 3625–3632.
17. Castelnovo, M.; Joanny, J.-F. *Langmuir* **2000**, *16*, 7524–7532.
18. Popov, Y. O.; Lee, J.; Fredrickson, G. H. *J. Polym. Sci., Part B: Polym. Phys.* **2007**, *45*, 3223–3230.
19. Lee, J.; Popov, Y. O.; Fredrickson, G. H. *J. Chem. Phys.* **2008**, *128*, 224908-1–224908-13.
20. Tsuchida, E.; Osada, Y.; Sanada, K. *J. Polym. Sci., Polym.Chem. Ed*. **1972**, *10*, 3397-3404.
21. Tsuchida, E.; Osada, Y.; Ohno, H. *J. Maccromol. Sci.* **1980**, *B17* (4), 683-714.
22. Kabanov, V. A.; Zezin, A. B. *Soviet Sci. Rev., Sect. B, Chem.Rev*. **1982**, *4*, 207-282.
23. Kabanov, V. A.; Zezin, A. B. *Pure & Appl. Chem.* **1984**, 56, 343-354.
24. Vermonden, T.; Branowska, D.; Marcelis, A. T. M.; Sudholter, E. J. R. *Tetrahedron* **2003**, *59*, 5039-5045.
25. Vermonden, T.; van der Gucht, J.; de Waard, P.; Marcelis, A. T. M.; Besseling, N. A. M.; Sudholter, E. J. R.; Fleer, G. J.; Cohen Stuart, M. A. *Macromolecules* **2003**, 36, 7035-7044.
26. Yan, Y.; Besseling, N. A. M.; de Keizer, A.; Marcelis, A. T. M.; Drechsler, M.; Cohen Stuart, M. A. *Angew. Chem. Int. Ed.* **2007**, *46*, 1807-1809.
27. Yan, Y.; Besseling, N. A. M.; de Keizer, A.; Cohen Stuart, M. A. *J. Phys. Chem. B* **2007**, *111*, 5811-5818.
28. Mckee, M. G.; Hunley, M. T.; Layman, J. M.; Long, T. E. *Macromolecules* **2006**, 39, 575-583.
29. Lan, Y. R.; Xu, L. M.; Yan, Y.; Huang, J. B.; de Keizer, A.; Besseling, N. A. M.; Cohen Stuart, M. A. *Soft Matter* **2011**, *7*, 3565–3570.

## Appendix

[1]H-NMR spectra of ligand, coordination complex, PDMAEMA and the mixture

$L_2EO_4$

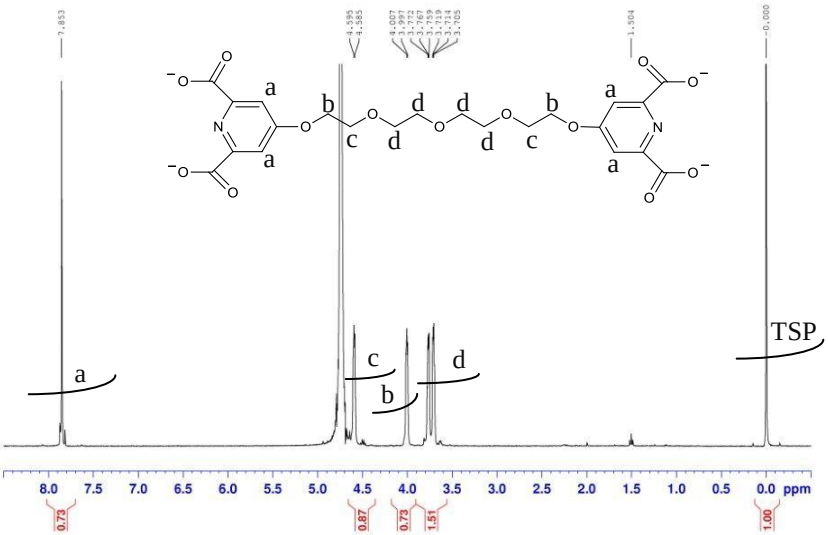


$Zn\text{-}L_2EO_4$

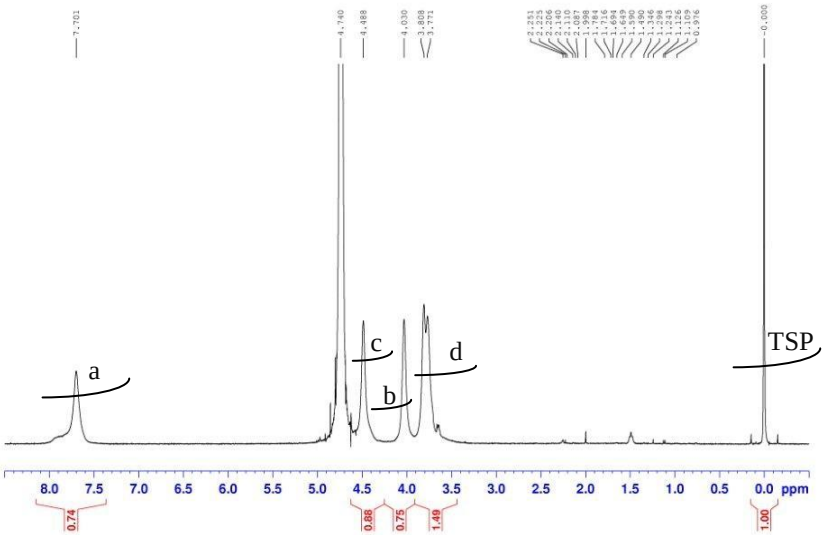

PDMAEMA

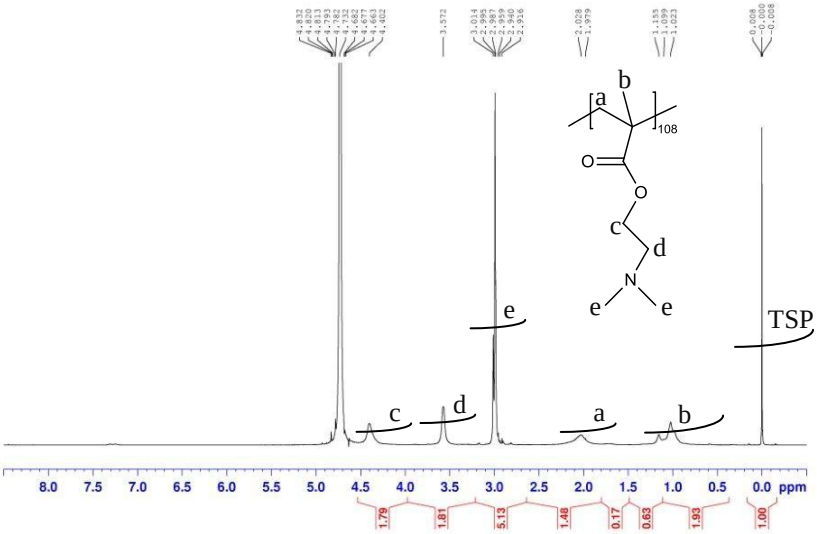


Mixture of Zn-$L_2EO_4$ and PDMAEMA

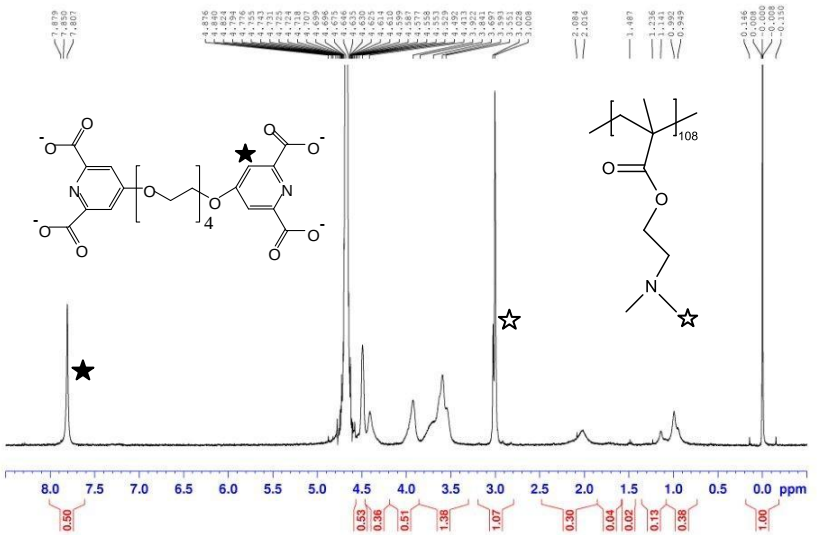


Samples were prepared in $D_2O$ with a controlled pH at 5 ± 0.2 and TSP as an internal standard. All the $^1$H-NMR measurements were carried out at 298 K on Bruker AMX-400 spectrometer (400 MHz). The star signs represent the characteristic protons used for analyzing polymer and ligand in the $^1$H-NMR spectrum of the mixture.

# Chapter 7

## Summary and General Discussion

## 7.1 Summary

Complex coacervate core micelles (C3Ms) have attracted increasing interest since their discovery in the middle of the 90s. The initial studies mainly focused on understanding the formation and structure of such micelles for a variety of polyelectrolytes. More recently, interest has shifted to develop C3Ms with novel properties for potential applications. For example, bio-signal sensitive C3Ms are believed to be good carriers for ionic pharmaceuticals, such as hydrophilic drugs, DNA and RNA.[1] Another attractive direction is combining organic polyelectrolytes together with coordination complexes, leading to C3Ms with metal ions in the core. The formed micelles are called metal containing complex coacervate core micelles (M-C3Ms) in this thesis, and we focus on their properties and their potential as imaging probes.

Magnetic Resonance Imaging (MRI) contrast agents are chemical compounds that are able to markedly short the relaxation times of water protons in tissues where they are distributed. Modern MRI examinations are performed widely with the use of contrast agents. Based on the different effects on the relaxation process, contrast agents can be divided into $T_1$ and $T_2$ contrast agents.[2] $T_1$ contrast agents mainly shorten the longitudinal (spin-lattice) relaxation time, and are usually complexes of paramagnetic metal ions, such as Fe(III), Mn(II), and Gd(III).[3-5] By contrast, $T_2$ contrast agents, such as superparamagnetic iron oxide, mainly shortens the transverse (spin-spin) relaxation time.[6] The efficiency of contrasts agents is presented as relaxivity $r_1$ or $r_2$, which is the ability to shorten the relaxation time per millimolar of the contrast agent.

In **Chapter 2** we focus on iron-containing C3Ms and study their formation and stability. Fe-C3Ms formed optimally at stoichiometric charge mixing ratio and are quite stable in time at room temperature. However, the micelles show a strong response to ionic strength: the scattering intensity decreases upon increasing salt concentration. This decrease is due to both a decrease in the number of micelles (or an increase in CMC) and a decrease in aggregation number. The salt dependence of the CMC and the aggregation number is explained using a scaling argument for C3M formation. Compared to Fe(II)-C3Ms, Fe(III)-C3Ms have a lower CMC and a higher stability against dissociation by added salt.

In **Chapter 3**, we study how these iron-containing micelles respond to pH. The hydrodynamic radius of Fe(III)-C3Ms is determined mainly by the corona and does not change very much in a broad pH range. The Fe(III)-$L_2EO_4$ complexes in the micellar core

form striped structures and the core shape changes from spherical shape (pH 4) to elongated shape (pH 5 - 7), and a mixture of elongated and branched structures (pH 8). The relaxation measurements indicate that the relaxivity $r_1$ of Fe(III)-C3Ms decreases from 2.5 to 0.5 $mM^{-1}$ $s^{-1}$ when the pH increases from 2 to 8. The low relaxivity is due to the strong binding between the ligand and $Fe^{3+}$ ions, which induces a strong crystal field around the metal ions and forces them into a low spin state. The strong pH effect on the relaxivity must be due to the binding of hydroxide ions.

**Chapter 4** presents a stable micelle system. The aim is to improve the stability of M-C3Ms, especially for the micelles based on transition metal ions. The dependence on ionic strength of M-C3Ms is due to the electrostatic driving force, which can be screened with increasing salt concentration. Hence, to avoid this salt-sensitivity, an alternative driving force for micellization is needed. To achieve this, we develop a diblock copolymer with ligand groups grafted covalently to one of the blocks. Added metal ions cross-link the ligand-carrying blocks together, while the hydrophilic blocks protect the formed coordination complex, leading to the formation of micelles. The micellization is based on strong coordination bonds between ligand and metal ions. The formed micelles show a high stability; adding salt and EDTA hardly affect the structures. The new modified diblock copolymers were mixed with different metal ions ($Zn^{2+}$, $Ni^{2+}$, $Mn^{2+}$, $Gd^{3+}$), and they all formed micelles, demonstrating the general applicability of this method for making stable metal containing polymer micelles.

In **chapter 5**, we study the formation and properties of combined Eu/Gd-C3Ms. Europium(III) is one of the most popular luminescent lanthanides for optical imaging, while gadolinium(III) based complexes are widely applied as MRI contrast agent since the metal ion has seven unpaired electrons, a large magnetic moment and low electronic relaxation.[7] By making a bimodal imaging probe, we hope to combine the high resolution of MRI and the high sensitivity of optical imaging together. Compared with transition metal ions ($Zn^{2+}$, $Fe^{2+/3+}$ …), lanthanide metal ions have nine coordination sites, so they can form branched structures with $L_2EO_4$ ligand at metal to ligand ratio 2/3. The branched structure seems to provide a strong stability against ionic strength: the formed Eu/Gd-C3Ms respond hardly to salt concentration up to 500 mM NaCl. Varying the Eu/Gd ratio does not change the micellar size but changes the luminescent emission intensity and the magnetic relaxation rate according to the $Eu^{3+}$ and $Gd^{3+}$ amount in a linear manner, indicating that Eu/Gd-C3Ms are highly tunable between luminescence and relaxation. The

stability of Eu/Gd-C3Ms is investigated further by putting micelles into different buffer solutions with different pH, salt concentration and competition ligand EDTA, and then record the decay of luminescence and relaxation rate over time. There is no decay over a period of 5 days. The light scattering and Cryo-TEM confirm that there is no change in micelle size and structure over this period. The high stability and tunability suggest great potential of Eu/Gd-C3Ms for use as bimodal imaging probes.

**In chapter 6**, we investigate the phase behaviour of metal containing coacervate complexes. This more fundamental research gives additional information about the stability of metal-containing coacervate complexes, which is helpful to develop new structures based on electrostatic interaction. The cationic polymer PDMAEMA has a fixed chain length, while the coordination polymer has a variable chain length depending on the environmental conditions. This difference between the two polymers leads to an asymmetric phase diagram: the coacervate complex phase tolerates an excess of coordination polymer much more than an excess of the homopolymer. The compositions of the complexes in both phases are studied. It turns out that the coacervate complex tends to choose the right amount of the three components under non-stoichiometric mixing. Both the metal to ligand ratio (M/L ≈ 1) and charge ratio ($f$ - ≈ 0.5) in the coacervate phase are around the stoichiometry, and the rest of the components just stay in the dilute phase.

## 7.2 General discussion

As a new category of coacervate micelles, M-C3Ms has been studied in this thesis. We mainly focus on paramagnetic metal ions, such as Fe(III), Gd(III) and luminescent lanthanides, such as Eu(III). The aim is to investigate the potential of these M-C3Ms for application as imaging contrast agents. In general, a good contrast agent should meet a few crucial requirements: [2,6,8]

1. high water solubility and good biocompatibility;
2. high thermodynamic stability and kinetic inertness: there should be no leakage of lanthanides or exchange with other metal ions in vivo , since free lanthanides are toxic;
3. high efficiency of gathering around tumor tissue, which can be achieved by introducing reactive moieties on the surface of the contrast agent.
4. for MRI contrast agents, a high relaxivity is desirable, because this means that a smaller dosage is needed for MRI examination, resulting in less toxicity and side effects.

However, it is quite difficult to develop one system that fulfills all these requirements, since these requirements all ask for different design strategies that partly contradict. For example, a higher stability for a MRI contrast agent is achieved by a full coordination of the metal ions with the ligand groups, but this makes the metal ion less accessible for water and leads to a lower relaxivity. The reported systems in current studies are therefore always compromises, which have advantages in some aspects but drawbacks in other.

For M-C3Ms, water solubility and biocompatibility are advantages. Fe-C3Ms have been studied systematically, including the formation, stability and relaxation properties. It turns out that both stability and relaxivity of iron micelles need to be improved for practical applications (Chapter 2 and 3). To improve the stability, we developed a new strategy in which ligand groups were grafted covalently to one block of the diblock copolymer, and the micelles form based on coordination directly, providing micelles that are stable against adding salt (Chapter 4). Gd-C3Ms seem very promising as MRI contrast agent due to a high stability and high relaxivity. Combined with Eu(III), Eu/Gd-C3Ms can be a good candidate for bimodal imaging probes. Further in vivo tests on these micelles are worth pursuing. It is also possible to introduce target groups on the surface by modifying the neutral block of the copolymer.[1] So in general, M-C3Ms are of interest for use as imaging contrast agents. Below, we propose some potential directions for future research, on both the fundamental and application aspects.

**Structure of M-C3Ms**

The core of a coacervate micelle consists of a complex coacervate of the two oppositely charged polyelectrolytes. The internal structure of this coacervate core is still poorly understood. Using a metal coordination polymer as one of the polyelectrolytes may have an advantage, because the metal ions provide contrast, which makes it possible to see the micellar core with Cryo-TEM. We have seen a striped structure with Fe(III)-C3Ms, and observed that the micellar core shape changes from spherical to elongated and branched with increasing pH (Chapter 3). Such striped structures were not found with micelles containing other metal ions ($Zn^{2+}$, $Fe^{2+}$, $Gd^{3+}$). We therefore hypothesize that iron hydroxide is involved in these structures, which is also the reason for the decrease of the relaxivity with increasing pH. However, a direct proof of this and an understanding of how these structures form are still lacking. Other techniques, such as WAXS and Mossbauer may be helpful to look deeper into these structures.

The coordination structure of the metal ions in the micellar core is another important issue to investigate, since this is related to the magnetic or luminescent functions. One crucial parameter is the hydration number, referring to the number of water molecule directly coordinated to the metal centre. For MRI contrast agents, the hydration number needs to be balanced because a higher hydration number in general enhances the relaxivity but reduces the stability of the structures. By contrast, for optical imaging probes, a higher hydration number is not favourable for luminescence emission. According to literature, the hydration number of luminescent lanthanide complexes can be obtained by measuring the luminescence lifetimes in water and deuterated water.[9] The same strategy can be applied to Ln-C3Ms, to obtain a better understanding of the structure and properties of these micelles.

The hydration number tests may also help to confirm the hypothesis used widely to explain the formation of M-C3Ms at low concentration of coordination complexes. In Vermonden's work, it was found that $Zn^{2+}$ and $L_2EO_4$ at 1/1 ratio formed small rings and short oligomers at low concentration.[10] These small structures can convert into linear chains with increasing concentration. Later, Yan and co-workers found that the oligomers formed at low concentration could form C3Ms in the presence of oppositely charged diblock copolymers, while free bisligands without metal could not, even though they have more negative charges compared to the oligomers formed at M/L=1/1.[11] This suggests that the oligomers at 1/1 can grow into longer chains upon mixing with cationic blocks due to the high local concentration in the coacervate core.[12] No experimental data confirms this hypothesis yet. Ln-$L_2EO_4$ complexes may have a similar transition from small structures into bigger branched structures during the coacervation. The metal ions in the small structures have more coordination sites occupied by water, so the hydration number of the coordination complexes in absence of the oppositely charged blocks is expected to be bigger than that of the complexes in micelles. By measuring the hydration number in different conditions, it should therefore be possible to observe the proposed structural transition of the coordination complexes during coacervation.

The kinetics of M-C3Ms formation and reorganization is another interesting topic of study. In our experiments, M-C3Ms (M= $Zn^{2+}$, $Fe^{2+/3+}$, $Ni^{3+}$, $Gd^{3+}$, $Eu^{3+}$, $Nd^{3+}$) are formed immediately upon mixing three components together and different orders of addition always give a similar size. This suggests that the micelles are equilibrium structures. However, the exchange between different metal ions within the coordination complexes and micelles has never been studied, even though this is very important, especially for

practical applications. To study this exchange, suitable metal pairs that can be distinguished in a quantitative manner have to be found first. In this regard, spectroscopy (UV, luminescence) or element analysis (ICP) may be useful techniques to carry out the studies on kinetic properties of M-C3Ms.

**Improving the stability of M-C3Ms**

One of the biggest obstacles of C3Ms for application is the low stability against ionic strength. In recent years, much effort has been made to improve the stability of C3Ms. One common way is to introduce a hydrophobic block into the diblock polyelectrolytes, so that the response to ionic strength is reduced by the hydrophobic interaction.[13] Another strategy is to cross-link the micellar core. To achieve this, functional groups (carbon double bond, -COOH, $-NH_2$) need to be introduced to the polymer backbones, that can be cross-linked later.[14,15] For example, Kotaoka and co-workers report a coacervate micelle system with thiol groups in the micellar core.[16] Adding oxygen oxidizes the thiol groups into disulfide bonds, providing micelles with a cross-linked core and high stability. In principle, M-C3Ms can be stabilized in similar ways. The only concern is that the coordination complexes are reversible, especially for the complexes from transition metal ions. The coordination complexes may therefore dissociate into small structures which leak out of the micellar core upon increasing the salt concentration, even though the core is combined with hydrophobic blocks or cross-linked. In chapter 4, we have discussed an alternative strategy, namely to graft ligand groups on the backbone of a diblock copolymer. In this case the micelles are formed directly by coordination bonds, without the need of ionic interactions. The formed micelles indeed show a high stability against ionic strength.

In chapter 5, we found that Gd-C3Ms have a much higher stability against ionic strength than micelles formed from transition metal coordination complexes. We demonstrate that this high stability is due to the branched structure and the high charge density of the coordination complexes. We believe that this strategy is worth pursuing further. As a structure with multiple ligand groups is preferred, star shaped PEO (with shorter arms) modified with ligand groups may be employed. The formed coordination complexes have a net-work structure and higher charge, and should therefore produce more stable M-C3Ms. This method is useful especially for micelles formed with coordination complexes from transition metal ions, since these cannot form branched structures with bisligand.

**Multi functional M-C3Ms**

M-C3Ms were found to contain a few hundred metal ions in the micellar core (Chapter 2 and 5). This gives us the opportunity to combine different metal ions in the micelle, giving multi functional M-C3Ms. We studied Eu/Gd-C3Ms in chapter 5. Eu-$L_2EO_4$ and Gd-$L_2EO_4$ complexes have a similar structure and charge density, and they are both small structures in the absence of oppositely charged polymer. Upon mixing with polyion-neutral diblock copolymer, the fast complexation process brings Eu-$L_2EO_4$, Gd-$L_2EO_4$ or mixed Eu/Gd-$L_2EO_4$ complexes into the micellar core in a proportion that is determined by statistical mixing, leading to micelles with mixed bimetallic coordination complexes in the core. The amount of metal ions and consequently the corresponding functional properties can be adjusted easily. In further studies, other metal ions can be incorporated into the micelle structure. For example, metal ions for imaging probes and therapy can be mixed together and provide visible therapy micelles.[17,18] Since mixed metal ions stay in one micellar core, the distance between different metal ions A and B may be short enough for energy transfer to take place from metal ion A to B.[19] This can be used to measure the degree of mixing of the metal ions in the core and prepare bi- or multi-metallic imaging probe. [20-22]

## References


1. Lee, Y; Kataoka, K. *Soft Matter* **2009**, *5*, 3810–3817.
2. Hermann, P.; Kotek, J.; Kubicek, V.; Lukes, I. *Dalton Trans*. **2008**, 3027-3047.
3. Caravan, P.; Ellison, J. J.; Mcmurry, T. J.; Lauffer, R. B. *Chem. Rev.* **1999**, *99*, 2293-2352.
4. Drahos, B.; Kotek, J. Hermann, P.; Lukes, I.; Toth E. *Inorg. Chem.* **2010**, *49*, 3224-3238.
5. Bottrill, M.; Kwok, L.; Long, N. J. *Chem. Soc. Rev.* **1999**, *99*, 557-571.
6. Na, H. B.; Song, I. C.; Hyeon, T. *Adv. Mater.* **2006**, *25*, 2133-2148.
7. Bonnet, C. S.; Toth, E. *C. R. Chimie* **2010**, *13*, 700-714.
8. Bunzli J. C. G. *Chem. Rev.* **2010**, *110*, 2729-2755.
9. Kimura, T.; Kato, Y. *J. Alloys Compd.* **1995**, *225*, 284-287.
10. Vermonden, T.; van der Gucht, J.; De Waard, P.; Marcelis, A. T. M.; Besseling, N. A. M.; Sudholter, E. J. R.; Fleer, G. J.; Cohen Stuart, M. A. *Macromolecule* **2003**, *36*, 7035-7044.
11. Yan, Y.; Besseling, N. A. M.; de Keizer, A.; Marcelis, A. T. M.; Drechsler, M.; Cohen Stuart, M. A. *Angew. Chem. Int. Ed.* **2007**, *46*, 1807-1809.
12. Yan, Y.; Besseling, N. A. M.; de Keizer, A.; Cohen Stuart, M. A. *J. Phys. Chem. B* **2007**, *111*, 5811-5818.
13. Yuan, X. F.; Harada, A.; Yamasaki, Y.; Kataoka, K. *Langmuir* **2005**, *21*, 2668-2674.
14. Bronich, T. K.; Keifer, P. A.; Shlyakhtenko, L. S.; Kabanov, A. V. *J. Am. Chem. Soc.* **2005**, *127*, 8236-8237.
15. Jaturanpinyo, M.; Harada, A.; Yuan, X. F.; Kataoka, K. *Bioconjugate Chem.* **2004**, *15*, 344-348.
16. Kakizawa, Y.; Harada, A.; Kataoka, K. *J. Am. Chem. Soc.* **1999**, *121*, 11247-11248.

17. Rafique, S.; Idrees, M.; Nasim, A.; Akbar, H.; Athar, A. *Biotechnol. Mol. Biol. Rev.* **2012**, *5*, 38-45.
18. Zielhuis, S. W.; Seppenwoolde, J. H.; Bakker, C. J. G.; Jahna, U.; Zonnenberg, B. A.; Van het Schip, A. D.; Hennink, W. E.; Nijsen, J. F. W. *J. Biomed. Mater. Res., Part A* **2007**, *82A*, 892-898.
19. Charbonniere, L. J.; Hildebrandt, N. *Eur. J. Inorg. Chem.* **2008**, 3241–3251.
20. Zhu, X. J.; Wong, W. K.; Wong, W. Y.; Yang, X. P. *Eur. J. Inorg. Chem.* **2011**, 4651–4674.
21. Matthes, P. R.; Holler, C. J.; Mai, M.; Heck, J.; Sedlmaier, S. J.; Schmiechen, S.; Feldmann, C.; Schnick, W.; Muller-Buschbaum, K. *J. Mater. Chem.* **2012**, *22*, 10179-10187.
22. Deiters, E.; Song, B.; Chauvin, A. S.; Vandevyver, C. D. B.; Gumy, F.; Bunzli, J. C. G. *Chem. Eur. J.* **2009**, *15*, 885–900.

# Samenvatting

Complex coacerate core micelles (C3Ms) zijn micellen waarvan de kern bestaat uit een complex coacervaatfase, die gevormd wordt door polyelektrolieten en van de oplossing gescheiden is door een corona, die meestal uit oplosbare polymeerblokken bestaat. C3Ms zijn ontdekt in het midden van de jaren 90 en staan sindsdien in het middelpunt van de wetenschappelijke belangstelling. Aanvankelijk werden de zelfassemblage en de structuur van C3Ms van verschilende polyelektrolieten bestudeerd. Recent is de aandacht meer gericht op het ontwikkelen van nieuwe C3Ms voor toepassing als capsules voor medicijnen en biomoleculen met een elektrostatische lading, zoals DNA en RNA. In een aanverwante onderzoeksrichting worden C3Ms gemaakt van organische polyelektrolieten en metaal-coördinatie complexen. Deze C3Ms hebben metaalionen in hun kern en worden daarom metaal-bevattende coacervaat micellen (M-C3Ms) genoemd. In dit proefschrift bestuderen we de eigenschappen van deze M-C3Ms en hun mogelijke toepassing als sonde voor gebruik bij beeldvorming op basis van optische visualisatie en magnetic resonance imaging (MRI).

In MRI-onderzoek worden op grote schaal contrastmiddelen gebruikt. Deze contrastmiddelen zijn meestal kleine moleculen of complexen die de relaxatietijd van de protonen van de watermoleculen in het weefsel waar ze worden aangebracht, drastisch kunnen verkorten. Het verkorten van de relaxatietijd kan op twee manieren gebeuren, en op grond hiervan worden contrastmiddelen dan ook ingedeeld in $T_1$ en $T_2$ contrastmiddelen. $T_1$ contrastmiddelen verkorten voornamelijk de longitudinale (spin-rooster) relaxatietijd van waterprotonen, en zijn meestal complexen van paramagnetische metaalionen, zoals Fe(III), Mn(III) en Gd(III). $T_2$ contrastmiddelen verkorten voornamelijk de transversale (spin-spin) relaxatietijd van waterprotonen, en zijn vaak superparamagnetisch, zoals ijzeroxide. De efficiëntie van contrastmiddelen per eenheid van hun concentratie kan worden aangegeven en onderling worden vergeleken met behulp van de grootheid relaxiviteit ($r_1$ of $r_2$, respectievelijk).

In hoofdstuk 2 onderzoeken we de vorming en stabiliteit van ijzerhoudende C3Ms. De optimale omstandigheden voor de vorming van Fe-C3Ms zijn te vinden bij een stoichiometrische verhouding van metaal, ligand en polyelektroliet. Deze micellen zijn

gedurende lange tijd stabiel bij kamertemperatuur, maar reageren sterk op de zoutconcentratie in de oplossing. We meten een afnemende intensiteit van lichtverstrooiing door een Fe-C3M dispersie met toenemende zoutconcentratie, omdat zowel het aantal Fe-C3Ms (de CMC neemt toe), als het aggregatiegetal van de Fe-C3Ms afnemen. We kunnen de afname van het aggregatiegetal verklaren met behulp van een schaalargument voor micelvorming. Wanneer we verschillende oxidatietoestanden van de ijzerionen met elkaar vergelijken, vinden we dat Fe(III)-C3Ms een lagere CMC hebben en stabieler zijn bij hoge zoutconcentraties dan Fe(II)-C3Ms.

In hoofdstuk 3 onderzoeken we het effect van pH op de Fe(III)-C3Ms uit het voorgaande hoofdstuk. De hydrodynamische grootte van deze micellen wordt voornamelijk bepaald door de grootte van de corona en verandert vrijwel niet wanneer de pH verhoogd of verlaagd wordt. De Fe(III)-ligand complexen vormen laagachtige structuren in de kern van de micellen. De vorm van de kern als geheel verandert onder invloed van pH van bolvormig (pH 4), naar ellipsoïde (pH 5-7), en uiteindelijk naar een mengsel van ellipsoïde en vertakte structuren (pH 8). Uit relaxatiemetingen volgt dat de relaxiviteit $r_1$ van deze micellen afneemt van 2.5 tot 0.5 $mM^{-1}$ $s^{-1}$ wanneer de pH toeneemt van 2 tot 8. De relatief lage waarde van de relaxiviteit wordt veroorzaakt door de sterke binding tussen de liganden en de Fe(III) ionen, die een sterk kristalveld rond de ijzerionen induceert en de ijzerionen zo in een toestand van lage spin brengt. Het grote effect van de pH op de relaxiviteit wordt veroorzaakt door binden van hydroxide-ionen door het ijzerion.

In hoofdstuk 4 onderzoeken we een manier om M-C3Ms van met name overgangsmetalen nog stabieler te maken. Het feit dat M-C3Ms uiteenvallen bij toenemende zoutconcentratie wordt veroorzaakt door de afschermende en afzwakkende werking die de zoutionen hebben op de elektrostatische drijvende kracht van complex coacervatie. Om dit effect te minimaliseren, hebben we hebben een diblokcopolymeer gemaakt met covalent gebonden ligandgroepen, die coördinatiebindingen met metaalionen kunnen vormen, aan een van de polymeerblokken. Wanneer we metaalionen toevoegen aan een oplossing van dit nieuwe diblokcopolymeer, worden meerdere metaal-ligand groepen binnen één diblokcopolymeer en tussen verschillende diblokcopolymeren via coördinatiebindingen met elkaar verbonden. Het tweede, neutrale, hydrofiele polymeerblok beschermt de gevormde coördinatiecomplexen en voorkomt ongeremd uitgroeien van het complex. Aldus ontstaan micellen die alleen door sterke metaal-ligand coördinatiebindingen bijeen worden gehouden en die stabieler zijn dan de M-C3Ms uit voorgaande hoofdstukken. Toevoeging

van zout en EDTA heeft amper invloed op de vorming van deze micellen. We hebben micellen gevormd met verschillende metaalionen ($Zn^{2+}$, $Ni^{2+}$, $Mn^{2+}$, $Gd^{3+}$) om aan te tonen dat deze methode algemeen toepasbaar is voor metaalionen.

In hoofdstuk 5 onderzoeken we de vorming en imaging-eigenschappen van M-C3Ms met zowel europium (Eu) als gadolinium (Gd) in hun kern. Eu(III) is een lichtgevende lanthanide die gebruikt wordt voor optische visualisatie. Gd(III)-complexen worden veel gebruikt als MRI-contrastmiddelen, omdat het metaalion zeven ongepaarde electronen heeft, een groot magnetisch moment en een trage elektronrelaxatie. We combineren de eigenschappen van deze beide metaalionen in een bimodale micel voor gelijktijdige MRI met hoge resolutie en optische visualisatie met hoge gevoeligheid. Waar overgangsmetalen ($Zn^{2+}$, $Fe^{2+/3+}$) zes coördinatiebindingen kunnen vormen, kunnen lanthanides er negen vormen. Daarmee is het mogelijk vertakte structuren met $L_2EO_4$ ligandgroepen te vormen bij een metaal/ligand mengverhouding van 2/3. De vertakte structuren vergroten de stabiliteit van de micellen, zodat Eu/Gd-C3Ms vrijwel niet uiteenvallen wanneer zout wordt toegevoegd tot een uiteindelijke concentratie van 500 mM NaCl. Wanneer we de verhouding Eu/Gd veranderen, verandert de grootte van de gevormde micellen niet. De luminescentie en magnetische relaxatie van de micellen veranderen wel evenredig met de hoeveelheid $Eu^{3+}$ en $Gd^{3+}$, respectievelijk. De visualisatie-eigenschappen van Eu/Gd-C3Ms zijn daarmee zeer gemakkelijk af te stemmen. We onderzoeken tot slot de stabiliteit van Eu/Gd-C3Ms door ze in bufferoplossingen met verschillende pH, zoutconcentratie en concurrerend ligand EDTA te brengen. Onder alle omstandigheden volgen we het tijdsverloop van de luminescentie en de relaxatiesnelheid van de micellen. We vinden dat noch de luminescentie, noch de relaxatiesnelheid van de micellen afneemt gedurende vijf dagen, ongeacht de gebruikte buffer. Lichtverstrooiingsmetingen en Cryo-TEM metingen bevestigen dat de grootte en structuur van de micellen inderdaad niet verandert gedurende deze vijf dagen. Samengevat hebben deze stabiele en gemakkelijk aanpasbare micellen groot potentieel voor gebruik als bimodale visualisatiemiddelen.

In hoofdstuk 6 onderzoeken we het fasegedrag van metaalhoudende complex coacervaten. Dit fundamentele onderzoek levert aanvullende informatie over de stabiliteit van de coacervaatfase die tevens de kern van M-C3Ms vormt. Het positief geladen polymeer PDMAEMA dat we in dit onderzoek gebruiken, heeft een vaste ketenlengte, terwijl het coördinatiepolymeer van metaalionen ($Zn^{2+}$) en bisliganden ($L_2EO_4$) een variabele ketenlengte heeft, die afhangt van omgevingsfactoren. Dit verschil leidt tot een

asymmetrisch fasediagram: de complex coacervaten verdragen een overmaat aan maat aan homopolymeer. We meten de samenstelling van zowel de complex coacervaatfase als de verdunde fase die daarmee in evenwicht is met behulp van NMR, als functie van de mengverhouding en de zoutconcentratie. Bij een niet-stoichiometrische mengverhouding is de samenstelling van de complex coacervaatfase altijd dicht bij de verwachte optimale verhouding, waarbij de verhouding metaal/ligand gelijk is aan 1 en de relatieve hoeveelheid positieve lading gelijk is aan 0.5. Extra hoeveelheden van metaal, ligand of homopolymeer komen in de verdunde fase terecht.

# Acknowledegement

Yes, I make my book finally!

But before I end it, I would like to thank all the people who have given their help and support on either professional or presonal aspects.

First of all, I would like to express my gratitude to my promoter Martien Cohen Stuart, not only for your science supervision with creative ideas, but also for your concern and help on my family things. Jasper van der Gucht, my dear supervisor, I can not imagine how I can finish this work without your help. Thanks for your continious guidance, inspring discussions, and your effort and patience working on my manuscripts. I am really enjoyed the working time together with you.

Secondly, I would like to thank my co-supervisor, Arie de Keizer. Your support and supervison encouraged me a lot at the beginning days. Also, thank you and your wife for the hospitality, I enjoyed the food very much. I thank my co-supervisor Henk Van As for his guidance in NMR part and arrangement for the collaboration with Italy part. And Frank J. Vergeldt, thank you for your help with NMR measurement and data analysis. Yan Yun (Peking Univeristy, China), based on your excellent work, I started this work. Thanks for your continuous contribution to this work. I also would like to thank the collaborators from University of Torino (Italy), Eliana Gianolio and Aime Silvio. I appreciate your effor and contribution to the MRI part. I am grateful to Aldrik H. Velders, who introduce me into the world of lanthanides and fluorescence. Remco Fokkink, thank you for your help with light scattering, data analysis, and the constructive discussions about light scattering. Evan Spruijt and Marc Lemmers, thanks for your kind help and discussions during the last four years. I thank Ton Marcelis (Laboratory of Organic Chemistry) for his help with ligand systhesis and modification. Barend van Lagen (Laboratory of Organic Chemistry), thanks for all the NMR measurement and spectrum analysis.

I would like to thank Josie Zeevat. I have been bothering you so many times: from the first favor with arranging visa things, till the final part of my thesis and defence. I can never forget your kindness, enthusiasm and encourage. I thank Anita ter Haar for her help with financial and tax things. Thanks to Mara Winkels for her patience and help with ordering

chemicals. I also thank Anton Korteweg and Ronald Wegh for their help with setting up experimental equipments and computers.

Also, I would like to thank my nice colleagues from FYSKO. I have spent a good time with you guys. I appreciated the harmony and friendly environment that we created and kept in the laboratory. I benefited from the group meetings, discussions and your generous suggestions. I enjoyed parties, barbecues, lab trips that we had spent together: talking, drinking, joking and dancing, so many good memories. With no more words, thank all of you.

感谢在瓦村认识的所有中国朋友们！

留学的日子是奋斗和漂泊的日子，正是因为有了你们的相伴和支持，才使得这里的生活和学习变得丰富多彩。 偶然邂逅也好，席间笑谈也好，结伴出游也好，相互帮忙也好，四年的时光结识了很多的朋友，留下了许多美好的回忆。“海内存知己，天涯若比邻”，希望我们友谊长存！感谢大家：卢玺峰，苏爱春，田利金，李肇颖，冯欢欢，郑婷婷，宁雷，李媛，乌婧，倪冉，杨娟，卢晶，李佳，程旭，宋彦儒，覃伟，宋春旭，马林，刘霞，丛汶峰，荆晶莹，林柯，张凝文，刘庆，杨婷，朱素贤，Dirk，李慧，郭学臻，牟文娟，彭金峰，赵越，贺远，付瑶，刘杰，李峰，张媛，李岩，张强，刘秉涛，武鸣，韩淼，尹家聪，杜羽，魏松红，郭长花，席梦利，郝彦玲。

最后，由衷地感谢我的父母及家人！感谢你们一直以来的支持，信任，包容，关心！特别地，感谢我深爱的妻子，郭军利女士。 从相识，相知，到相恋，相爱，感谢你一路的陪伴，感谢你真挚的爱与信任，感谢你默默的支持，无私的奉献，感谢你为我们这个小家所做的一切！千言万语，汇成一句，“执子之手，与子偕老”！

致我亲爱的女儿，贝贝，你的到来给了爸爸无限的欢乐和动力，谢谢你！愿宝贝儿永远健康，快乐！

Junyou Wang (王俊有)

Wageningen

October 2012

# Curriculum Vitae

Junyou Wang was born on 3rd of September, 1982 in Ci County, Hebei Province, China. After getting his BSc in Chemistry in 2005 at Hebei Normal University, he went to Nankai University and started his master study at Institute of Polymer Chemistry. He joined Dr. Xinlin Yang's group and worked on the systhesis and self-assembly of polymer nanoparticles. In July 2008 he received his master degree as excellent graduate (*cum laude*) of Nankai University. In September 2008 he started his PhD study at Wageningen University in the group of Physical Chemistry and Colloid Science, under supervision of prof. Martien Cohen Stuart and dr. Jasper van der Gucht. The research was focused on developing metal containing polymer micelles as potential imaging probes. The outcome of the research is presented in this thesis.

# List of Publications

**This thesis**

- **Junyou Wang**, Arie de Keizer, Remco Fokkink, Yun Yan, Martien A. Cohen Stuart, Jasper van der Gucht, Complex Coacervate Core Micelles from Iron-Based Coordination Polymers, *J. Phys. Chem. B* **2010,** *114*, 8313–8319. (Chapter 2)

- **Junyou Wang**, Arie de Keizer, Herman P. van Leeuwen, Yun Yan, Frank J. Vergeldt, Henk Van As, Paul H. H. Bomans, Nico A. J. M. Sommerdijk, Martien A. Cohen Stuart, Jasper van der Gucht, Effect of pH on Complex Coacervate Core Micelles from Fe(III)-Based Coordination Polymer, *Langmuir* **2011**, *27*, 14776–14782. (Chapter 3)

- **Junyou Wang**, Martien A. Cohen Stuart, Antonius T. M. Marcelis, Mathieu Colomb-Delsuc, Sijbren Otto, Jasper van der Gucht, Stable Polymer Micelles Formed by Metal Coordination, *Macromolecules* **2012**, *45*, 7179–7185. (Chapter 4)

- **Junyou Wang**, Aldrik H. Velders, Eliana Gianolio, Silvio Aime, Frank J. Vergeldt, Henk Van As, Yun Yan, Markus Drechsler, Arie de Keizer, Martien A. Cohen Stuart, Jasper van der Gucht, Controlled Mixing of Lanthanides(III) Ions in Coacervate Core Micelles, Submitted. (Chapter 5)

- **Junyou Wang**, Martien A. Cohen Stuart, Jasper van der Gucht, Phase Diagram of Coacervate Complexes Containing Reversible Coordination Structures, *Macromolecules* in press, DOI: 10.1021/ma301690t. (Chapter 6)

**Other Publications**

- **Junyou Wang**, Hao Li, Xinlin Yang, Preparation of Hollow Composite Spheres with Raspberry-like Structure Based on Hydrogen Bonding Interaction, *Polym. Adv. Technol.* **2009**, *20*, 965-971.

- Min Ji, Bin Liu, Xinlin Yang, **Junyou Wang**, Synthesis of Hollow Polymer Microspheres with Movable Polyelectrolyte Core and Functional Groups on the Shell-layer, *Polymer* **2009,** *50***,** 5970-5979.

- **Junyou Wang**, Xinlin Yang, Synthesis of Core-Corona Polymer Hybrid with Raspberry-like Structure by Heterocoagulated Pyridinium Reaction, *Langmuir* **2008,** *24***,** 3358-3364.

- **Junyou Wang**, Xinlin Yang, Raspberry-like PVPy/$SiO_2$ Composite Particles by Self-assembled Heterocoagulation Based on a Hydrogen-bonding Interaction, *Colloid Polymer Sci.* **2008,** *286*, 283-291.

- Guoliang Li, Xiaoying Yang, Bin Wang , **Junyou Wang** , Xinlin Yang, Monodisperse Temperature-responsive Hollow Polymer Microspheres: Synthesis, Characterization and Biological Application, *Polymer* **2008,** *49***,** 3436-3443.

- Guoliang Li, Xinlin Yang, **Junyou Wang**, Raspberry-like Core-corona Polymer Composite Particles via Electrostatic Self-assembled Heterocoagulation, *Colliod surface A* **2008**, *322*, 192～198.

# Overview of Completed Training Activities

**Courses**

Colloid Science, Wageningen, (The Netherlands), 2009

Biophysical Imaging, Wageningen, (The Netherlands), 2009

Advanced soft matter, Wageningen, (The Netherlands), 2010

22th Hen-sur-Lesse winter school, (Belgium), 2011

13th European School on Rheology, Leuven (Belgium), 2011

**Conferences and Symposia**

Dutch Polymer Days, Lunteren, The Netherlands, 2009

8th Dutch Soft Matter Meeting, Wageningen, The Netherlands, 2010

10th Dutch Soft Matter Meeting, Utrecht, The Netherlands, 2011 *

CHAINS 2011-Chemistry As Innovating Science, Utrecht, The Netherlands, 2011 #

Dutch Polymer Days, Lunteren, The Netherlands, 2012

9th International Symposium on Polyelectrolytes, Lausanne (Switzerland), 2012 *

**Other meetings and activities**

Group meetings, 2008-2012

PhD trip 2009, Switzerland and France

PhD trip 2011, Southeast Asia

---

Notes: * oral presentation, # poster

Cover Image: disigned and made by Junyou Wang

Printing: Ponsen en Looijen b.v., Ede